HIGHWAY RESEARCH RECORD

Number 457

Soil Slopes and Embankments

8 reports
prepared for the
52nd Annual Meeting

Subject Areas

61 Exploration-Classification (Soils)
63 Mechanics (Earth Mass)

HIGHWAY RESEARCH BOARD
DIVISION OF ENGINEERING NATIONAL RESEARCH COUNCIL
NATIONAL ACADEMY OF SCIENCES—NATIONAL ACADEMY OF ENGINEERING
Washington, D.C. 1973

NOTICE

These papers report research work of the authors that was done at institutions named by the authors. The papers were offered to the Highway Research Board of the National Research Council for publication and are published here in the interest of the dissemination of information from research, one of the major functions of the Highway Research Board.

Before publication, each paper was reviewed by members of the HRB committee named as its sponsor and accepted as objective, useful, and suitable for publication by the National Research Council. The members of the review committee were chosen for recognized scholarly competence and with due consideration for the balance of disciplines appropriate to the subject concerned.

Responsibility for the publication of these reports rests with the sponsoring committee. However, the opinions and conclusions expressed in the reports are those of the individual authors and not necessarily those of the sponsoring committee, the Highway Research Board, or the National Research Council.

Each report is reviewed and processed according to the procedures established and monitored by the Report Review Committee of the National Academy of Sciences. Distribution of the report is approved by the President of the Academy upon satisfactory completion of the review process.

ISBN 0-309-02190-1
Library of Congress Catalog Card No. 73-16620
Price: $2.20

CONTENTS

FOREWORD

This RECORD will be of interest to design, construction, and soils engineers who are faced with the vexing problems of earth cut-slope stability and embankment stability and settlement.

McGuffey emphasizes that earth cut slopes need to be designed rather than just excavated. He presents and assesses the relations among cost of treatment, factor of safety, and dependability of investigative and testing data. Corrective treatments are also described.

Mohan, Mendez, and Lovell present a computer program having wide capabilities for correcting the "sliding block" mode of failure in either natural or man-made slopes. Ten sliding surfaces can be concurrently analyzed for the factor of safety.

Kuesel, Schmidt, and Rafaeli describe the use of sand drains and surcharge to minimize post-construction settlements and to maintain stability during construction over a soft marine clay. Instrumentation and careful measurements were provided to alleviate the dangers of failure. Controlled construction loading rates were imposed depending on the measurements. A special bid item for "delay time" was included to provide for the unforeseen. Valuable experience and guidance for future projects were obtained from the project.

Jumikis presents a settlement influence-value chart for a homogeneous, elastic medium applicable to rigid circular foundations laid on the ground surface.

Hopkins and Deen report on the field use of mercury-filled gauges in investigating the settlements of compressible foundations beneath highway bridge approach embankments. Up to 10 units per gauge were used in this study, and all performed well. Settlements as large as 10 ft (3 m) can be measured. Settlement points up to 370 ft (110 m) from the measurement gauge were measured successfully after as long as 2 years.

Krizek and Krugmann describe a study that had as an objective the preparation of a series of charts and computer programs that the practicing engineer can use as guidelines in establishing (a) the rate an embankment may be preloaded and (b) the associated settlements.

A comprehensive case history of stress and deformations measured by field instrumentation of a 200-ft (60-m) highway embankment is given by Chang and Forsyth. A finite-element method of analysis was used to predict the stresses and deformation, and the results agreed reasonably well with the measured field data.

Huang presents a method, using a high-speed computer, to determine the stresses and strains in a viscoelastic multilayer system subjected to a circular load moving at a constant speed on the surface.

EARTH CUT-SLOPE DESIGN IN NEW YORK STATE

Verne C. McGuffey, New York State Department of Transportation

A method of designing stable earth cut slopes is presented for glaciated New York State soils conditions. The cut-slope design procedures were developed from detailed studies of natural landslides and highway cut-slope failures occurring during and after construction. These failures are classified according to mechanism of failures, and a description of corrective treatment is discussed for each classification. Emphasis is placed on essential design input considerations other than the mechanics of stability analyses. The design procedure relates the importance of investigative procedures, laboratory testing, stability analyses, alternate methods of treatment, and effects of changing conditions. Relations among cost of treatment, factor of safety, and dependability of data are discussed. Also, guides are given for selecting locations for cut-slope design investigation and for the amount of investigation and analysis required.

•CONSTRUCTION of highways using modern geometric standards has increased the frequency and magnitude of earth cuts. Failures of the cut slopes are often very expensive to correct and may result in loss of support to land and structures beyond the right-of-way. A design procedure is therefore needed to predict the degree of stability of cut slopes to be made in critical locations. Finding the "correct" method of stability analysis is only part of the answer to the cut-slope design problem. The design procedure must include suitable investigative techniques, stability analyses, methods of corrective treatment, and guides to interpreting the importance of all components of the design for the situation being studied.

The procedures described are based on studies of cut-slope failures in New York State. Failures are common in all types of glacial till deposits, but morainic deposits and "sloughed till" (colluvium) usually have a potential for greater problems. Dissected lacustrine clay deposits and fine-grained delta deposits also are prone to cut-slope failures. Average rainfall in New York State is about 3 ft per year, and the frost penetration over much of the state exceeds 3 ft. Because the stability of a cut slope depends directly on the geology and climate of an area, the procedures described may not be directly applicable to other situations.

CLASSIFICATION OF CUT-SLOPE FAILURES

An understanding of the types of cut-slope failures is needed before a design is started. Cut-slope instability can be classified into two basic categories: shallow failures and deep failures.

Shallow Failures

Shallow failures will not affect adjacent facilities or lands beyond the top of the cut slope and are usually handled by localized spot-maintenance procedures. Shallow failure mechanisms are categorized into three types (Fig. 1):

1. Sod slides are grass and sod that travel down the slope after the spring thaw or heavy rains (they usually occur on the north- or west-facing slopes on very dense or plastic soils),

Publication of this paper sponsored by Committee on Embankments and Earth Slopes.

2. Piping failures are funnel-shaped washouts in areas of high seepage in sand or silt soils that often occur as isolated pockets or as a line of washouts where a sand or silt soil overlays a less permeable soil, and

3. Sloughing failures are seashell-shaped areas of sliding soil that occur in silty soils with high seepage.

Corrective treatment for shallow failures is largely cosmetic, consisting of cleaning the ditches where necessary, reseeding sod slide areas, and placing a 2-ft thick blanket of coarse stone in the areas of piping or sloughing. Installation of underdrains along the interface of a sand or silt soil to a less permeable soil is often included as part of the design to prevent loss of support of the upper materials.

The stone "slope protection" blanket lowers the groundwater and adds confining pressure at the point of seepage eruption. The stone used for stabilizing the shallow cut failures in New York State has the following gradation: a 6-in. top size, no more than 30 percent smaller than 2 in., and less than 10 percent passing the $\frac{1}{4}$-in. sieve. Where the cost has not been prohibitive, coarse-aggregate crushed stone has been used with success. This stone blanket is usually placed a minimum of 2 ft in thickness; thinner blankets will not work. The filter criteria (1) for the stone slope protection blanket are not satisfactory for many of the fine-grained soils that it has stabilized. However, the only distress evident from inspections of hundreds of successful applications was some minor silting in the ditch and in the toe of the stone blanket. The silting was traced to surface water entering the slope protection and flowing at the rock-soil interface with sufficient velocity to erode the surface of the soil. Diversion of surface runoff has stopped the silting. At one time New York State used a slope protection blanket that was fine enough to meet the filter criteria for most of the native silty soils. However, many failures of this type of material occurred because of inability of the slope protection blanket to carry away the seeping water without becoming completely saturated and sliding off the slope.

Deep Failures

Deep failures usually extend beyond the top of slope and are categorized into three types (Fig. 2):

1. Slumps are failures in soils with high groundwater seepage. This is a large slough or a series of sloughs that may extend to the top of slope.

2. Shear failures are circular arc failures in plastic soils that, in most cases, do not extend more than 20 ft beyond the top of the cut slopes. Occasionally failures result from oversteepening of the slope, which causes initial overstress and failure of the in-place (undrained) shearing-strength conditions. Also failures occur after a long period of time as a result of stress release when the residual (drained) shear strength (2) predominates.

3. Block failures are failures that are controlled by the subsurface profile. These are types of wedge failures with cracks starting near the top of the cut and secondary movements occurring beyond the top of the cut soon after the first movements. They usually result from shallow soils over sloping rock surfaces, thin layers containing high water pressure, or sloping plastic layers.

These three types of failure mechanisms result in loss of support for the ground beyond the top of the cut slope, and, as such, the damage that can result from any movements is often very costly. The design procedure described here is therefore confined exclusively to design of earth cut slopes to prevent deep failures.

CUT-SLOPE DESIGN PROCEDURES

Cut-slope design is a complex study of the consequences of instability versus the cost of reasonable treatment to prevent the instability. Soil strength and groundwater conditions in earth cuts usually change with time, which makes the design process more difficult. Cuts in overconsolidated soil result in a release of overburden stress and a loss in shearing strength of the soils with time. Many overconsolidated soils in

New York State have had major cut-slope failures 8 years after construction. In granular soils and many of our complex, multigrained till soils, the water level draws down over a period of time. As a result, cut-slope failures that occur when the initial cut is made will be permanently stable as soon as the water table reaches equilibrium after grading is completed.

The soils engineer must decide whether to institute a design for an earth cut slope or to take a chance on using a "standard" slope angle. Facilities are not available to provide a detailed investigation of all cuts on highway projects. However, it is imperative that an investigation be made of all cuts that support important adjacent lands or structures. It is also essential that locations of existing landslides be identified before the highway alignment is fixed. Stabilization of existing landslides into which a cut has been made is perhaps the most expensive change precipitated by "unknown" soil conditions. Therefore, all locations with topography not consistent with the geology of the area should be investigated to determine whether it is an old landslide.

Investigative Techniques

Development of proper input for a cut-slope investigation depends on understanding the mechanism of failure. A simplified expression of the stresses applied to a natural slope is shown in Figure 3. More detailed discussions of the failure mechanism are available, but it appears that the current inability to obtain exacting input of present and expected conditions precludes the use of most of the more rigorous solutions. The basic inputs required for cut-slope stability analyses are surface geometry, subsurface geometry, shearing strength of the critical soil (or soils), groundwater conditions, and changes in the groundwater conditions and soil strengths that can be expected.

Surface Geometry—For surface geometry, cross sections and topography are required including accurate locations of utilities, streams, roads, etc. For side hill conditions, cross sections must be carried up to the top of the hill or to a controlling feature such as a rock outcrop.

Subsurface Geometry—The location and characteristics of the critical soil strata are usually obtained by taking continuous split spoon samples in borings located strategically along the proposed cut. A minimum of two borings on a cross section are needed, one in the ditch line and one at the top of slope. Additional borings may be needed above the top of cut if the slope continues to rise. The number of borings required longitudinally depends on the continuity of the soil conditions and the extent of the possible problems. The use of test pits is helpful in obtaining undisturbed samples. Also, knowledge of the continuity of subsoil conditions (if the critical soils are not too deep) is helpful.

Twenty-three borings were taken at one landslide location with only two borings giving an indication of clay near the surface of the rock. Deep test pits were then used to determine the cause of failure. These showed a thin, discontinuous clay layer at the rock surface. Now, for geologically similar areas where thin clay over rock is expected, it is first assumed that the clay layer exists, and then the exploration program tries to prove that it does not.

Seismic investigations are the prime tool if the rock surface is a major influencing factor. Other investigators have had success with the electrical resistivity method of investigation. In New York State, however, resistivity methods have only been successful in determining the groundwater table.

Shearing Strength—Consolidated drained triaxial tests are run to determine the drained friction angle of the critical soil. A rate of shear of about one-tenth of the drainage rate determined from a consolidation test (3) is used.

Consolidated undrained tests are used for short-term analyses on plastic soils. Also, consolidation and permeability tests are used to estimate the rate of drawdown of the groundwater table and the rate of stress release.

Explorations in, and analysis of, existing landslides are helpful in evaluating the shearing strength in similar geologic soil deposits.

A preliminary relation between plasticity index and drained friction angle is shown in Figure 4. This curve is based on data taken from existing landslide situations that

were analyzed and checked against laboratory test data with reasonably good comparisons (1). It has been used with apparent success to advance development of designs when time is not available to obtain adequate tests.

Groundwater Conditions—Past landslide studies have shown as many as three indicated groundwater tables: one in the underlying rock, one in a granular layer within a glacial till deposit, and one within the glacial till. Therefore, the method of obtaining the groundwater condition must be capable of separating these tables. In New York State various methods are employed, use of which depends on the conditions expected from a geologic evaluation. Separate observation wells sealed into each soil or rock deposit are often used.

Changes in Condition—Normal seasonal groundwater fluctuations can be obtained from periodic readings on observation wells. However, the drawdown that occurs after the cut is made can only be estimated. An approximate theoretical solution for drawdown curves at different times is currently being checked by field instrumentation in New York State. These solutions are for uniform soils only because many layered soil systems do not exhibit significant drawdown.

Consolidated undrained triaxial tests give a good value for the shearing strength of a soil deposit when the cut is made. However, the stress release resulting from the excavation reduces the strength of overconsolidated soils to a value approaching that obtained from the consolidated drained test. The shear strength at failure is somewhat above the drained strength for slopes that have not moved before. For slopes that have failed before (old landslides), the shear strength at failure is the same as the drained strength. An approximate procedure to relate the rate of groundwater drawdown (improving stability) to the rate of stress release (decreasing stability) is being studied in New York State. Because of the length of time required for complete stress release (about 8 years for the upper 20 ft for some slopes), it is doubtful that a good method of estimating the time to failure will be developed for many years.

Stability Analyses

Various methods of stability analyses have been computerized and are available. Because most landslides and cut-slope failures that have been evaluated failed under conditions of drained shear strength with seepage forces (or artesian water pressures) included, the stability analysis should have these capabilities. New York State is currently using a computerized circular-arc stability analysis that has these and other capabilities (4). The modified Swedish stability analysis appears to provide the best correlation to field conditions for sliding types of wedge failures. Because this analysis has not yet been programmed for a computer, it must be done manually. However, a modified "NAVDOCKS" wedge (5) has been programmed for a desk-top calculator and is only slightly conservative for most cases.

In addition to the methods of analyses previously mentioned, a solution for the infinite slope stability analysis for the drained strength conditions with seepage forces has been presented in graphical form (6). An example of one situation applicable to silty glacial till soils is shown in Figure 5. The curves (Fig. 5) are used as a preliminary evaluation tool to help in determining whether a problem could be expected under generalized soil conditions, slope angles, and water table. These curves can be used where the failure mechanism is expected to be shallow by using the slope angle as the angle of the proposed cut. They can also be used with reasonable accuracy for a deep-seated failure on a subsurface plane, provided that the slope of the subsurface plane is taken as the slope angle on the curves.

Numerically, the following guides for acceptable factors of safety are used:

1. Factors of safety less than 0.95 for drained or undrained strength conditions are considered unsatisfactory because a failure will occur and treatment must be anticipated in design.
2. Factors of safety between 0.95 and 1.15 for the drained strength condition are considered conditionally acceptable for the plastic soils that are expected to lose strength with time, provided that the undrained factor of safety is in excess of 1.25 and the possible damages are not great. In most cuts, the groundwater table will draw

Figure 1. Shallow-cut failures.

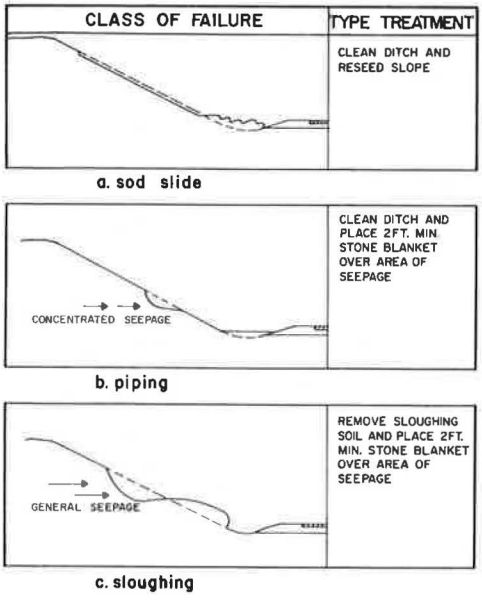

Figure 2. Deep-cut failures.

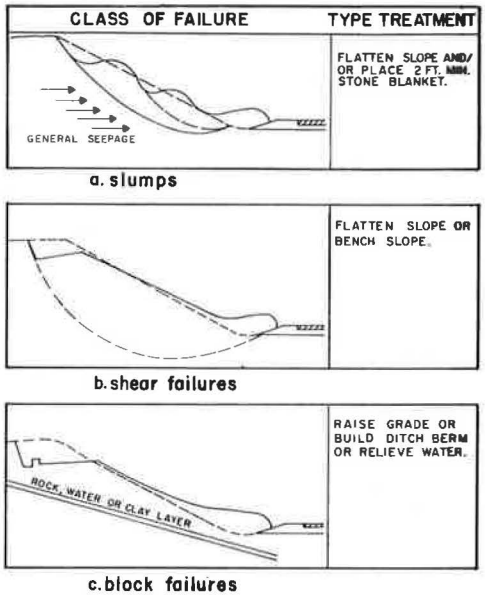

Figure 3. Simplified stresses on natural slopes.

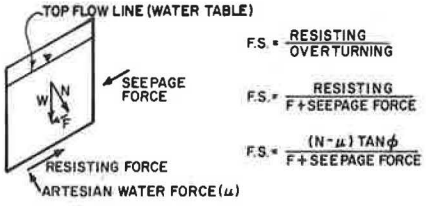

Figure 4. Drained strength and plasticity index.

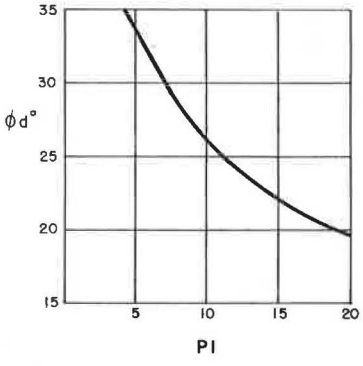

Figure 5. Infinite slope analysis.

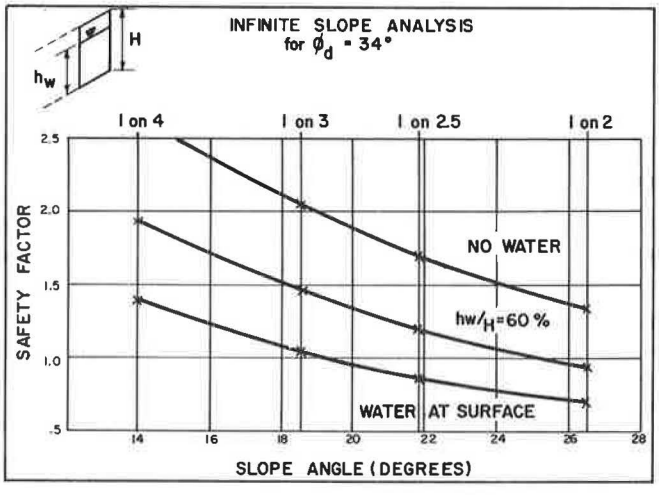

down during the period of stress release, which improves the factor of safety to an adequate value before reaching a condition approaching the drained strength.

3. The normal factor of safety used is 1.15 provided that the maximum expected cyclical fluctuations of groundwater do not leave a factor of safety of less than 1.0.

METHODS OF STABILIZATION

Commonly used methods of cut-slope stabilization are shown in Figure 2 and discussed in this section.

Slumps

Methods of treatment include flattening the slope, placing a minimum 2-ft thick stone slope protection blanket over the slope, installing subsurface drainage controls, and correcting failures after they occur. Because cutting into the groundwater surface normally causes a lowering of the groundwater and resultant reduction of seepage force, it is often best to allow failures to occur during construction. If a stable condition is not reached before the end of the construction period, some positive method of stabilization must then be used.

Shear Failures

Methods of treatment include flattening the slope or constructing a wide bench in the slope. (Narrow benching of cut slopes to control runoff is not effective in the soils and climate of New York State. The drainage becomes blocked with ice and snow causing the top of the bench to become saturated and fail with resultant destruction of the bench.)

Cut-slope failures in the varved clays in New York State have been virtually eliminated. In most of our varved clays, stable slopes result at the following slopes: 0 to 20 ft (1 vertical on 2 horizontal), 20 to 70 ft (1 vertical on 3 horizontal), and more than 70 ft (flatter). These guides are based on laboratory testing and design analyses using the drained shear strength and anticipated water table and are verified by natural gulley slopes that have reached a stable inclination.

Block Failures

Methods of treatment are usually determined by the type of discontinuity in the subsurface profile. Some common methods of treatment are as follows:

1. Installation of subsurface drainage is made to reduce the seepage forces or artesian water pressure. This treatment has been used with only limited success in New York State because it is difficult to locate the source of groundwater and more difficult to design and install a filter system that will permit permanent drainage of the critical soil layer. In recent years a slotted polyvinylchloride pipe has been developed and is now available in the eastern United States. Because the width of slots can be very small and varied to meet soil conditions, this may be the solution to the filter problem.
2. Total removal of soils above the sliding surface is usually not economical and in some instances would require stripping a complete hillside. Flattening the slope is not a suitable solution in many cases because it may cause greater instability by reducing the overburden stress on the failure surface without reducing the water pressure.
3. Raising the roadway grade (or relocating the roadway) to reduce the effective depth of cuts is the best solution if it can be determined in the planning or early design phase before the highway geometrics are fixed.
4. Narrowing the roadway section and constructing a berm in the ditch requires placing underdrains in the ditch area and filter materials between the original slope and the berm. Narrowing the roadway section often reduces sight distance and causes snow-removal and pavement-drainage problems.
5. Constructing a retaining wall at the ditch line can only be used where the base of the wall can be located below the failure surface and becomes very expensive if the earth pressures are high. Generally, walls are not considered a satisfactory solution

because more serious failures may be started by the normal wall installation procedures. Drilled-in-place walls were used successfully in Seattle, Washington.

SELECTION OF STABILIZATION METHOD

Selection of a suitable stabilization method for a potentially unstable cut slope is somewhat difficult and confusing. Two examples relating factors that affect the choice of treatment may provide a better understanding of the problem.

Slump Failure

If we assume a 75-ft deep cut, the normal choices of stabilization in New York State would be (a) to flatten the slope from the normal 1 vertical on 2 horizontal to 1 vertical on 3 horizontal or (b) to dig out 2 ft of the surface materials and replace it with 2 ft of stone slope protection blanket. For the slope-flattening treatment, the factor of safety would be increased by approximately 0.4, and the cost would be in the order of $10,000 per station plus an increase of approximately 75 ft of right-of-way. For the second choice, using a slope protection blanket, the factor of safety would be increased only by approximately 0.1, and the cost would be in the order of $6,000 per station; however, there would be no increase in the right-of-way required.

The deciding factor for the choice of treatment is usually the amount of damage that could result if a failure did occur after the treatment was completed. A number of expensive residences along the top of slope make the slope-flattening treatment economically undesirable even for an increase in the factor of safety of 0.4. However, it might also be undesirable to increase the factor of safety by only 0.1 when some unknown, such as a series of sewage drain fields behind the slope, might cause failures that would destroy the valuable building.

When the choice of treatment is not clearly defined, more specialized treatments, such as horizontal drains or massive toe walls, are used to improve the factor of safety and reduce the possibility of large damage costs.

Shear Failure

A 70-ft deep cut was planned in a soft clay deposit within the Albany, New York, area. The slope stability analyses indicated that a 1 vertical on 3 horizontal would be satisfactory. For aesthetic reasons, the designers chose a longitudinal transition of slopes in this area from a 1 vertical on 2 horizontal in a stable gravel deposit to 1 vertical on 3 horizontal in the clay deposit under a proposed bridge. This resulted in an average slope through the clay deposit adjacent to the bridge site of approximately 1 vertical on $2\frac{1}{2}$ horizontal, which still provided an adequate factor of safety against immediate failure (undrained strength conditions) but a marginal factor of safety for the long term (drained strength conditions). However, during construction the contractor further changed the design conditions by overexcavating behind one of the piers for the structure in the area. This resulted in a temporary equivalent slope of approximately 1 vertical on $1\frac{1}{2}$ horizontal. Within 2 weeks there was a shear failure that filled the excavation and dropped the ground at the top of the cut slope, breaking sewer lines and endangering a house close to the top of the cut. Because of the contractor's operations, a failure had occurred, the strength of the clay was reduced, and excess pressures were induced such that there was a combination of drained and undrained phenomena occurring within the slope. A type of bench cut was designed adjacent to the bridge to account for the undrained strength parameters that applied as a result of the contractor's improper overexcavation. This required relocating the sewer lines and taking additional property at the top of slope. Additional expense was incurred to permit safe construction of the abutment near the top of the 1 vertical on 3 horizontal slope. This required changing the type of pile from cast-in-place to H-piles and using lightweight expanded shale aggregate as the backfill behind the abutment.

The original soils design report was not complete in that it did not point out the importance of controls during construction. It is not possible to estimate all possible situations that would cause a cut slope to fail. However, a greater effort is needed to

inform the construction personnel of the importance of temporary construction operations on the stability of cut slopes at critical locations.

The factors influencing the choice of cut-slope stabilization methods discussed here include indicated factor of safety, cost, dependability of the limits of variables, changing conditions, outside influences (aesthetics, special use properties, etc.), temporary construction conditions, and added costs resulting from failures. Other situations will include different influencing factors or will show a greater emphasis on certain factors than discussed in the previous examples.

The selection of an appropriate method of stabilization and an adequate factor of safety must be tailored to the individual situation being studied, with emphasis placed on the importance of the adjacent land.

CONCLUSIONS

Cut-slope stability studies must be approached in a manner different from embankment stability studies. With minor exceptions, embankment stability conditions improve with time as consolidation and strength gain occur, and changes in factor of safety with time are not considered to be detrimental. The stability of cut slopes, however, may improve or become worse with time after construction. Permanent water table drawdown improves the stability, but stress release and loss of shearing strengths reduce the factor of safety. Also, normal seasonal water fluctuations alternately increase or decrease the factor of safety. A season with unusually high rainfall may cause cut-slope failures that would never be predicted from prior records.

Currently, it is not possible to design all cut slopes without failures under all possible conditions. However, cut-slope failures at critical locations can and should be eliminated by adequate investigation and design.

Areas of old landslides can and must be identified because cut-slope failures in old landslides are usually the most expensive to correct.

Investigative techniques and design analyses are available now that can usually predict areas of major cut-slope problems where no surface indications exist. Although not yet perfected, these procedures can, with an intimate knowledge of the local geology, be used with reasonable success.

REFERENCES

1. Soil Mechanics, Foundations, and Earth Structures. Bureau of Yards and Docks, Dept. of the Navy, NAVDOCKS DM-7, 1971, p. 7-8-13.
2. Skempton, A. W. Long Term Stability of Clay Slopes. Geotechnique, June 1964, pp. 77-101.
3. Bishop and Henkel. The Measurement of Soil Properties in the Triaxial Test. 1957, pp. 124-127.
4. Computerized Analysis of the Stability of Earth Slopes. Soil Mechanics Bureau, New York State Dept. of Transportation, Albany, SDP-1, Oct. 1970.
5. NAVDOCKS Wedge Analysis by Desk Top Computer. Soil Mechanics Bureau, New York State Dept. of Transportation, Albany, Feb. 1972.
6. Infinite Slope Analysis. Soils Mechanics Bureau, New York State Dept. of Transportation, Albany, Feb. 1972.

COMPUTERIZED SLOPE STABILITY ANALYSIS: THE SLIDING BLOCK

Aditya Mohan, Carlos Mendez, and C. W. Lovell, Jr., Purdue University

This paper presents a computer program for a common type of analysis of the slope stability problem: the possibility of slope failure by translation of a massive block along a weak layer of soil. The problem, which can occur in either natural or man-made slopes, is most generally referred to as the sliding block problem. Variation in the water surface position requires three subroutines or cases. The program automatically sequences selected potential sliding surfaces one by one, then selects the desired water surface case, and finally computes the factor of safety against sliding along the base of the central block. The analysis is based on total unit weights and boundary forces. It is possible to consider 10 different soil types having very different soil parameters, such as unit weight, Mohr-Coulomb cohesion intercept, and Mohr-Coulomb angle of friction. A maximum of 12 continuous soil layers at any inclination can be considered in the present program. A total of 10 vertical strip loads of different intensities can be placed on the ground surface anywhere below the toe and above the crest. Finally, with all this information, 10 sliding surfaces can be concurrently analyzed for the factor of safety. This factor is applied to the strength of the soil at the base of the central block, assuming that there is limiting equilibrium for the active and passive earth pressure forces at the ends of the central block.

•THE stability of man-made and natural slopes has always been an important topic of discussion in the field of civil engineering. Yet, failure of man-made fills and cuts probably occurs more frequently than all other failures of civil engineering structures combined. Although an understanding of the major factors that contribute to failure of slopes has improved considerably, our predictive ability remains less than satisfactory.

This paper addresses the problem of the sliding block, i.e., an essentially rigid mass sliding in a weak layer. At first glance, this seems to be a rather simple problem; however, when practical variations in soil profile are considered, as well as water levels, boundary geometries and loadings, and uncertainties of position and shape of the most critical sliding surface, the solutions require reasonably large computer systems.

When a slope is underlain by one or more strata of very soft or loose materials, the most critical sliding surface may not be even approximately circular, as shown in Figure 1. Rather there is a three-plane surface of potential sliding in which a maximum amount of the surface lies within the weak material.

An initial programmed solution (11) was quite general with respect to the shape of the three-plane surface, but to accommodate this feature the profile was simplified to two soil layers, i.e., a strong soil over a weak one. A second program, reported in this paper, makes simplifying assumptions with respect to the shape of the sliding surface but is quite versatile with respect to the profile and boundaries. This second

Publication of this paper sponsored by Committee on Embankments and Earth Slopes.

program seems to better meet the analytical requirements of the Indiana State Highway Commission.

SLOPE FAILURE BY SLIDING

The type of failure usually assumed in slope stability analysis is the one-piece slide (10). The failure is one in which the moving body is essentially rigid and the failing mass is separated from the unmoved one by a surface of assumed shape. Where the soil is grossly homogeneous, it seems logical that the failure surface would be roughly circular, and, in the interest of simplicity, it is usually made exactly so. A recent overview of the circular analysis, involving the well-known methods of slices, is given elsewhere (4).

Where there is evidence of definite differences in shearing resistance in the soil profile, it is well to consider potential failure surfaces that follow the surfaces of weakness. Several methods of handling irregular surfaces are reported elsewhere (4, 12, 14).

The irregular sliding surface is shown in Figure 1, where the potential failure planes have a maximum length in the weaker materials. The potential failing block is actually a combination of active and passive wedges, with a central trapezoidal block based in a weak layer. Examples of simplified solutions to this problem are given elsewhere (5, 6, 11).

GENERAL SOLUTION TO THE SLIDING BLOCK PROBLEM

Figure 2 shows the free body diagram with a full quota of complexities in boundary geometries and forces; i.e., these could be simpler in a given instance. Incorporation of a water surface and associated water forces into the problem makes it convenient to consider three cases, each with its appropriate subroutine in the computer solution. The upper boundary slopes reading left to right in Figure 2 are referred to as the down slope and the middle slope or simply the slope and the upper slope. The cases are as follows:

1. Case 1—when the water surface is below the trial sliding surface,
2. Case 2—when the water surface is partly above and below the ground surface but above the trial sliding surface, and
3. Case 3—when the water surface is anywhere below the ground surface but above the trial sliding surface.

It is assumed that the right-hand wedges are in a state of limiting active earth pressure, and the left-hand wedges are in a state of limiting passive earth pressures. Simplifying assumptions are employed with respect to the inclinations of the wedge surfaces and the directions of the earth pressure forces. Although the right-hand and left-hand wedges are assumed to be on the verge of sliding, there is in general an incomplete mobilization of the shearing resistance along the base of the block; i.e., the factor of safety is defined with respect to the shearing resistance-shearing force ratio along this surface.

The wedge inclination and earth pressure force direction assumptions are those that apply for a simple Rankine case. They are employed by others (5) and have been shown to be good approximations of the most critical values for a number of cases tested by Mendez (11).

To be certain that all assumptions inherent in the solution are understood, we are listing them as follows:

1. Problem is two-dimensional;
2. The ground surface is defined by three slopes and a well-defined toe and crest;
3. Soil strata are laterally continuous;
4. Soil properties in layers are defined by γ, c, and ϕ (where c or ϕ can be equal to zero);
5. Sliding surface is at the base of the block, and between the slide wedges is a plane;

6. All lateral forces on vertical wedge boundaries are normal to these boundaries (i.e., there are no shear forces on these boundaries);

7. The factor of safety is figured for the base of the sliding block only, and the movement required to mobilize limiting active and passive pressures is smaller than the movement required to mobilize the shearing strength of the weak soil strata;

8. The wedge slip surfaces are at $45 + \phi/2$ and $45 - \phi/2$ with the horizontal for active and passive wedges respectively;

9. The active and passive forces are computed by satisfying static equilibrium (after verifying assumptions 6 and 8); and

10. Seepage, if any, is in a steady state; however, water pressures are calculated at any point as if they were hydrostatic.

The analysis of forces is shown in Figures 2, 3, and 4. The analysis is divided into three parts: calculation of forces on central block due to active wedge, calculation of forces on central block due to passive wedge, and calculation of base forces on central block and of the factor of safety against sliding along this base.

The analysis of forces is illustrated for water surface case 2, but the other cases follow directly.

Figure 2 shows a rather complex problem space section, with multiple soil layers at variable inclinations and with very different soil properties.

Analysis of Active Forces on Central Block

Figure 3 shows the active wedge (Fig. 2) divided into small wedges governed by the intersection of the assumed slip surface and soil boundaries.

Let us consider a typical polygon of forces for any (n th) wedge shown in Figure 3. Summing all the forces in the x- and y-directions and equating to zero yield the following equations:

For $\Sigma F_x = 0$,

$$PAn = UARn - UALn - UAn \cos(45 - \phi n/2) + NA'n \cos(45 + \phi n/2) - CAn \cos(45 + \phi n/2) \quad (1)$$

and for $\Sigma F_y = 0$,

$$WAn = CAn \sin(45 + \phi n/2) + UAn \sin(45 - \phi n/2) + NA'n \sin(45 + \phi n/2) \quad (2)$$

Elimination of NA'n from Eqs. 1 and 2 yields an expression for the incremental active force for the n th wedge,

$$PAn = WAn \tan(45 - \phi n/2) - 2\,CAn \cos(45 + \phi n/2) + (UARn - UALn) + UAn\,[\cos(45 - \phi n/2) - \tan(45 - \phi n/2) \sin(45 - \phi n/2)] \quad (3)$$

Analysis of Passive Forces on Central Block

Figure 4 shows the forces acting on the passive wedge shown in Figure 2. Consider a typical polygon of forces acting for an n th passive wedge in Figure 4. Forces in the x- and y-directions are summed, and equilibrium is equated to zero.

For $\Sigma F_x = 0$,

$$PPn = U\beta_n \sin\beta_1 + CP_n \cos(45 - \phi n/2) + ULn + UPn \cos(45 + \phi n/2) - URn + NP'n \cos(45 - \phi n/2) \quad (4)$$

and for $\Sigma F_y = 0$

$$WPn = NP'n \sin(45 - \phi n/2) - U\beta_n \cos\beta_1 - CPn \sin(45 - \phi n/2) + UPn \sin(45 + \phi n/2) \quad (5)$$

Figure 1. Slope in stratified soil profile.

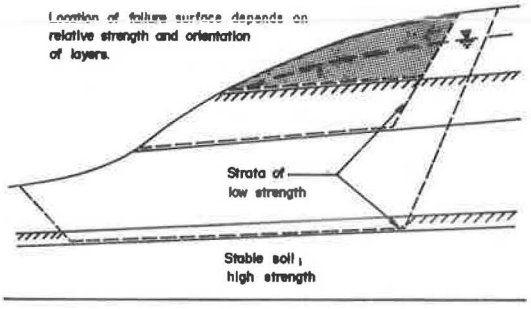

Figure 2. General problem of sliding block with submerged water (case 2).

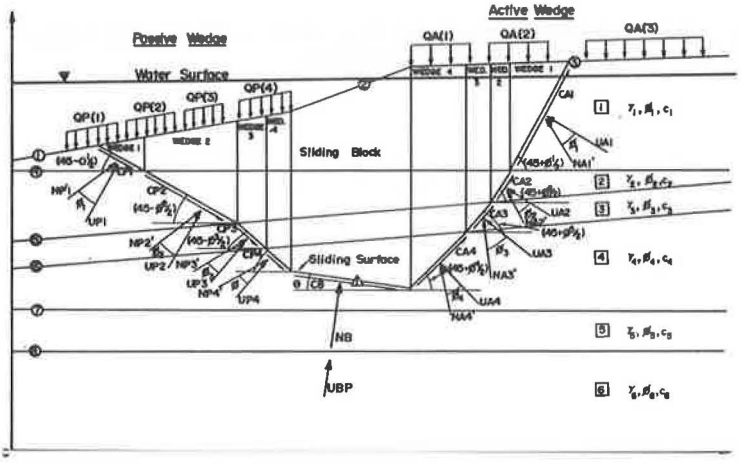

Figure 3. Analysis of forces on active wedge (case 2).

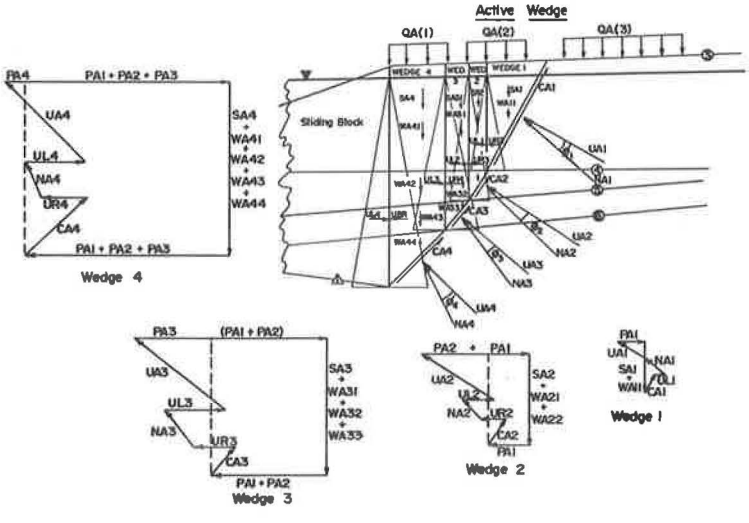

V = 196.25 metric tons = 196,250 kg. The influence values S for m = 3.00 are taken from Figures 1 and 2 and are given in column 6 of Table 1. The settlements as successive displacement differences,

$$\Delta s_n = \left(\frac{V}{E \times R_o}\right)(S_n - S_{n-1}) \tag{15}$$

for each layer are given in column 9 of Table 1. By stepwise calculations, the total settlement s of this soil-foundation-load system is found as the sum of the settlements of each individual layer:

$$s = \sum_{1}^{4}(\Delta s_n) = 2.41 \text{ cm}$$

Method of Equivalent Layers

Because in the multilayered soil system each layer may be of different homogeneity with large differences in elastic characteristics, use of these charts (Figs. 1, 2, and 3), which are prepared for a homogeneous monolayer, to make $\bar{\sigma}_z$ stress and settlement s calculations necessitates that the stratified, multilayered soil system be converted or homogenized into an equivalent (fictitious), homogeneous hemispace. The homogenization is accomplished by the so-called method of equivalent layers h_e. This method works with fictitious substitute heights h_e for each thickness h_1, h_2, h_3, . . . , h_n of the real strata. The principle involved in this method is to determine an ideal, equivalent thickness h_e of a uniform, homogeneous soil column (or beam) that, upon loading, will bring about a deflection equal to the sum of the deflections (viz., settlements) of each of the strata in the multilayered system. Thus, the charts here developed are directly applicable to such an equivalent, homogeneous hemispace, or, in other words, the charts are also indirectly applicable as an approximation of multilayered soil systems.

The homogenization of multiple layers into a single, ideal, equivalent homogeneous monolayer is based on the principle that two layers of various thickness with differing moduli of elasticity are equivalent when these two layers are of the same stiffness, i.e., when

$$E_1 \times I_1 = E_2 \times I_2 \tag{16}$$

or

$$\frac{E_1 \times h_1^3}{(12)\left(\frac{m_1^2 - 1}{m_1^2}\right)} = \frac{E_2 \times h_2^3}{(12)\left(\frac{m_2^2 - 1}{m_2^2}\right)} \tag{17}$$

where

h_1 and h_2 = heights of a column of soil, namely, thickness of soil layers, and
m_1 and m_2 = Poisson's numbers for layer one and layer two respectively.

If it can be assumed that $m_1 \approx m_2$ for all courses, then the equivalent height h_e for a two-layered system calculates as

$$h_2 = h_e = h_1 \sqrt[3]{\frac{E_1}{E_2}} \tag{18}$$

Thus, it is here assumed that the rigid circular foundation and the individual layers form a compound unit. Upon deformation, a two-layered soil system, it is assumed, would deflect uniformly and retain its unity. When $\sqrt[3]{E_1/E_2} = 1$, we have a uniform mass—a monolayer.

Figure 4. Self-settlement influence values (SO) for rigid circular foundation.

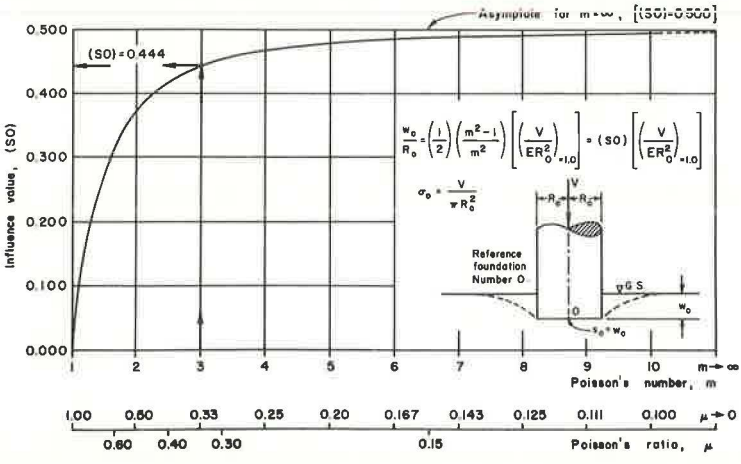

Table 1. Calculation of settlement.

Number of Layers (1)	Soil Material (2)	Thickness of Each Layer (m) (3)	Depth to Bottom of Each Layer (m) (4)	Relative Depth (5)	Influence Value (6)	Modulus of Elasticity of Each Layer (kg/cm^2) (7)	Load Factor (cm) (8)	Successive Settlement Difference for Each Layer, $\Delta s_n = (8)(S_n - S_{n-1})$ (9)
1	Sand	3.0	3.0	$z_1/R_o = 3/2.50 = 1.20$	$s_1 = 0.14351$	$E_1 = 150$	$\frac{785}{150} = 5.233$	$\Delta s_1 = (5.233)(0.14351) = 0.75$
2	Silt	2.0	5.0	$z_2/R_o = 5/2.50 = 2.00$	$s_2 = 0.22838 - \frac{0.14351}{0.08487}$	$E_2 = 120$	$\frac{785}{120} = 6.542$	$\Delta s_2 = (6.541)(0.22838 - 0.14351) = (6.541)(0.08487) = 0.56$
3	Silty clay	4.0	9.0	$z_3/R_o = 9/2.50 = 3.60$	$s_3 = 0.31306 - \frac{0.22838}{0.08468}$	$E_3 = 100$	$\frac{785}{100} = 7.8500$	$\Delta s_3 = (7.850)(0.31306 - 0.22838) = (7.850)(0.08468) = 0.66$
4	Clay	5.0	14.0	$z_4/R_o = 14/2.50 = 5.60$	$s_4 = 0.35772 - \frac{0.31306}{0.04466}$	$E_4 = 80$	$\frac{785}{80} = 9.8125$	$\Delta s_4 = (9.8125)(0.35772 - 0.31306) = (9.813)(0.04466) = 0.44$
5	Gravel	—	—	—	—	$E_5 = \infty$	—	—

Figure 2. Settlement influence-value chart for rigid circular foundations.

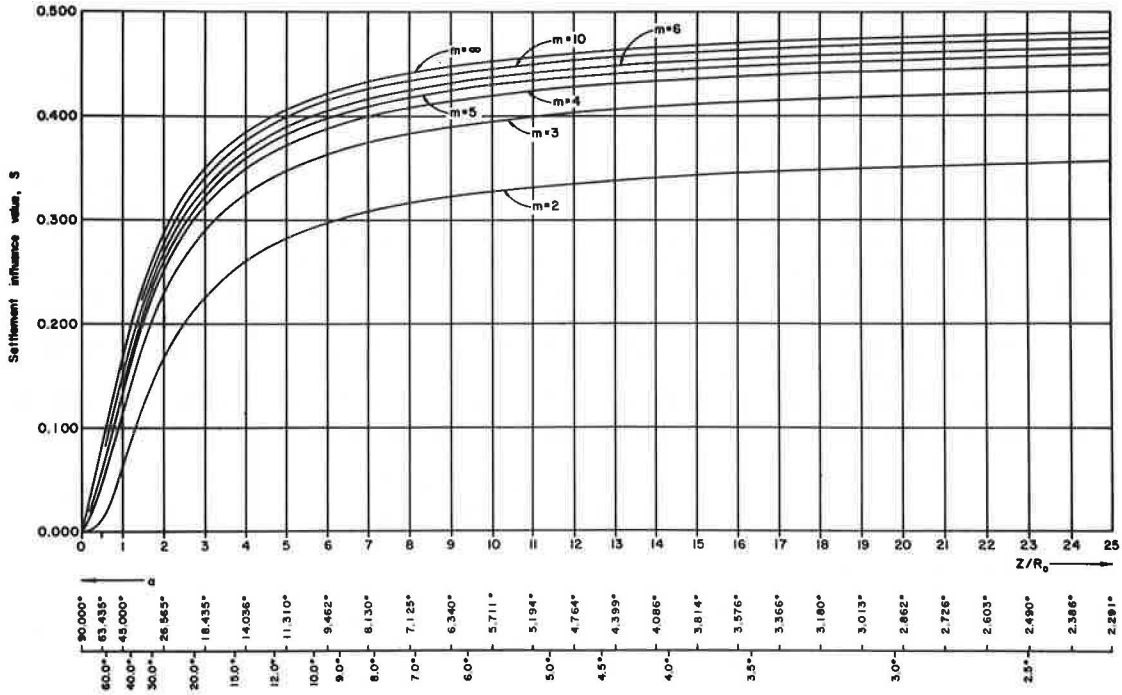

Figure 3. Enlargement of Figure 2 for z/R_0 ratios.

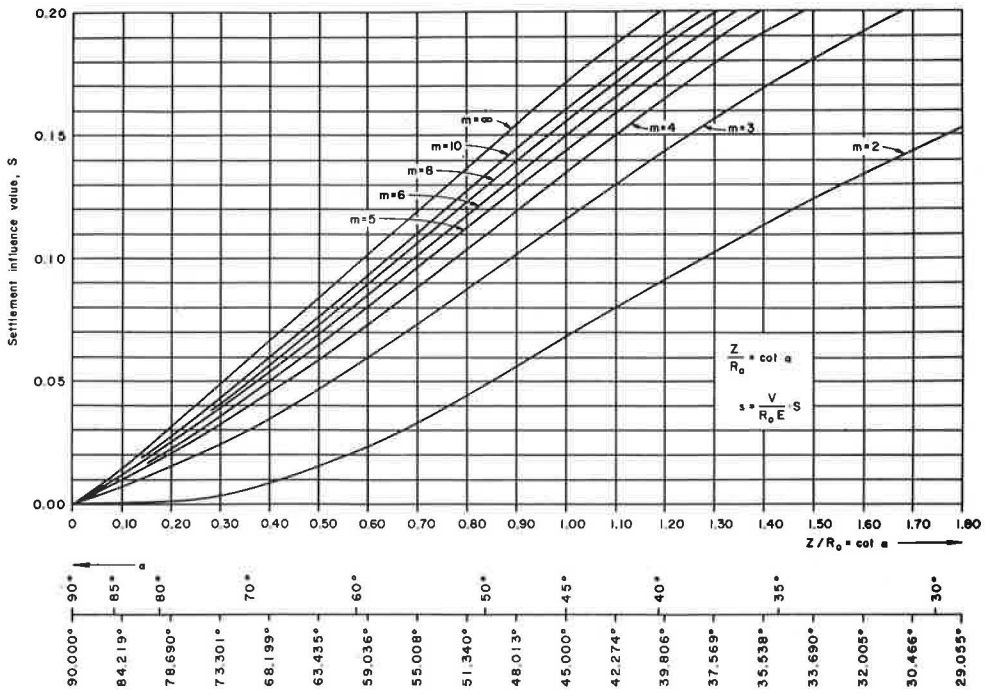

Settlement s may be obtained by multiplying the corresponding settlement influence value S by the factor $V/(E \times R_o)$:

$$s = (S)\left(\frac{V}{E \times R_o^2}\right)(R_o) = (S)\left(\frac{V}{E \times R_o}\right) \tag{12}$$

Settlement Influence-Value Charts

The dimensionless influence values were programmed for computer calculations and compiled in tabular form for various Poisson's numbers (13). By means of such tables, the settlement influence-value charts (Figs. 1, 2, and 3) were prepared for quick, effective, and practical use. Figure 3 is an enlargement of Figure 2 for z/R_o ratios from 0 to 1.80 (for settlement influence values from S = 0.00 to S = 0.20). For the purpose of comparison, in Figure 1 there is also shown for m = 2 the vertical σ_z stress influence-value curve $i_z = \sigma_z/\sigma_o$ for limply arranged single uniform stresses (σ_o) over a circular area on a homogeneous, hemispatial medium.

For a hemispace of infinite extent, $z = \infty$ and $\alpha = 0$; thus the total settlement [elastic settlement according to Boussinesq's theory of elasticity (9, 12-16)] is

$$s_o = w_o = \left(\frac{1}{2}\right)\left(\frac{m^2 - 1}{m^2}\right)\left(\frac{V}{E \times R_o}\right) \tag{13}$$

or, in terms of influence value,

$$\frac{w_o}{R_o} = \left(\frac{1}{2}\right)\left(\frac{m^2 - 1}{m^2}\right)\left(\frac{V}{E \times R_o^2}\right) = (SO)\left(\frac{V}{E \times R_o^2}\right) \tag{14}$$

Here (SO) is the influence value of the so-called self-settlement $s_o = w_o$ of the circular rigid foundation (Fig. 4). If, for example, m = 3.0, E = 120 kg/cm^2, V = 196,250 kg, and R_o = 2.50 m, then the self-settlement $s_o = w_o$ of the rigid circular foundation (which is the total vertical displacement in the z = 0 plane) calculates (Fig. 4) as

$$s_o = w_o = (SO)\left(\frac{V}{E \times R_o}\right) = (0.444)\left[\frac{196{,}250}{(120)\ (250)}\right] = (0.444)\ (6.541) = 2.90 \text{ cm}$$

MULTILAYERED SOIL SYSTEM

Stress distribution and settlement in a multilayered soil system differ considerably from those in a uniform, massive (infinitely thick), homogeneous monolayer only in cases where there exists a sharp difference in elasticity characteristics of the various individual deformable component layers in the multilayered soil. If the differences are small, then the influence-value chart renders a reasonably satisfactory approximation for determining settlement of such multilayered soil systems.

Example for Use of the Settlement-Influence Chart

The influence chart may also be used for calculating approximative total elastic settlement of a multilayered soil system. There exist two principal methods for doing this, namely,

1. The method of successive displacement-difference steps where the total settlement is obtained by adding the so-called partial settlements (i.e., settlements of each layer in the multilayered soil system), and
2. The method of equivalent layers.

Successive Settlement-Difference Step Method

A multilayered soil system consisting of four layers of compressible soil over a gravel (Table 1) is given here. The radius of the rigid circular foundation is R_o = 2.50 and m = 2.50 cm. The magnitude of the central-symmetrical load is given here as

Figure 1. Vertical stress and settlement influence-value charts.

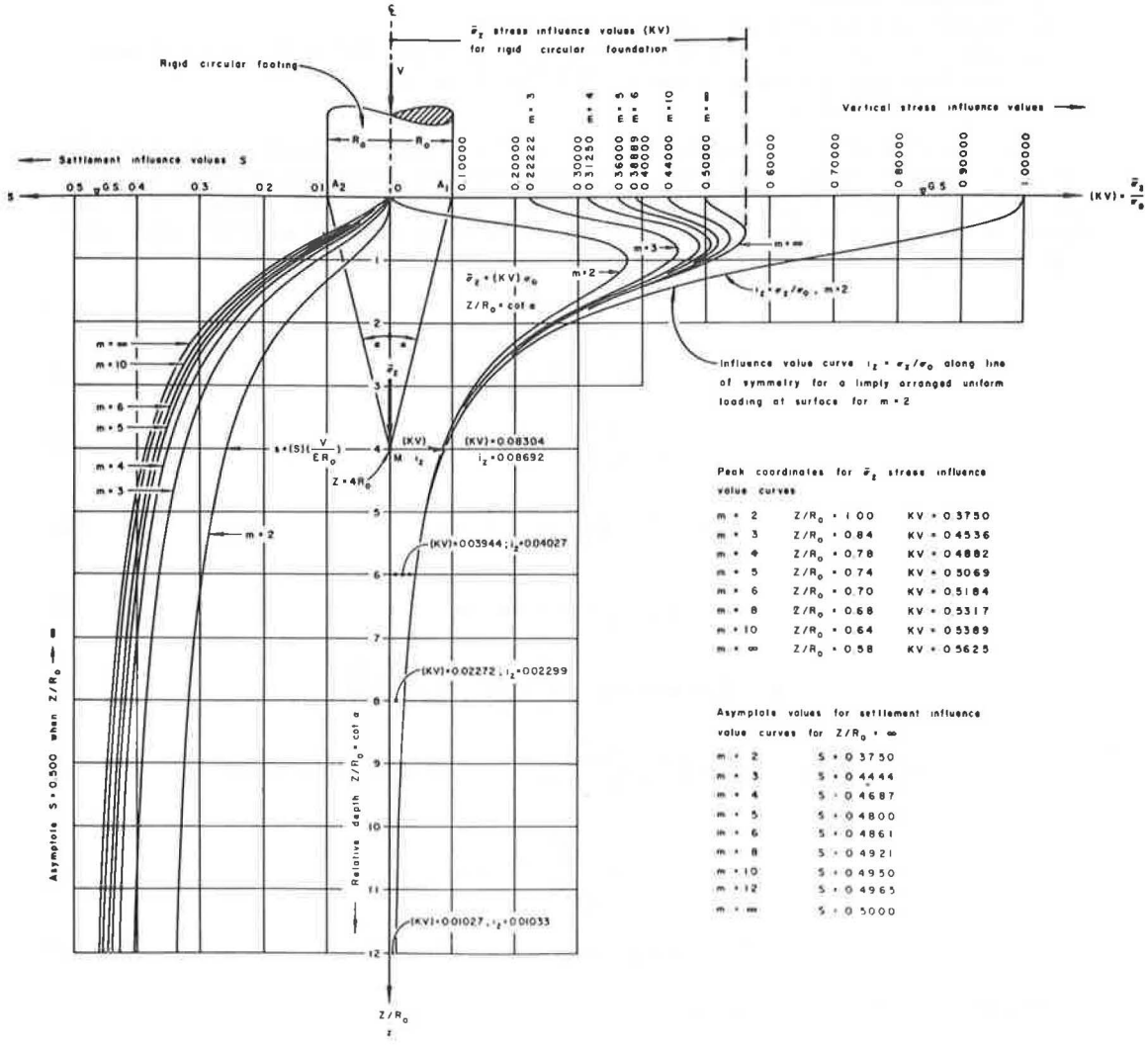

Peak coordinates for $\bar{\sigma}_z$ stress influence value curves

m = 2	Z/R_0 = 1.00	KV = 0.3750
m = 3	Z/R_0 = 0.84	KV = 0.4536
m = 4	Z/R_0 = 0.78	KV = 0.4882
m = 5	Z/R_0 = 0.74	KV = 0.5069
m = 6	Z/R_0 = 0.70	KV = 0.5184
m = 8	Z/R_0 = 0.68	KV = 0.5317
m = 10	Z/R_0 = 0.64	KV = 0.5389
m = ∞	Z/R_0 = 0.58	KV = 0.5625

Asymptote values for settlement influence value curves for $Z/R_0 = \infty$

m = 2	S = 0.3750
m = 3	S = 0.4444
m = 4	S = 0.4687
m = 5	S = 0.4800
m = 6	S = 0.4861
m = 8	S = 0.4921
m = 10	S = 0.4950
m = 12	S = 0.4965
m = ∞	S = 0.5000

$m = 1/\mu$ = Poisson's number;
μ = Poisson's ratio;
$\bar{\sigma}_z$ = spatial (triaxial) vertical stress (Eqs. 8-14);
α = arc cot (z/R_o) = one-half of the central angle at point M on the vertical centerline beneath the center of the circle (Fig. 1); and
z = depth coordinate.

The derivation of the settlement influence values S can be developed using the cylindrical coordinate system: Boussinesq's contact pressure distribution under a central symmetrically loaded rigid circular foundation with a smooth base, laying of the foundation on the ground surface, and use of the following system of equations (especially Eqs. 8 through 14):

$$\sigma_{zo} = \frac{V}{2\pi R_o (R_o^2 - x^2)^{1/2}} \tag{1}$$

$$V = \pi R_o^2 \times \sigma_o \tag{2}$$

$$\epsilon_z = \frac{1}{E}\left(\sigma_z - \frac{2}{m} \times \sigma_x\right) \tag{3}$$

$$\epsilon_z \times E = \bar{\sigma}_z = \sigma_z - \frac{2}{m} \times \sigma_x \tag{3a}$$

$$\sigma_z = \frac{1}{2} \times \sigma_o \times \sin^2 \alpha \tag{4}$$

$$\sigma_x = \frac{1}{4} \times \sigma_o \times \sin^2 \alpha \left(\frac{m+2}{m} - 2\cos^2 \alpha\right) \tag{5}$$

$$\bar{\sigma}_z = \frac{1}{2} \times \sigma_o \times \sin^2 \alpha \left(\frac{m+1}{m}\right)\left(\frac{m-2}{m} + 2\cos^2 \alpha\right) \quad \text{(Eqs. 8-14)} \tag{6}$$

$$s = \frac{1}{E}\int_0^z \bar{\sigma}_z \times d_z \tag{7}$$

$$z/R_o = \cot \alpha, \text{ or } \alpha = \text{arc cot } (z/R_o) \tag{8}$$

The settlement s calculated as

$$s = \left(\frac{1}{2\pi}\right)\left(\frac{m+1}{m}\right)\left[2\left(\frac{m-1}{m}\right)\left(\frac{\pi}{2} - \alpha\right) - \sin\alpha\cos\alpha\right]\left(\frac{V}{E \times R_o}\right) \tag{9}$$

Settlement Influence-Value Equation

The settlement equation (Eq. 9) can be rewritten in a dimensionless form as

$$\frac{s}{R_o} = \underbrace{\left(\frac{1}{2\pi}\right)\left(\frac{m+1}{m}\right)\left[2\left(\frac{m-1}{m}\right)\left(\frac{\pi}{2} - \alpha\right) - \sin\alpha \times \cos\alpha\right]}_{S}\left(\frac{V}{E \times R_o^2}\right) \tag{10}$$

or

$$\frac{s}{R_o} = (S)\left(\frac{V}{E \times R_o^2}\right) \tag{11}$$

where S is the elastic settlement influence value for a homogeneous, elastic hemispace of infinite depth (a monolayer).

1. Boussinesq's theory of elasticity is applicable.
2. Particularly, the foundation-supporting monolayer of soil is an elastic, homogeneous, isotropic, weightless, linearly deformable solid of semi-infinite extent. It obeys Hooke's law of proportionality between stress and strain. Hence, stresses are compatible with strains.
3. The modulus of elasticity E of the hemispatial material is constant throughout.
4. Originally, before loading, the soil is free of stress caused by force fields or thermal effects.
5. The circular footing laid on the ground surface is assumed to be a completely rigid, nondeformable body as compared with the rigidity of the soil—a situation that is frequently encountered in practice.
6. Cohesive and frictional forces between soil and foundation are disregarded in the development of this chart although slips or horizontal displacements can occur along the contact surface between the base of the footing and the soil. Only vertical displacements are reckoned with. In practice, these assumptions are used in the case of many uniform soils and many stress-strain problems in soil mechanics. Hence, they can also be used for elastic settlement calculations.

Relative to theoretical settlement calculations in multilayered soil systems, the following further assumptions are made:

1. The individual, horizontal soil layers are weightless and of infinite lateral extent.
2. Each individual soil layer in the multilayered system has its own elastic properties and is of perfect homogeneity and isotropy.
3. The stress distribution used is that predicted by Boussinesq's theory for a homogeneous half-space; the varying moduli of each layer are assumed not to influence the stress distribution.
4. Also, in this study, no consideration is given to the drainage (filtration) and rate problems as in a consolidating soil. Only total, elastic settlements are dealt with.
5. These charts do not apply to eccentrically loaded, rigid circular footings.
6. In these elastic settlement calculations of rigid circular foundations loaded only vertically and centrally and shallowly laid on the ground surface, only the vertical reactive soil resistance at the base of the foundation is considered. Hence, soil lateral resistance against the walls of the foundation does not enter into these calculations. Even if the footing were laid below the ground surface, a shallow embedment would mobilize a soil lateral resistance that would be relatively small as compared with the relative resistance vertically induced by a structural load. Also, if in the future there should arise a need for excavating a part of the embedded foundation and hence loosening the soil around it (for the purpose of repairs, utility installations, or laying of new foundations adjacent to a structure already in service, for example), then the soil lateral surcharge would be removed, and the stability of the soil-foundation system may become impaired.

SETTLEMENT EQUATION

The following notation is used in this paper:

σ_{z_o} = Boussinesq's general vertical contact pressure at the base of a rigid circular die;
V = externally applied single, vertical, concentrated load on a rigid circular foundation;
R_o = radius of circle;
x = a coordinate;
$\sigma_o = V/(\pi \times R_o^2)$ = average calculated vertical stress from applied load V;
ϵ_z = elastic, vertical relative deformation (stress) of an element at depth z under a triaxial (spatial) stress condition;
E = modulus of elasticity of soil;
σ_x, σ_z = orthogonal stress components;

SETTLEMENT INFLUENCE-VALUE CHART FOR RIGID CIRCULAR FOUNDATIONS

Alfreds R. Jumikis, Rutgers University, The State University of New Jersey

The paper presents a settlement influence-value chart for a homogeneous, elastic medium applicable to rigid circular foundations laid on the ground surface. The chart, which is based on Boussinesq's theory of elasticity pertaining to elastic deformation of an ideal, elastic, hemispatial medium from a rigid surface loading, is suitable for quick assessment of uniform, elastic settlement from a circular symmetrically and statically loaded, rigid circular foundation laid on the boundary surface of a homogeneous, hemispatial medium (monolayer). A numerical example of settlement calculation is used to demonstrate the routine of the easy-to-use chart prepared for Poisson's numbers. It may also be used for evaluation of approximative settlement of a multilayered soil system under a rigid circular foundation. Derivations of the settlement equation, settlement value equation, and settlement value charts are explained. The method of successive "displacement-difference steps" and the method of "equivalent layers," which may be used for calculating the approximate total elastic settlement of a multilayered soil system, are detailed.

•FOR uniform, circular elastic loading there are stress and strain tables available for one-, two-, and three-layered elastic hemispace systems. They are prepared based on the theory of elasticity and are used primarily in highway pavement design. Stress and strain tables have been developed by Burmister (1), Acum and Fox (2), and Jones (3). Vertical, spatial stress distribution tables for uniformly loaded, flexible circular plates on the surface of a homogeneous hemispace, for Poisson's number m = 2 and for any point in the elastic medium inside and outside the circular contour, have been published by Jumikis (4, 5).

Based on Jones's stress tables, Peattie (6) presented stress-strain factors graphically. The Jones tables give stresses at interface points on a vertical centerline under a uniformly distributed load over a circular area for a three-layered soil system for Poisson's number m = 2 and with full friction in layer interfaces for various ratios of the modulus of elasticity, the stress-strain relation being linear.

The flexible solutions are not applicable to settlement calculations of foundations whose footings are rigid relative to the foundation-supporting soil. In such cases the displacement, namely, uniform settlement of a rigid foundation, must be computed on the basis of a specified, uniform vertical displacement over the loaded area.

ASSUMPTIONS

In deriving formulas and charts for calculating theoretical elastic settlement of a single layer of soil of semi-infinite extent under a rigid circular, shallow foundation or die loaded central symmetrically with a single, vertical, concentrated point load V only, the following assumptions are made:

Publication of this paper sponsored by Committee on Mechanics of Earth Masses and Layered Systems.

6. Although the selection of elastic constants, especially of Poisson's ratio, is difficult, finite-element methods can be used to estimate the rough magnitudes of horizontal displacements;
7. Inclinometer data, especially the rates of horizontal displacements, were successfully used to monitor the safety against slope failures;
8. The inevitable uncertainties in predicting settlement rates and rates of strength increase may be compensated for by including a bid item for delay time in the contract documents, to be invoked if field data indicate rates slower than the fastest anticipated; and
9. With this approach, field instrumentation and interpretation become very important parts of the design.

The results and procedures described here are applicable in general to any major project involving sand drains and surcharge, particularly if a strength increase of the clay is required for stability of fill slopes and thus a programmed surcharge is called for. Specifically, the soil data are representative of many clays in coastal and estuarine areas of the U. S. eastern seaboard.

ACKNOWLEDGMENTS

The authors thank D. N. Tanner, R. B. Stevenson, W. C. Grantz, V. Tanal, and K. Chung for their assistance. Also acknowledged are J. N. Clary, C. R. Moxley, R. B. Peck, and D. B. Gedney.

REFERENCES

1. Steuerman, S., and Murphy, G. J. Foundation of the Hampton Roads Tunnel. Proc., 4th Internat. Conf. on Soil Mech. and Found. Eng., Vol. 3, 1957, pp. 437-443.
2. Bickel, J. O. The Design and Construction of the Hampton Roads Tunnel. Jour. Boston Society of Civil Engineers, Vol. 45, 1958, pp. 369-390.
3. Rafaeli, D. Design of the South Island for the Second Hampton Roads Crossing. Spec. Conf. on Performance of Earth and Earth-Supported Structures, Proc. ASCE, Purdue Univ., Vol. 1, Part 1, 1972, pp. 361-378.
4. Bjerrum, L. Geotechnical Properties of Norwegian Marine Clays. Geotechnique, Vol. 6, 1954, pp. 49-69.
5. Gray, H. Simultaneous Consolidation of Contiguous Layers of Unlike Compressible Soils. Trans. ASCE, Vol. 110, 1945, pp. 1327-1356.
6. Richart, F. E. A Review of the Theories for Sand Drains. Trans. ASCE, Vol. 124, 1959, pp. 709-739.

Figure 6. Cross section A-A showing horizontal displacements.

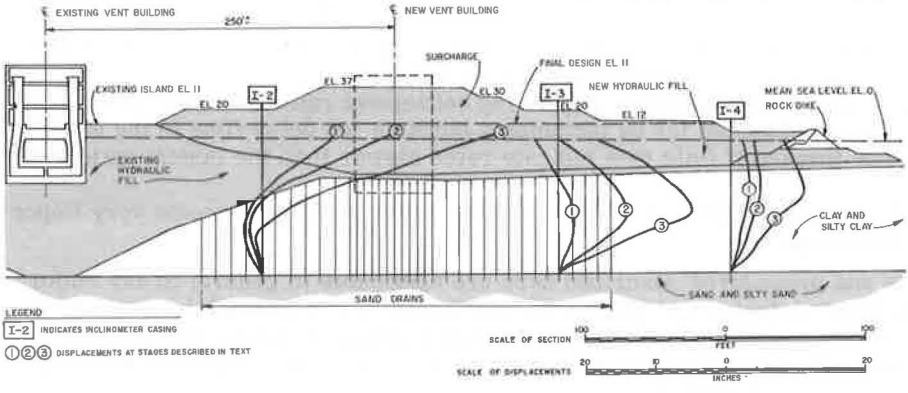

Figure 7. Time settlement curves at station 936+70.

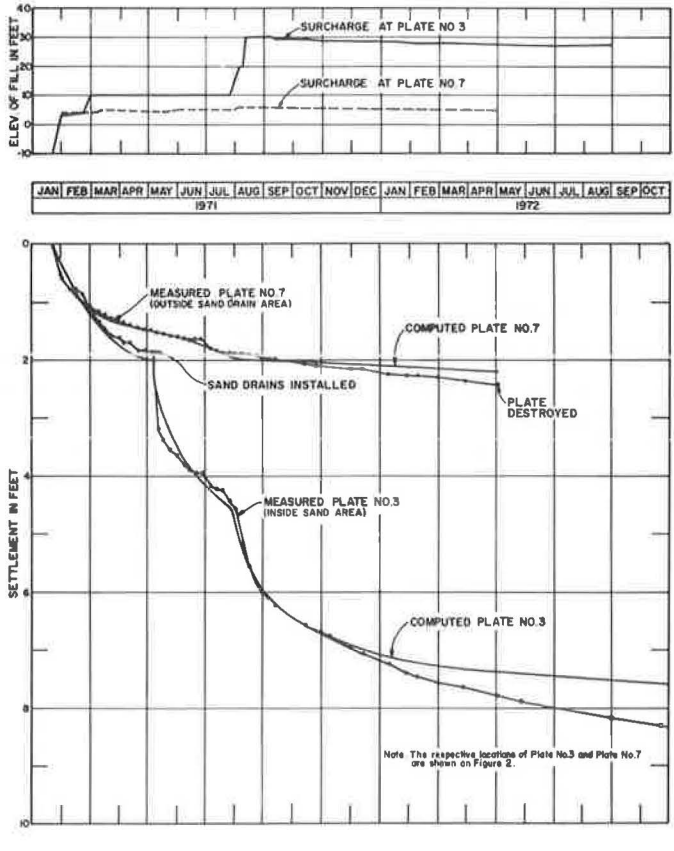

consolidation (5), and the program includes the effect of sand drains according to the theory presented by Richart (6). The program accommodates loading in stages by calculating the average pore pressures in the two layers at the end of each stage and adding the vertical stresses due to the new load to these pore pressures. The computer then calculates the dissipation of the new pore pressures, degree of consolidation, settlement, and compression of the individual layers with time.

The settlement data were analyzed to determine the field values of the consolidation coefficients c_v and c_h. A large number of computer analyses were run with different parameters to achieve the best fit with the observed surface and subsurface settlements. Values of c_v were determined by fitting settlement data unaffected by sand drains. With these c_v values, c_h was determined from settlement data in the sand drain area. The best fit between computed and measured settlement curves was, in general, achieved with values of c_h equal to c_v.

In general, it was not possible to fit computed and measured curves unless a reduction of c_v and c_h with time was assumed. Typically, at effective stresses between 1,000 and 2,000 lb/ft^2 (50 and 100 kN/m^2) above the initial stresses, the coefficients were reduced by 50 to 75 percent. This is in reasonable agreement with typical consolidation test data such as those shown in Figure 4.

One year after the beginning of the filling operation, the settlement rate in the sand drain area was about 2 in. (5 cm) per month. At this time, primary consolidation in this area was almost 100 percent complete in the upper clay and about 92 percent complete in the lower clay. Outside the sand drain area, the corresponding values were 96 percent and 34 percent for the upper and lower clays respectively. On the basis of consolidation tests (Table 1), the rate of secondary settlement at this time would be between 0.5 and 1 in. (1.3 to 2.5 cm) per month.

The calculated field values of c_v and c_h vary significantly along the island. The initial values for the upper clay vary from more than 300×10^{-4} cm^2/sec to about 50×10^{-4} cm^2/sec, whereas those for the lower clay vary between about 50×10^{-4} cm^2/sec and 10×10^{-4} cm^2/sec. The lowest field values are in the high range of those determined in the laboratory, whereas the highest field values correspond to those based on field permeability tests. With progressing consolidation, c_v and c_h decreased to within the medium-to-high range of the laboratory values at the appropriate stress levels.

Figure 7 shows typical settlement data from plates inside and outside the sand drain area. The computed curves shown for both plates are based on the back-figured initial values $c_v = c_h = 100 \times 10^{-4}$ cm^2/sec for the upper clay and 20×10^{-4} cm^2/sec for the lower clay, decreasing to 30×10^{-4} cm^2/sec and 6×10^{-4} cm^2/sec at approximately 60 percent consolidation under the full load. In both locations, the measured and computed curves parted after about 300 days because the computations did not include settlements due to secondary consolidation.

CONCLUSION

This case history demonstrates that a surcharge and sand drain scheme can be designed reliably on the basis of laboratory data supplemented by field tests. The important specific findings of this study are summarized as follows:

1. The values of the $c/\bar{p}$ ratio determined in the laboratory were verified in the field but were substantially greater than would be expected from correlation with plasticity data;
2. The compression index C_c varied appreciably both in the laboratory and in the field, but it fell within the same ranges;
3. The field data showed the horizontal consolidation coefficient c_h to be essentially equal to the vertical coefficient c_v for this installation of jetted sand drains;
4. The laboratory values of c_v and c_h were several times smaller than those indicated by initial settlement data (the values derived from field permeability tests, though on the high side, were in better agreement);
5. A substantial decrease of c_v and c_h was noted as a result of the compression of the clay with time;

essentially undrained and are governed by a relatively high modulus of deformation and a low volume change, i.e., a Poisson's ratio close to 0.5. Displacements caused by consolidation, on the other hand, are mostly vertical and are associated with considerable volume change. The appropriate Poisson's ratio for these movements would be small, and the modulus would be that determined from consolidation tests.

As a conservative compromise, the movements were analyzed using moduli determined from consolidation tests and a Poisson's ratio of 0.45. In the analyses, the fill load was applied at the clay surface without regard to the rigidity of the fill.

For a typical cross section analyzed in this manner, the maximum predicted settlement would be 7 ft (2.1 m), the maximum predicted horizontal displacement in the clay about 13 in. (0.33 m), and the movement of the existing tunnel about ½ in. (1.3 cm) with a slight tilt. Tensile stresses and movements toward the new fill were predicted in a wide band between the old and the new islands.

The existing tunnel did, in fact, settle a maximum of ½ in., but no measurable tilt or horizontal displacement took place. A few tension cracks, about ⅛ in. wide and 20 to 30 ft long, were observed on the surface of the existing island above the edge of the tunnel (Fig. 5).

Selected inclinometer data are shown in Figure 6. Curve 1 indicates displacements that occurred during the last 2 months' fill (at elevation of +12) but does not include the displacements during filling to elevation +12 and the following 3 months. Filling from +12 to +37 took place in a 2-week period, and curve 2 shows the inclinometer displacements immediately after this filling operation. Curve 3 shows the displacements 6 months later.

Curve 3 for inclinometer I-2 indicates a displacement at elevation zero of 30 in. (76 cm) toward the centerline of the fill or about 6 times the displacement predicted by the computer analysis at that location. This discrepancy was anticipated and is caused by the fact that the computer analyses assumed the same elastic soil properties in tension and in compression.

For inclinometers I-3 and I-4, maximum predicted horizontal displacements were 13 in. (0.33 m) and 9 in. (0.23 m) respectively. The maximum measured displacements were 19.3 in. (0.49 m) and 10.2 in. (0.26 m) respectively. As mentioned previously, these do not include the initial displacement.

At inclinometer I-3, the horizontal displacements that took place in the 6-month consolidation period after placement of the surcharge were approximately equal to the displacements during the 2-week filling period. For comparison, the settlements during the consolidation period were more than three times greater than the settlements during filling.

Inclinometer I-4 was located 130 ft (40 m) away from the surcharge fill. Here, only small horizontal displacements took place during filling, but the consolidation displacements were only slightly smaller than at I-3.

The measured displacements are somewhat larger than those predicted by the finite-element analysis. The analysis considered only displacements of an elastic nature, and it may be presumed that some elastic deformations took place. However, the rate of displacements decreased with time, indicating the relative stability of the slope and its foundation and that delay time was not invoked.

The computer solution used for these problems was rather crude. Better predictions could have been obtained by assigning a low, or zero, tensile modulus to the soil material and by using a compressive modulus decreasing with the shear stress and increasing with the normal stress. Nonetheless, the experience gained from this project indicates the utility of even a simple-minded computer solution.

SETTLEMENT RATES

A computer program was used to estimate and back-calculate settlements and degree of consolidation in the two clay layers as a function of time. This program uses Boussinesq stress distribution to calculate stresses and simple consolidation theory to calculate total settlements, without accounting for secondary settlements. The degree of consolidation is calculated by using an approximate two-layer solution for vertical

Figure 3. Coefficients of vertical (c_v) and horizontal (c_h) consolidation.

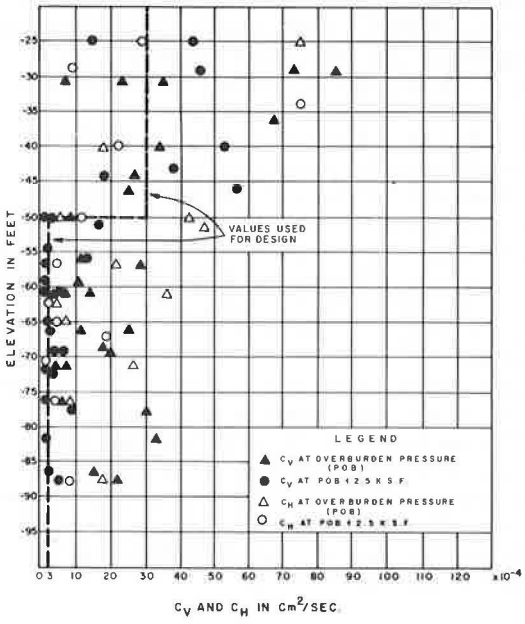

Figure 4. Typical consolidation test data, lower clay.

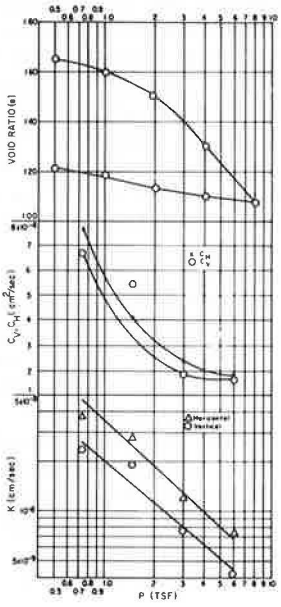

Figure 5. Settlement contours as of October 23, 1972.

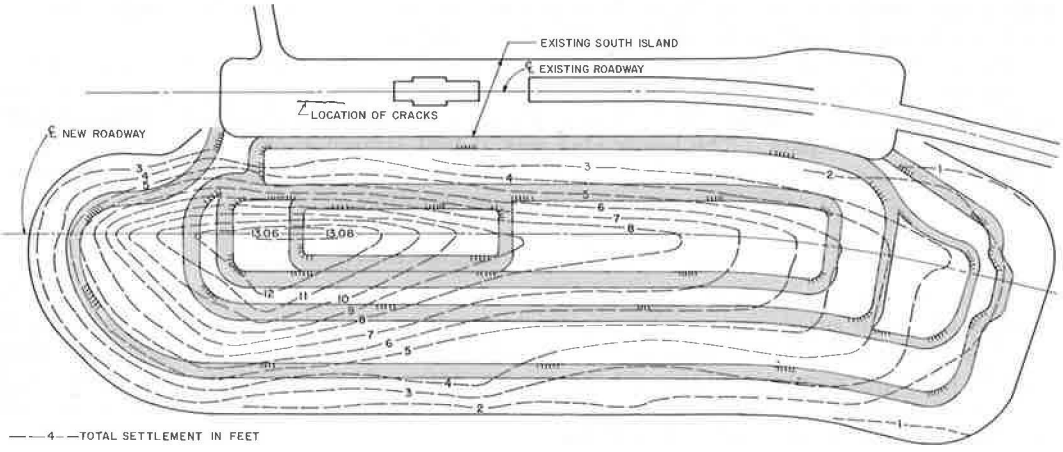

alternative. The new tunnel approach should be close enough to the old one to take advantage of the existing island yet far enough away to avoid exposing or endangering the existing structures and generating undue displacements in them. The requirement of minimal residual settlements after construction, stability of fill slopes during construction, and stability of the excavation for the approach and ventilation building in the middle of the new finished island indicated surcharging at a controlled rate, the consolidation being accelerated by sand drains.

Settlement plates were installed after a few feet of hydraulic sand fill were placed, and sand drains were installed by the jetting method in the central areas with three different spacings after the fill reached elevation +12. Piezometers and deep settlement points were installed at the same time. At this time four additional borings were made to verify the strength increase of the clay under the initial loading. Inclinometers were installed to warn against excessive horizontal displacements at any stage of filling. Such excessive horizontal displacements would indicate plastic shear and possible impending slope failure. Figures 1 and 2 show the final configuration of the island with its surcharge and the location of the instruments.

Computerized stability analyses of the Bishop type indicated that slopes to an elevation of +20 (+6 m) would be only marginally stable with the in situ clay strength. At this time, all field data were carefully analyzed to determine if delay time should be invoked. On the basis of the favorable strength increase measured in the additional boreholes, the rate of settlements observed, and the nominal displacements measured by the inclinometers, it was concluded that adequate safety against slope failure had been achieved, and construction was permitted to proceed without invoking the delay time. The surcharge was placed to its full height without incident.

SHEAR STRENGTH INCREASE

The original design had been based on conservative ratios of $c/\overline{p} = 0.15$ for the upper clay and 0.25 for the lower clay, ratios smaller than those obtained by tests but in line with past experience (4). If the field values of $c/\overline{p}$ were indeed that low, delay time would have been required to achieve adequate strength.

The additional borings, however, verified the laboratory tests. In the upper clay, which was nearly consolidated under the load to elevation +12, the $c/\overline{p}$ ratio was between 0.30 and 0.35 as determined by field vane shear tests and unconfined compression tests on undisturbed samples. The lower clay was at that time not consolidated, and the strength increase in the lower clay was nominal. The strength of the upper clay, however, was the most critical parameter for slope stability.

VERTICAL DISPLACEMENTS

The total vertical settlements occurring about 21 months after filling began, and 15 months after the surcharge reached its final elevation, are shown as contours in Figure 5. The settlements at this time were nearly complete in the sand drain area and more than 70 percent complete outside the sand drain area. The maximum settlement of 13 ft (4.0 m) occurred under the highest fill near the north end of the island, where the clays are thickest and more plastic than average.

Field values of the compression index C_c, back-calculated from surface and deep settlement data varied from 0.30 to 0.50 for the upper clay and from 0.65 to 1.10 for the lower clay, increasing from south to north. Thus, the entire range of C_c values from laboratory tests was in fact experienced at various points along the island.

HORIZONTAL DISPLACEMENTS

It was important to estimate the possible movements of the existing tunnel and ventilation structures caused by the weight of the new island and its surcharge. An elastic finite-element computer program was employed for this purpose.

The movements that take place under and around a fill such as this island fill are of two kinds. Movements caused by shear stresses occur relatively quickly after the placement of the fill load and include horizontal displacements. These movements are

Figure 1. Longitudinal profile of South Island.

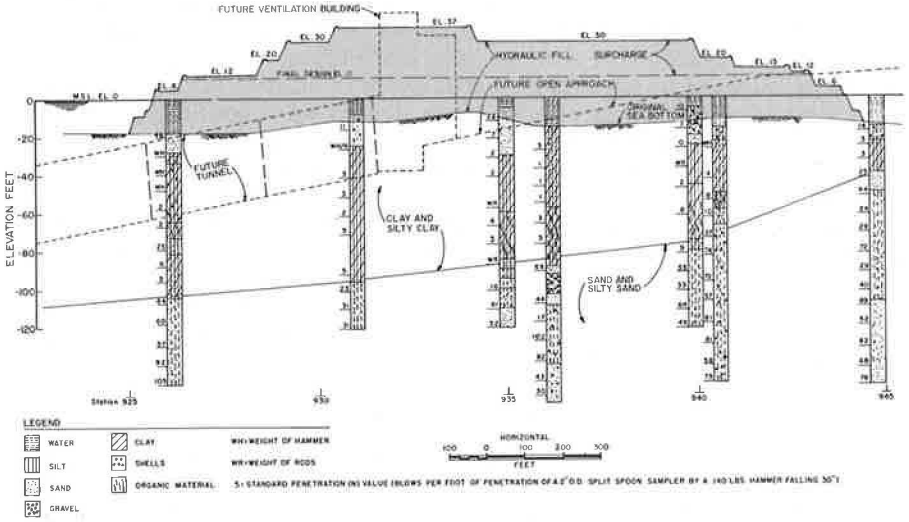

Figure 2. General plan of South Island.

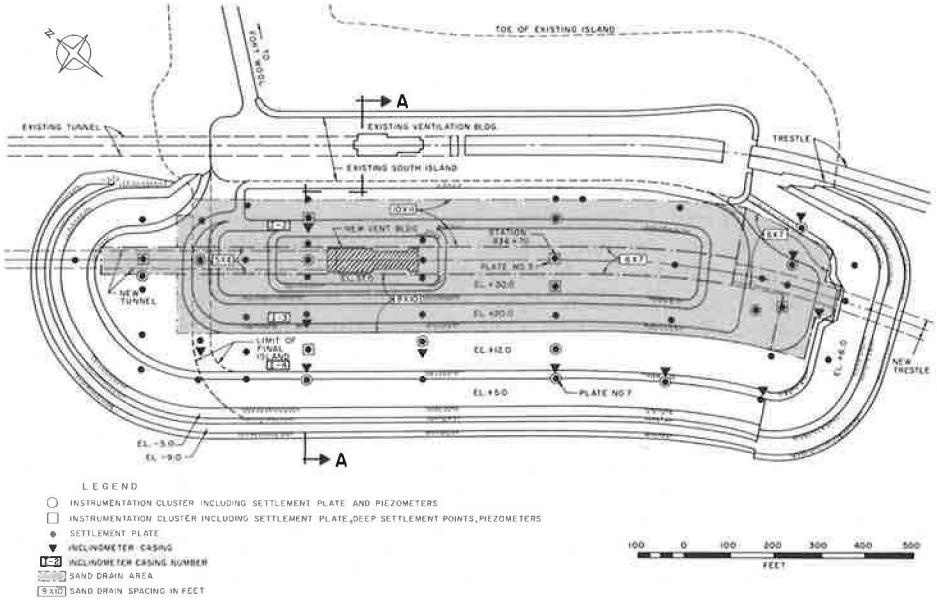

Table 1. Soil properties from laboratory tests.

Test	Upper Clay Layer	Lower Clay Layer
Liquid limit, percent	32 ± 8	75 ± 30
Plasticity index, percent	15 ± 10	45 ± 25
Moisture content, percent	35 ± 4	65 ± 15
Void ratio, e_o	1.1 ± 0.3	1.8 ± 0.2
Compression index, C_c	0.45 ± 0.10	0.85 ± 0.20
Coefficient of secondary consolidation, C_α	0.005 ± 0.002	0.011 ± 0.005
Shear strength, lb/ft^2	450 ± 200	950 ± 300

In its natural state, the soft clay did not have sufficient shear strength to support the full weight of the surcharge. Although the soil would gain strength under the fill load, the time required for adequate strength gain depended on the rate of consolidation, which was only imperfectly predictable through laboratory tests. Furthermore, very large strains would be imposed by anticipated settlements of 10 ft (3 m) or more under the full surcharge load, and the effects of such large strains were not fully predictable.

These concerns were met without excessive cost by basing the design on reasonable assumptions of soil parameters, but the construction contract included an extensive instrumentation program to monitor field performance, with control over the rate of fill placement to be exercised if dangerous conditions were indicated by the field measurements. This was accomplished by providing a separate bid item for delay time, which could be invoked by the engineer after fill had been placed to a specified height, thus compensating the contractor for the cost of idle equipment and crews. The bid price received for delay time was $4,000 per day, so that a potential delay of 60 days implied a financial risk of $240,000.

SOIL CONDITIONS

Figure 1 shows the soil profile in the longitudinal direction of the island and also the island elevations when the surcharge was at its highest. Figure 2 shows a plan of the island. Through most of the length of the island, the clay extends from sea bottom at elevation -12 to -18 down to elevation -80 to -95, a thickness of 65 to 80 ft (20 to 24 m). In the vertical direction, two strata of clay can be distinguished, with increasing plasticity with depth. A summary of the properties of the two clay layers, separated approximately at elevation -50, as determined by laboratory tests, is given in Table 1.

Although the distinction between the two layers is clear from the test data, there is a considerable random variation, horizontally as well as vertically, of the soil parameters within each layer. There is a trend, however, to greater plasticity and compressibility with increasing clay thickness toward the north.

For the economical design of a sand drain installation, prediction of the time-dependent behavior of the soil is important. For this reason a large number of consolidation tests were run to determine the coefficient of consolidation, on samples cut in both the horizontal and vertical directions. The test results are shown in Figure 3. Not unexpectedly, the scatter of the data is wide, but the coefficients are clearly much greater for the upper layer than for the lower layer. The ratio between the horizontal and vertical coefficients of consolidation, c_h/c_v, varies but is generally equal to or slightly greater than unity. The results of a typical consolidation test from the lower clay layer are shown in Figure 4. Except for the top parts of the two clay strata, the consolidation tests indicated that the clays were normally consolidated.

Five constant-head permeability tests performed in observation wells, and field pumping tests with observation wells, gave permeabilities between 2×10^{-6} and 3×10^{-6} cm/sec for the upper clay and between 1.8×10^{-7} and 3.3×10^{-7} cm/sec for the lower clay. Such tests tend to reflect the greater of the horizontal and vertical permeabilities. The consolidation coefficients, c_v or c_h, computed from the field permeability data, using average a_v values from consolidation tests, would be 300×10^{-4} cm^2/sec for the upper clay and 40×10^{-4} cm^2/sec for the lower clay, substantially greater than the values determined in the laboratory.

Using the statistical relation between plasticity index and $c/\bar{p}$ ratio reported by Bjerrum (4), one would have expected $c/\bar{p}$ ratios of about 0.15 to 0.20 for the upper clay and 0.25 to 0.30 for the lower clay. Consolidated-undrained and unconsolidated-undrained field vane tests and laboratory triaxial tests, however, indicated a $c/\bar{p}$ ratio of 0.30 to 0.35 for both layers.

DESIGN, CONSTRUCTION, AND INSTRUMENTATION

For the South Island of the first crossing, the clay was removed and replaced with hydraulic fill. Environmental restrictions on disposal of dredged materials and the proximity of the first island precluded a similar design for the second island, and a controlled accelerated surcharge compression design was selected as the most economical

SETTLEMENTS AND STRENGTHENING OF SOFT CLAY ACCELERATED BY SAND DRAINS

Thomas R. Kuesel, Birger Schmidt, and David Rafaeli,
Parsons, Brinckerhoff, Quade and Douglas

The 24-acre south portal island for the second Hampton Roads Crossing in Virginia was surcharged and the compression and strengthening of underlying soft clay were accelerated by jetted sand drains to meet the requirements of an economical construction scheme, to minimize post-construction settlements, and to maintain stability during construction. The island was extensively instrumented, and the paper presents analyses and conclusions from selected data. Both laboratory and field data indicate a much higher ratio of undrained shear strength to overburden pressure than would be expected from well-known correlations between this ratio and plasticity indexes. Laboratory values of the horizontal and vertical consolidation coefficients were lower than indicated by measured settlement rates; values derived from field permeability tests proved more reliable. Horizontal displacements in the soft clay, estimated by finite-element analyses and measured by inclinometers, proved to be useful indicators of the overall safety of the slopes. The effect of unknown factors and variable soil parameters was minimized by construction documents written with a specific bid item for "delay time," a device that proved financially beneficial. The solutions to the problems of this site can be used for similar sand drain projects where there is substantial uncertainty and variation of the soil parameters. The soil parameters reported are, of course, applicable only to similar extensive nonstratified clay deposits.

•CONSTRUCTION of the second Hampton Roads Bridge-Tunnel Crossing, connecting Norfolk with Hampton in Virginia, began in 1970 and is expected to be finished in 1975. It will consist of a 6,900-ft (2,100-m) long two-lane sunken-tube tunnel between two man-made islands and two trestles connecting the islands with the mainland. The first Hampton Roads Crossing, which was opened in 1957 (1, 2), parallels the new crossing at a distance of 250 ft (76 m).

Of the two man-made islands, the North Island is founded on sands and silty sands and presents no substantial settlement or stability problems. At the South Island, however, about 80 ft of normally consolidated clay overlies sandy soils, and sand drains and programmed surcharge were required to construct a stable island with a minimum of residual settlements. The design of the South Island was described by Rafaeli (3), and the present paper will discuss the results of an extensive instrumentation program, the behavior of the clay, and the performance of the sand drains.

The new South Island is approximately 1,950 ft long and 570 ft wide (600 x 175 m) and covers an area of 24 acres (0.1 km^2). The average water depth was 15 ft (5 m), and the final island elevation is +11 ft (3.4 m). The surcharge was built up to a maximum elevation of 37 ft (11.3 m), and a total volume of 1,130,000 yd^3 (860,000 m^3) of sand fill and surcharge was placed.

Publication of this paper sponsored by Committee on Embankments and Earth Slopes.

of the new programs is an inability of old ones to accommodate the desired level of physical complexity.

ACKNOWLEDGMENTS

The authors wish to recognize the financial support made available through the Joint Highway Research Project, Purdue University, and the technical advice of the Materials and Test Division, Indiana State Highway Commission.

REFERENCES

1. Bell, J. M. General Slope Stability Analysis. Jour. Soil Mech. and Found. Div., Proc. ASCE, Vol. 94, No. SM6, 1968.
2. Bell, J. M. Noncircular Sliding Surfaces. Jour. Soil Mech. and Found Div., Proc. ASCE, Vol. 95, No. SM3, 1969.
3. Bishop, A. W. The Use of the Slip Circle in the Stability Analysis of Slopes. Geotechnique, Vol. 5, 1955.
4. Carter, R. K., Lovell, C. W., Jr., and Harr, M. E. Computer Oriented Stability Analysis of Reservoir Slopes. Water Resources Research Center, Purdue Univ., Tech. Rept. 17, 1971.
5. Soil Mechanics, Foundations and Earth Structures. Bureau of Yards and Docks, Dept. of the Navy, NAVDOCKS DM-7, 1971.
6. Steel Sheet Piling. United States Steel, ADUSS 25-3848-03, 1972.
7. Fellenius, W. Erdstatische Berichnungen mit Reibung and Kohasion (Adhasion). Ernst, Berlin, Germany, 1927.
8. Hamel, J. F., and Flint, M. K. Failure of Colluvial Slope. Jour. Soil Mech. and Found. Div., Proc. ASCE, Vol. 98, 1972.
9. Landslides and Engineering Practice. HRB Spec. Rept. 29, 1958.
10. Little, A. L., and Price, V. E. The Use of an Electronic Computer for Slope Stability Analysis. Geotechnique, Vol. 15, 1958.
11. Mendez, C. Computerized Slope Stability; The Sliding Block Problem. Water Resources Research Center, Purdue Univ., Tech. Rept. 21, 1972.
12. Mohan, A. Computerized Slope Stability; Slip Surface Defined by a Polynomial of Any Degree. Purdue Univ., Internal Rept. 11, 1971.
13. Mohan, A. Computerized Slope Stability Analysis; A Sliding Block Model. Joint Highway Research Project Rept., Purdue Univ., Oct. 1972.
14. Morgenstern, N. R., and Price, W. E. The Analysis of the Stability of General Slip Surface. Geotechnique, Vol. 15, 1965.
15. Taylor, D. W. Stability of Earth Slopes. In Contributions to Soil Mechanics 1925-1940, Boston Society of Civil Engineers, 1940.
16. Terzaghi, K. Mechanism of Landslides. In From Theory to Practice in Soil Mechanics, John Wiley and Sons, New York, 1960, pp. 202-245.
17. Terzaghi, K. Theoretical Soil Mechanics. John Wiley and Sons, New York, 1965.

Figure 7. Illustration problem 1.

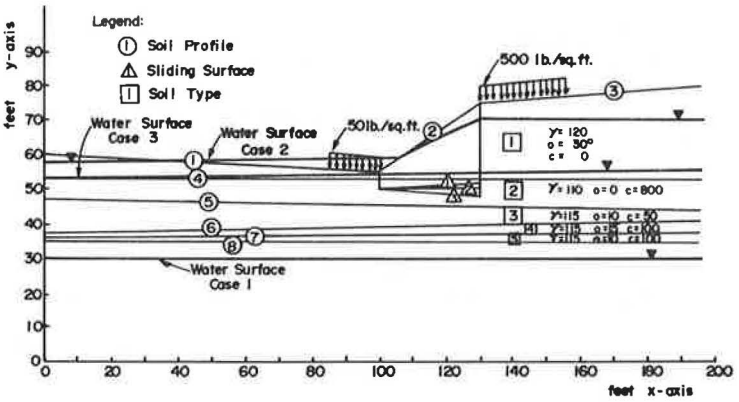

Figure 8. Illustration problem 2.

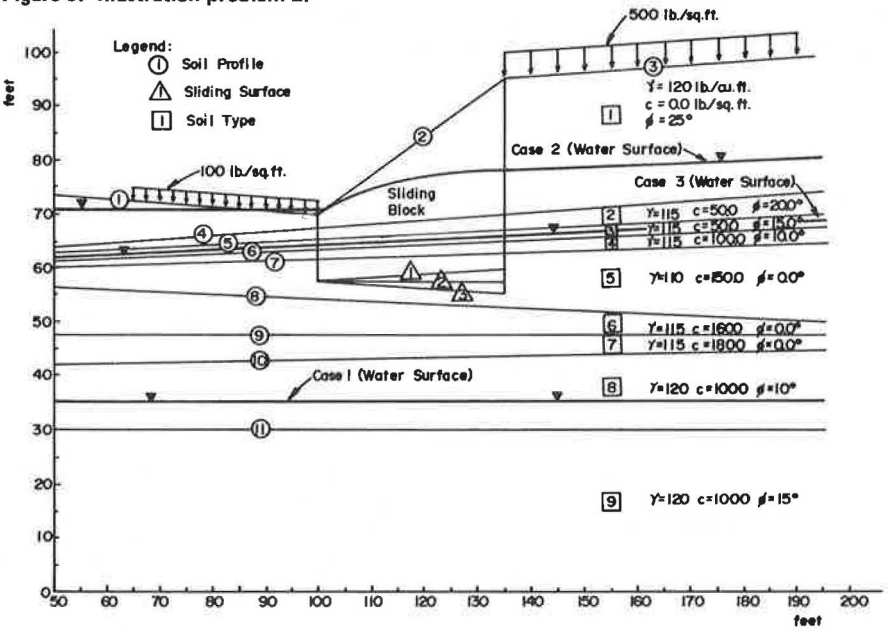

Table 1. Summary of results for illustration problems.

Case Analyzed	Number and Slope of Sliding Surface	Factor of Safety	
		Problem 1	Problem 2
1	1, θ^+	1.94	2.07
	2, $\theta = 0$	1.87	2.24
	3, θ^-	1.83	2.42
2	1, θ^+	1.66	1.83
	2, $\theta = 0$	1.65	1.98
	3, θ^-	1.64	2.12
3	1, θ^+	1.84	1.84
	2, $\theta = 0$	1.52	1.81
	3, θ^-	1.66	1.75

2. Top ground surface is made up of three slopes and well-defined toe and crest points;
3. Soil properties are defined by γ, c, and ϕ (c or ϕ can equal zero);
4. Multiple (up to 10) uniform strip loads are on ground surface of the upper or lower slopes or both;
5. Water surface is anywhere in the problem space (the water surface is defined by continuous straight lines or a nonlinear surface defined by seven or fewer known coordinates or both); and
6. Multiple trial sliding surfaces are at the bottom of the central block and can be at any inclination (as many as 10 can be analyzed in a single run).

Specific trial surfaces are input for analysis. No searching technique (for identification of a minimum FS) is recommended although some ideas on this are contained elsewhere (4).

The active and passive force subroutines are potentially valuable in the solution of lateral earth pressure problems.

ILLUSTRATION PROBLEMS

The purpose of the illustration problems is threefold: to demonstrate the use of the computer program, to show the versatility and several options of the program, and to serve as a check for duplicated decks. Two separate hypothetical problems are chosen for this purpose.

Problem 1

The first illustration problem involves a simple soil profile shown in Figure 7. Solutions are obtained for three central block sliding surfaces and for three locations of the water surface for each sliding surface (Table 1).

Problem 2

The second problem is more complex and is shown in Figure 8. This problem is also solved for three slopes of sliding surfaces in combination with three locations of the water surface for each sliding surface (Table 1).

CONCLUSIONS AND RECOMMENDATIONS

The primary objective of this research was the development of a computer-assisted system for rapid prediction of the factor of safety of slopes where the mode of failure is a sliding block. The resulting program is sufficiently versatile to accommodate a three-slope ground surface and a subsurface profile with spatial variations in material properties, a steady-state flow domain, and uniform strip ground surface loadings. Up to 10 trial sliding surfaces can be analyzed concurrently, with the base of the central wedge at any inclination in any selected soil layer. The program automatically sequences the trial sliding surfaces, computing a factor of safety for each. Because many sliding surfaces may have to be examined (i.e., there is no systematic search technique that ensures identification of a minimum), this is a most important feature.

It was desired to develop a system that would be used on smaller computers. Consequently, the program uses a small storage and short computation time.

Hopefully, the program will enable a designer to check against this mode of instability for any slope where there is reason to suspect that it may occur. Such suspicion would ordinarily result from study of boring logs and profiles. Sliding blocks can be based in any soil stratum of below-average strength. Where there is no evidence of weak layers, it is likely that some common form of the circular or rotational slump analysis will be employed. In questionable cases, both types of analysis may be undertaken and factors of safety compared.

Any computer program should be tested for reliability by generation of solutions to common problems through different programs or manual calculations. Unfortunately, this is usually possible for only simple examples because the motivation for development

Figure 4. Analysis of forces on passive wedge (case 2).

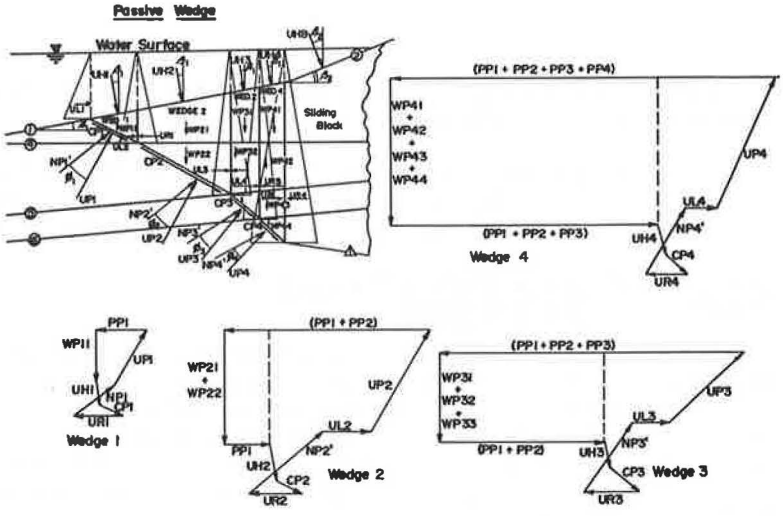

Figure 5. Forces on sliding block (case 2).

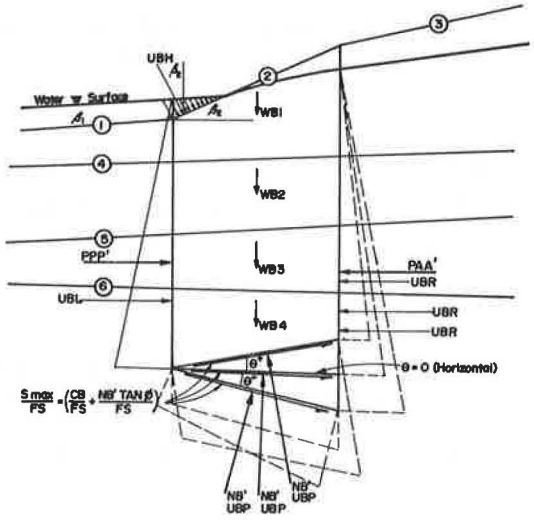

Figure 6. Flow chart of block program.

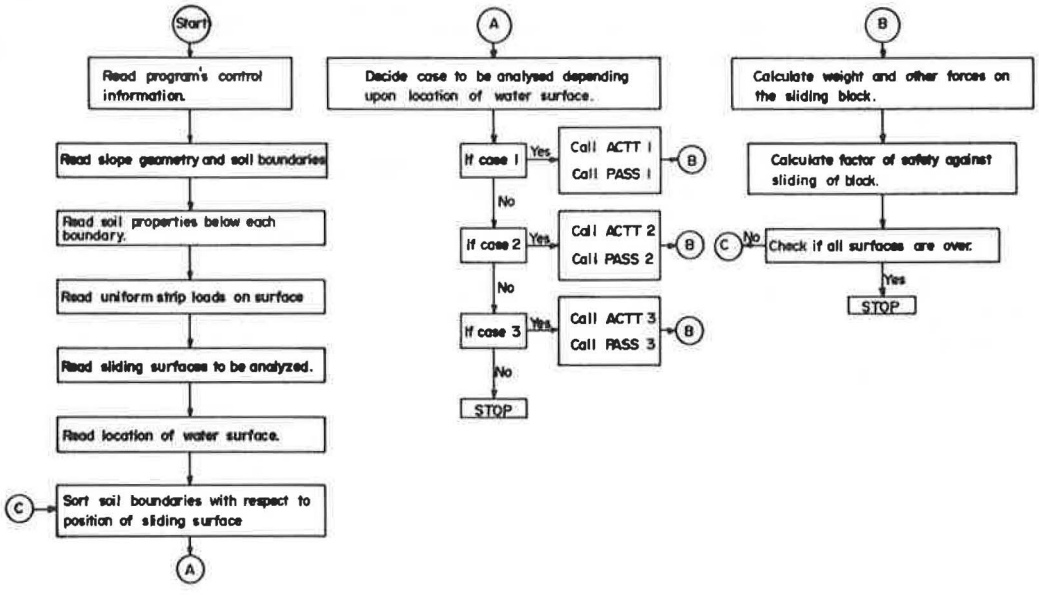

Elimination of NP'n from Eqs. 4 and 5 yields an expression for the incremental passive force for the nth wedge.

$$PPn = WPn \tan(45 + \phi n/2) + 2\,CPn \cos(45 - \phi n/2) + U\beta_n [\sin\beta_1 + \cos\beta_1 \tan(45 + \phi n/2)] + (ULn - URn) + UPn [\cos(45 + \phi n/2) - \sin(45 + \phi n/2) \tan(45 + \phi n/2)] \quad (6)$$

Analysis of Forces on Central Block and Calculation of Factor of Safety

Figure 5 shows the appropriate free body (Fig. 2). The factor is commonly called the factor of safety (FS), although it is better interpreted as a strength reduction factor; i.e., if the real strength were divided by this factor, a reduced strength would obtain at which failure would impend. Note that the base sliding surface can be inclined up (θ^+) or down (θ^-) with respect to the horizontal, or may be horizontal ($\theta = 0$).

For θ^- and where forces are summed normal (N) and tangential (θ) to the sliding surface, for $\Sigma F_N = 0$

$$NB' + UBP = PAA \sin\theta - PPP \sin\theta + WB \cos\theta + UBH \cos\beta_2 \cos\theta - UBL \sin\theta + UBR \sin\theta - UBH \sin\beta_2 \sin\theta \quad (7)$$

and $\Sigma F_\theta = 0$

$$\frac{CB}{FS} + \frac{NB' \tan\phi}{FS} = PAA \cos\theta - PPP \cos\theta - WB \sin\theta - UBH \cos\beta_2 \sin\theta - UBH \sin\beta_2 \cos\theta - UBL \cos\theta + UBR \cos\theta \quad (8)$$

Elimination of NB' from Eqs. 7 and 8 yields an expression for the factor of safety for a particular trial sliding surface,

$$FS = \frac{CB + (PAA \sin\theta - PPP \sin\theta + WB \cos\theta + UBH \cos\beta_2 \cos\theta - UBL \sin\theta + UBR \sin\theta - UBP - UBH \sin\beta_2 \sin\theta) \tan\phi}{(PAA - PPP) \cos\theta - WB \sin\theta - UBH \cos\beta_2 \sin\theta - UBH \sin\beta_2 \cos\theta - UBL \cos\theta + UBR \cos\theta} \quad (9)$$

For θ^+,

$$FS = \frac{CB + (PPP \sin\theta - PAA \sin\theta + WB \cos\theta + UBH \cos\beta_2 \cos\theta + UBL \sin\theta - UBR \sin\theta - UBP + UBH \sin\beta_2 \sin\theta) \tan\phi}{(PAA - PPP) \cos\theta + WB \sin\theta + UBH \cos\beta_2 \sin\theta - UBH \sin\beta_2 \cos\theta - UBL \cos\theta + UBR \cos\theta} \quad (10)$$

For $\theta = 0$ (horizontal slope),

$$FS = \frac{CB + (WB - UBP + UBH \cos\beta_2) \tan\phi}{(PAA - PPP) - UBH \sin\beta_2 - UBL + UBR} \quad (11)$$

THE COMPUTER PROGRAM AND ITS CAPABILITIES

The flow chart for the program is shown in Figure 6. The program has been written in FORTRAN IV language, and at present it is workable on the CDC 6500 computer. It is made up of a main program and six supporting subroutines. The program makes use of common storage to optimize use of high-speed core and minimum computation time.

The program is capable of handling the following variables:

1. Multiple (up to 11) continuous soil layers are at any inclination, and layer boundaries are straight;

After homogenization, stresses and settlements are then calculated as if the rigid circular foundation with its load V were placed at the surface (fictitious ground surface) of the equivalent layer. The $\bar{\sigma}_z$ stress curve is then plotted along the centerline from the fictitious ground surface. Then the same $\bar{\sigma}_z$ stress curve for layers h_1 and E_1 is plotted from the real ground surface. Within layer h_1, these two $\bar{\sigma}_z$ stress curves are then connected by a smooth transition curve to obtain the resultant vertical $\bar{\sigma}_z$ stress distribution curve in the real two-layered system.

The settlements should be calculated for the thickness z_a of the compressible active layer. Calculations may become difficult when there exist between the individual layers courses of soil having very large differences in moduli of elasticity. In such cases the equivalent height h_e may become very large with the angle $\alpha = \text{arc cot}(z/R_o)$ approaching a value close to zero. Also, there may arise a difficulty in interpretation of results and hence the use of the charts when the lower layer has a very great value ($E \to \infty$) of the modulus of elasticity, which in the process of homogenization gives an equivalent height h_e whose value is zero.

LIMITATIONS OF CHARTS

The assumptions made in developing the theoretical settlement influence-value chart for a central symmetrically loaded, rigid circular foundation also point out the chart's limitations. Thus, the main limitations pertain to an idealized soil, smooth base, smooth interface contact, weightless elastic medium, rigid circular foundation laid at the ground surface, displacement differences, elastic settlements are calculated for a homogeneous, semi-infinite elastic hemispace. Hence, the theoretical settlement influence values give approximative values only as compared with the real conditions in a soil. In reality, rock, gravel, sand, clay, or mixtures thereof are frequently encountered in single layers, as well as forming multilayered soil systems in various sequences of their stiffness. Such situations necessitate approximations and simplifications in pertinent calculations. The approximative nature of these calculations may also be seen in the approximative values of the elastic modulus E and Poisson's number m assumed for use in these theory-of-elasticity calculations.

Depth of Foundation

Although these charts do not include the embedment depth effects on stress and settlement distribution in soil, the settlement influence-value chart may, nevertheless, also be used if the foundation is laid t-units below the ground surface, rendering approximative results. In such a case, the $\bar{\sigma}_z$ stress may be calculated by substituting $(\sigma_o - \gamma t)$ for σ_o in Eq. 6. Approximative settlement s is calculated by substituting $(V - \pi R^2 \gamma t)$ for V in Eqs. 9, 10, 11, and 12.

Smooth and Rough Bases

Carrier and Christian (17) have shown that there is essentially no difference between a rough rigid plate and a smooth rigid one when $n = 0$ or $n = 1$ for $\mu = 0.5$, where n is a power in the E-equation defining a hemispace where E varies with depth: $E = E_o\left(\frac{z}{2R_o}\right)^n$. To quote these authors: "It is probable, therefore, that roughness has no influence for intermediate values of n for a rigid or uniform circular load when $\mu = 0.5$." The same opinion has been expressed by Gibson (18) and Schiffman (19).

Smooth Soil Interfaces and Rough Soil Interfaces

In the absence of reliable stress and settlement measurement data relative to interface roughness or smoothness for two-layered and multilayered soil systems under externally loaded, rigid circular foundations, it is, unfortunately, impossible to say anything about the probable accuracy of the settlement determination method by this chart when it is applied to rigid-soft or soft-rigid soil systems.

Elastic Layer of Finite Thickness Overlying a Rigid Deposit

Generally, stress distribution in a two-layered system differs from that in a homogeneous, semi-infinite medium only in cases where there are sharp differences in elasticity characteristics among the various single deformable layers of soil. Therefore, on determination of the stressed condition in the soil, consideration of nonuniformity should be given only when deformation characteristic values of the various nonuniform soils, composing nonuniform natural earth masses, differ sharply one from another. In such a case, the theory used in this study for the development of tables and charts for approximative stress and settlement evaluation is applicable as for a nearly homogeneous monolayer.

If in a two-layered soil system there is immediately below the base of a rigid circular footing an elastic compressible layer of finite thickness overlying a practically incompressible rigid deposit such as rock, then stress distribution in the upper compressible layer depends primarily on the ratio of the thickness of the compressible layer ($z = h$) to the diameter ($2R_o$) of the rigid footing. Figure 1 shows that, beginning with a relative depth of $z/R_o = 4$ (or from a depth of two diameters and down), the vertical stresses $\bar{\sigma}_z$ for all Poisson's numbers are practically the same and are small. Hence, it is believed that, within the zone of thickness of two (or three) diameters, the chart is applicable as for a homogeneous soil of infinite depth (monolayer).

Figure 1 also shows that, within a depth zone of one diameter ($z/R_o = 2$), there exist large stresses in soil below the footing. Thus, if the massive rock is located at a depth shallower than two diameters, the soil-rock system should be treated as a two-layered system by means of the method, say, of the equivalent layer.

Rigid Layer of Finite Thickness Overlying an Elastic Deposit

If in a two-layered soil system a rigid layer overlies a compressible one, the vertical stresses distribute through the upper, rigid layer on the surface of the compressible layer over a larger area than the size of the circle on the ground surface. Hence, on the interface plane between the rigid and soft layers, the $\bar{\sigma}_z$ stress is smaller than that in a uniform monolayer mass. As in almost every theoretical settlement calculation, so here the calculated deflections tend to be larger than the actual ones.

CONCLUSIONS

Based on the foregoing discussion, some general conclusions relative to the practical application of the settlement influence-value chart may be made as follows:

1. Regardless of some of the limitations imposed in developing this settlement influence-value chart, and in its application to real soils, the chart is nonetheless a very useful one in practical soil mechanics and foundation engineering for calculating approximative settlements in homogeneous monolayers as well as in multilayered soil systems. The chart is easy to use.
2. Because it influences the magnitude of the vertical stress distribution and that of the settlement, the real modulus of elasticity E must be known and used in these calculations and must be determined from appropriate tests.
3. Figure 1 shows that Poisson's number m has a remarkable effect on the vertical, spatial stresses in and settlement of an elastic layer.
4. For a compressible, homogeneous monolayer soil, settlement calculations can be practically based on the thickness of the active zone.
5. If in a multilayered soil system the soil elasticity characteristics of the individual layers do not differ greatly, the chart may be used for approximative settlement evaluation in the same way as for a nearly uniform, homogeneous monolayer. Otherwise, the multilayered soil system should be homogenized into an equivalent, homogeneous monolayer.
6. In a two-layered soil system that is elastic-rigid, within the depth zone, the thickness of which is about two diameters below the base of the footing, the chart is applicable as for a homogeneous soil of infinite depth (monolayer). In a two-layered

soil system of rigid-elastic consistency, the $\bar{\sigma}_z$ stresses on the rigid-elastic interface are smaller than in a uniform monolayer mass, but the settlement here tends to become smaller.

7. The uniform, elastic settlement influence-value chart derived for a rigid centrically loaded circular foundation may also be used effectively for approximating the settlements imposed by a rigid square foundation whose area is equivalent to that of the circle:

$$4A^2 = \pi R_o^2;\ R_o = 2A\sqrt{1/\pi} = 1.128A$$

where

2A = length of side of the square, and
R_o = radius of circle.

This approximation is thought valid for side ratios of up to 1 to 5 only, according to Schleicher (14).

8. Because the bearing capacity of a pier (rigid die) and/or of a massive pile depends on their tolerable settlement, the settlement influence-value chart may also be used with some limitations for evaluation of the bearing capacity of circular (and quadratic in cross section) rigid piers and piles where no mantle resistance (skin friction) applies (in water, for example).

In general, the chart would tend to give conservative answers because the theory neglects depth effect on stress distribution and also neglects skin friction on the sides of the piers, which would both tend to reduce the observed amount of settlement as compared with the calculated ones.

ACKNOWLEDGMENTS

In preparing the charts, and this paper, the author acknowledges support given to him by the following persons: E. C. Easton, Dean of the College of Engineering; R. C. Ahlert, Executive Director of the Bureau of Engineering Research, and J. Wiesenfeld, Chairman, Department of Civil and Environmental Engineering, all of Rutgers University. The author also appreciates the discussions about this paper afforded to him by R. D. Barksdale of the School of Civil Engineering, Georgia Institute of Technology.

REFERENCES

1. Burmister, D. M. The Theory of Stresses and Displacements in Layer Systems and Application to Design of Airport Runways. HRB Proc., Vol. 23, 1943, pp. 126-149.
2. Acum, W. E. A., and Fox, L. Computation of Load Stresses in a Three-Layer Elastic System. Géotechnique, London, Vol. 2, 1951, pp. 293-300.
3. Jones, A. Tables of Stresses in Three-Layer Elastic Systems. HRB Bull. 342, 1962, pp. 176-214.
4. Jumikis, A. R. Vertical Stress Tables for Uniformly Distributed Loads on Soil. College of Engineering, Rutgers Univ., New Brunswick, N.J., Engineering Research Publ. 52, 1971, pp. 381-472.
5. Jumikis, A. R. Influence Value Graphs for Circular Bearing Areas. Highway Research Record 405, 1972, pp. 45-50.
6. Peattie, K. R. Stress and Strain Factors for Three-Layer Elastic Systems. HRB Bull. 342, 1962, pp. 215-253.
7. Boussinesq, J. V. Application des potentiels à l'étude de l'équilibre et du movement des solides élastiques, principalement au calcul des déformations et des pressions que produisent, dans ces solides, des efforts quelconques exercés sur une petite partie de leur surface ou de leur intérier. Gautier-Villars, Paris, 1885.
8. Borowicka, H. Ueber ausmittig belastete starre Platten auf elastisch-isotropem Untergrund. Ingenieur-Archiv, Vol. 14, No. 1, 1943, pp. 1-8.
9. Boussinesq, J. V. Application des Potentiels. Gautier-Villars, Paris, 1885, p. 140.

10. Fischer, K. Zur Berechnung der Setzung einer starren, mittig belasteten Kreisplatte auf geschichteter Unterlage. Beton und Stahlbetonbau, Vol. 10, 1957, pp. 257-259.
11. Fröhlich, O. K. Die starre Kreisplatte auf elastisch-isotroper Unterlage. Geologie und Bauwesen, Vienna, No. 4, 1943, p. 125.
12. Jumikis, A. R. Theoretical Soil Mechanics. Van Nostrand Reinhold Co., New York, 1969, pp. 160-163.
13. Jumikis, A. R. Stress and Settlement Tables for Centrically Loaded, Rigid Circular Foundations on Multilayered Soil Systems. College of Engineering, Rutgers Univ., New Brunswick, N.J., Engineering Research Publ. 54, 1973, pp. 7-22.
14. Schleicher, F. Zur Theorie des Baugrundes. Der Bauingenieur, No. 49, 1926, pp. 949-952.
15. Timoshenko, S. P., and Goodier, J. N. Theory of Elasticity, 2nd Ed. McGraw-Hill, New York, 1951.
16. Timoshenko, S. P. History of Strength of Materials. McGraw-Hill, New York, 1953, pp. 328-334.
17. Carrier, W. D., III, and Christian, J. T. Analysis of an Inhomogeneous Elastic Half-Space. Jour. Soil Mech. and Found. Div., Proc. ASCE, Vol. 99, No. SM3, March 1973, pp. 301-306.
18. Gibson, R. E. Some Results Concerning Displacements and Stresses in a Non-homogeneous Elastic Halfspace. Géotechnique, London, Vol. 17, March 1967, pp. 58-67; Vol. 18, June 1968, pp. 274-276; and Vol. 19, March 1969, pp. 160-161.
19. Schiffman, R. L. The Influence of Adhesion on the Stresses and Displacements in an Elastic Half-Space. Highway Research Record 282, 1969, pp. 17-24.

MERCURY-FILLED SETTLEMENT GAUGE

Tommy C. Hopkins and Robert C. Deen,
Kentucky Department of Highways

A description is given of a remote-sensing, multiple-point, mercury-filled settlement gauge designed for measuring in-place settlements. The gauge consists of settlement units positioned at locations where settlement measurements are desired and a monitoring unit located outside of construction limits. Settlement readings are observed on a mercury manometer located at the monitoring site and are equal to the differences in initial and subsequent pressure-head readings. Comparisons of measurements obtained at a highway construction site from mercury gauge settlement units and conventional settlement platforms are presented and show very good agreement. With the mercury gauge, a large amount of settlement information can be obtained per installation, and the gauge does not have many of the disadvantages associated with the settlement platform.

CONSTRUCTION of certain engineering structures, for example, highway embankments and buildings, frequently results in settlements that can adversely affect the performance and even the stability of the structure. Hence, it is important to be able to measure in-place settlements and to compare observed settlements with theoretical predictions.

Since 1964, the Kentucky Department of Highways has focused attention on the development of a remote-sensing gauge. As a result, a multiple-point mercury-filled settlement gauge has been developed. Such gauges do not have many of the disadvantages associated with settlement platforms and other types of gauges. Furthermore, the multiple-point gauges provide much more settlement information per installation than can be obtained from a settlement platform.

GAUGE DETAILS

Description

Components and arrangement of the multiple-point, mercury-filled settlement gauge, capable of measuring several points of settlement per installation, are shown in Figure 1. The gauge contains two units: the monitoring site located at some convenient site outside the loaded area and settlement units positioned at points where settlement measurements are desired.

At the monitoring site, tube 1 (Fig. 1) leads from a tee connector mounted on a control panel, loops through the area where measurements are desired, and returns to the monitoring site. A portion of the return end of tube 1 is fixed in a vertical position to an aluminum pipe anchored in concrete. The middle portion is coiled and "stacked" around the pipe. Tube 2 leads from the tee connector to a mercury-filled manometer having a resolution of 0.1 in. and the capacity to measure a pressure head as large as 10 ft. The third end of the tee is connected to an array of valves, mounted on the control panel for fine control of applying and releasing nitrogen pressure, and to a bottled nitrogen supply.

Settlement units (Fig. 1) consist of stainless steel tube connectors inserted into the return portion of tube 1 at points where settlement measurements are desired. The

Publication of this paper sponsored by Committee on Embankments and Earth Slopes.

connectors are machined in such a way that the cut ends of tube 1 fit tightly into each end of the connector, and a constant diameter is maintained throughout tube 1. A practical limit of settlement units is 2 per foot of gauge length. Normally, 6 to 10 points have been used per gauge installation. In Figure 1, only two units are shown.

Insulated electrical wires 1 and 2 are connected (soldered) to each stainless steel insert and extended from each settlement unit through a push-button switch to an ohmmeter located on the control panel. The settlement unit is insulated and protected by casting it in an epoxy resin of a type commonly used for splicing communication cable. At the base of the vertical portion of tube 1, a stainless steel connector of the same construction as the settlement units is inserted. Insulated electrical wire 3 leads from that point to the ohmmeter.

Toggle valve 1 permits an instantaneous shutoff of the release of nitrogen pressure from the gauge system. The nitrogen tank is recharged through check valve 2. Metering valve 3 provides an extremely fine release of nitrogen pressure from the gauge system. On-off valves 4 and 5 control the direction of flow of the nitrogen.

Mercury is introduced into tube 1 through a detachable plexiglass reservoir. The bottom portion of the reservoir is funnel-shaped. The diameter of the stem portion of the funnel is equal to the inside diameter of tube 1. Sufficient mercury to fill the return portion of tube 1 reaching from the farthest settlement unit to the bottom coil at the monitoring site is first introduced into the cylinder positioned horizontally. With a quick motion, the filled reservoir is tilted vertically, and the mercury is allowed to drain into tube 1. This normally permits introduction of a mercury column into tube 1 free of breaks. Mercury remains in tube 1 until all settlement readings have been obtained; thereafter, it is recovered. Nitrogen is used to prevent condensation of moisture in tube 1, which, if present, could cause breaks in the mercury column. The valves, nitrogen tank, and ohmmeter are housed in a portable carrying case. The manometer can be either transported or stored (mounted) at the site. By using flexible tubing, the manometer can be coiled and conveniently transported to the site.

An effort is made to position settlement units and the coiled portion of tube 1 at the same elevation. With this arrangement, settlements as large as 10 ft can be measured. Otherwise, the maximum settlement that can be measured is 10 ft minus the initial difference in elevation between the settlement unit and the coiled portion of tube 1. Measurements can be obtained even if the monitoring site is located at an elevation below the settlement units.

Theory and Operation

The operation of the gauge is shown in Figure 2. Figures 2a, 2b, and 2c show steps necessary to obtain a pressure-head reading, h_o, when the settlement unit is situated in an initial position. To obtain subsequent pressure-head readings, h, for the settlement unit in a new position (Fig. 2d), we repeat the steps shown in Figures 2a, 2b, and 2c.

When nitrogen pressure is applied to the two mercury columns (Fig. 2) and the columns are adjusted to some static state such as shown in Figure 2c, the difference, h_o', in level between the ends of the mercury column, A and B, equals the initial pressure head, h_o, observed on the manometer at the monitoring site. That is, when the columns of mercury are at rest, all velocity heads and head losses are zero, and Bernouilli's equation for the system reduces to

$$h_o' = h_o = P_o/\gamma_m \tag{1}$$

where

P_o = pressure applied to the two mercury columns,
γ_m = unit weight of mercury, and
P_o/γ_m = pressure head.

A change, h_s, in elevation of the settlement unit from its initial elevation (Fig. 2d) will result in an equal change in pressure head observed on the manometer. Hence,

for this new position of the settlement unit,

$$h' = h = P/\gamma_n \tag{2}$$

and

$$h_s = h' - h_o' = h - h_o \tag{3}$$

where P/γ_n = subsequently applied pressure head.

Contact of the end of the mercury column in tube 1 (Fig. 2b) at each settlement unit is recognized by completion of an electrical circuit via the ohmmeter, the wire extending from the ohmmeter to the stainless steel connector (point C) at the monitoring site, the mercury column in tube 1, the stainless steel connector of the settlement unit, and a wire extending from the settlement unit to the ohmmeter. As nitrogen pressure is applied (Fig. 2b), the mercury column in tube 1 will contact the stainless steel connector at the monitoring site completing the circuit, and the ohmmeter needle deflects. Pressure application is discontinued at the instant the ohmmeter needle deflects to zero. By an extremely fine release of pressure (Fig. 2c) through the metering valve, the column of mercury is allowed to move toward the stainless steel connector of the settlement unit. At the instant the column contacts the stainless steel connector, as signaled by a deflection of the ohmmeter needle, toggle valve 1 is closed, locking the pressure in the system. Hence, the pressure head observed on the manometer at the monitoring site can be recorded accurately and conveniently. This procedure is repeated for each settlement unit on the gauge length.

Length of the mercury column in tube 1 is affected by (a) volume change in tube 1 due to creep or relaxation and (b) difference in temperature of mercury in tube 1 and mercury in the manometer at the monitoring site. In the former case, the level of the end of the mercury column at B, Figure 2c, must be referenced initially to a fixed datum. In each subsequent settlement reading, the position of the end of the column is noted with respect to the initially fixed datum. If the end of the column is below the initial point, then a correction, M, must be added to the observed manometer reading; if above the point, the correction is subtracted. Equation 3 then becomes

$$h_s = (h \pm M) - h_o \tag{4}$$

However, this correction can be practically eliminated by using tubing that is not subject to large expansion and contraction and by coiling the tubing at the monitoring site in a manner shown in Figure 1.

Because the temperature of the mercury in tube 1 and in the manometer at the monitoring site may differ, there may be an error, ϵ, proportional to the temperature difference and applied pressure. Consequently, the difference in the levels of the mercury column in tube 1 will not equal the observed pressure head on the manometer at the monitoring site. The error can be computed from

$$\epsilon = h\,(T_g - T_m)/(9{,}988 - T_g) \tag{5}$$

where

h = observed pressure head on the manometer at monitoring site;
T_g = temperature in deg F of mercury in tube 1, normally ground temperature; and
T_m = temperature in deg F of mercury in the manometer at the monitoring site, normally air temperature.

Equation 4 then becomes

$$h_s = (h \pm M + \epsilon) - h_o \tag{6}$$

The error, ϵ, can be minimized and usually ignored. If settlement readings are obtained when ground and air temperatures are nearly equal, the error can be ignored.

Figure 1. Gauge components.

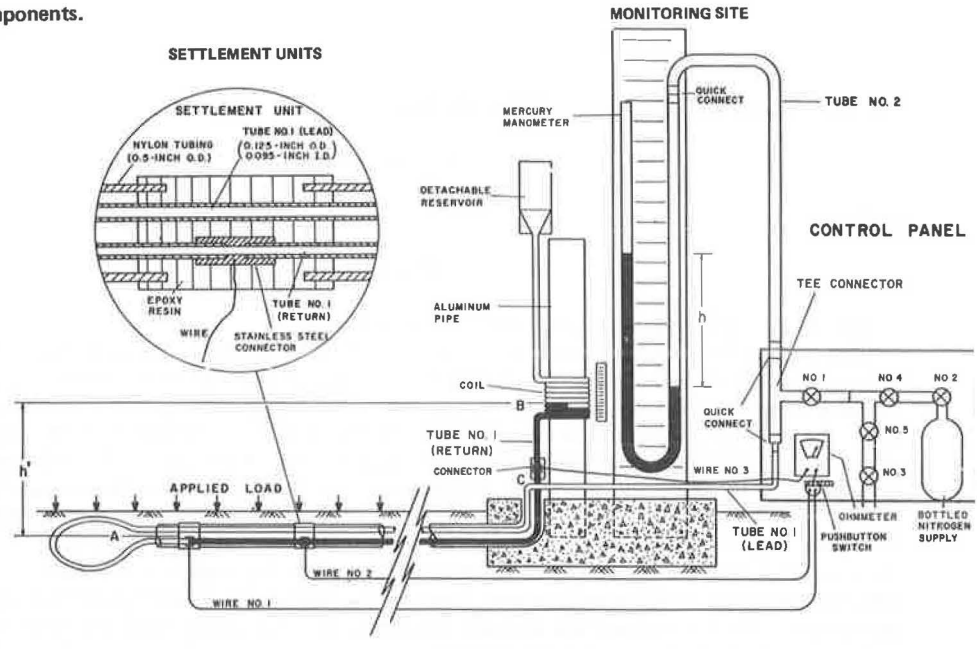

Figure 2. Gauge operation.

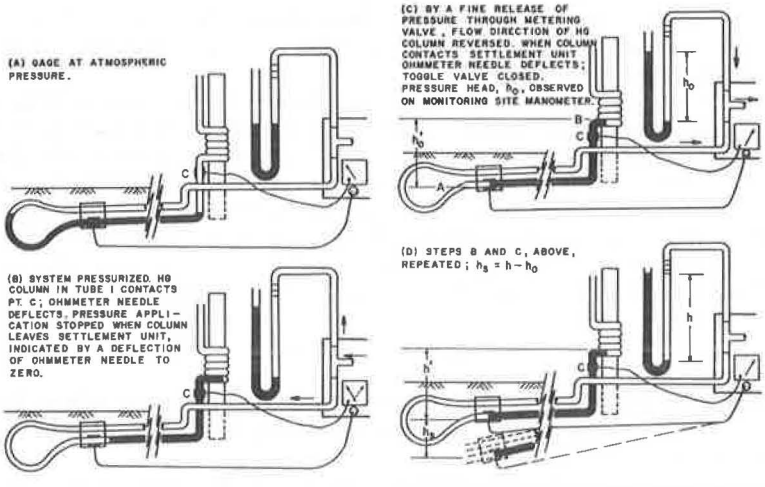

Figure 3. Plan view of Green River site.

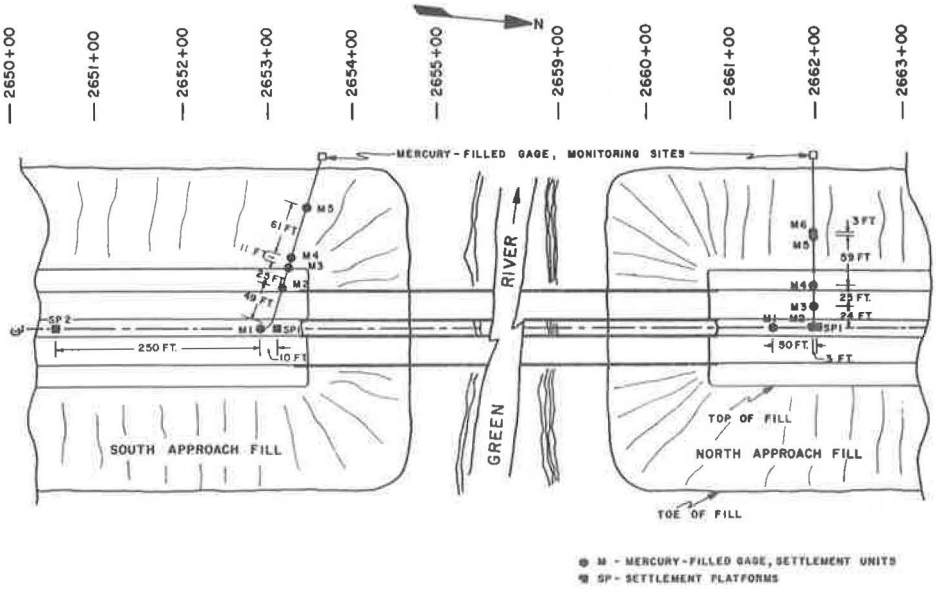

The computed error for an observed pressure head of 40 in. is 0.04 in. per 10-deg temperature difference. In cases where large settlements and temperature differences are anticipated, the error could be significant.

This temperature differential problem can be resolved by monitoring the ground and air temperatures, computing the error, and correcting the readings or by coiling the tubing as shown in Figure 1. When the gauge is read initially, ground and air temperatures may differ. Thus, an initial error, ϵ_o, is introduced. Generally, ground temperature is constant; therefore, the density of mercury in tube 1 is constant. Because all subsequently observed pressure heads are referenced to the initially observed pressure head, the problem reduces to one of noting the air temperature at the time of the initial reading and in each subsequent reading and computing the initial and subsequent errors. Equation 6 becomes

$$h_s = (h \pm M + \epsilon) - (h_o + \epsilon_o) \quad (7)$$

Consequently, all settlement readings can be readily corrected in a simple manner by merely observing air temperatures (or by measuring directly the temperature of the mercury in the manometer at the monitoring site) during each reading. However, the error can be eliminated completely by coiling tubing 1 as shown in Figure 1. Because the largest expected error is on the order of 0.6 in., the end of the mercury column will remain in the initially marked coil of tube 1. This coil is essentially in a horizontal plane, and thus the elevation of the initial reference does not vary significantly. Therefore, no accuracy is lost because of the effects of temperature differences and applied pressures.

In the event the vertical position of the monitoring site is changed, thereby disturbing the initially marked point (B, Fig. 2c), a correction C must be applied to Eq. 7 so that finally

$$h_s = (h \pm M \pm C + \epsilon) - (h_o + \epsilon_o) \quad (8)$$

FIELD PERFORMANCE

Fourteen mercury-filled settlement gauges have been used during the period 1966 to 1972 at 10 highway construction sites primarily to investigate settlements of compressible foundations located beneath highway bridge approach embankments. Field reliability of the mercury gauge system at four of those sites is being checked by positioning settlement units of the mercury gauge as close as practical to settlement platforms and comparing measurements obtained from the two devices. A discussion follows of the results obtained to date (April 1972) from one of the construction sites.

The site involved major construction of the Bowling Green-Owensboro Parkway Bridge across the Green River in Kentucky. Two settlement platforms were located on the southern foundation, and one was situated on the northern foundation. The risers were not encased and therefore were subjected to negative friction. A multiple-point, mercury-filled settlement gauge was installed on each approach foundation (Fig. 3). The mercury gauge on the north side measured 270 ft in length and contained six settlement units. On the south side, the mercury gauge contained five settlement units and was 225 ft in length.

The most useful check of the reliability of the mercury gauge was made on the north side where settlement unit 2 (M2) was positioned within 3 ft of a settlement platform (SP 1, Fig. 3). Settlement-logarithm time curves obtained from the settlement platform and mercury gauge unit 2 are compared in Figure 4. Fill height-logarithm time curve and a typical soil profile of the northern foundation are also shown in Figure 4.

All individual settlement measurements obtained from the settlement platform (SP 1) and mercury gauge unit 2 (M2) were within ±0.25 in. of the mean of the two measurements. For 80 percent of the measurements, the differences were within ±0.14 in. Half of the readings were within ±0.08 in. of the mean. The largest differences occurred during the time periods of about 50 to 90 days and 105 to 160 days (Fig. 4). During those periods, when there was a pause in loading, consolidation of the fill

Figure 4. Settlement curves for north approach foundation, Green River site.

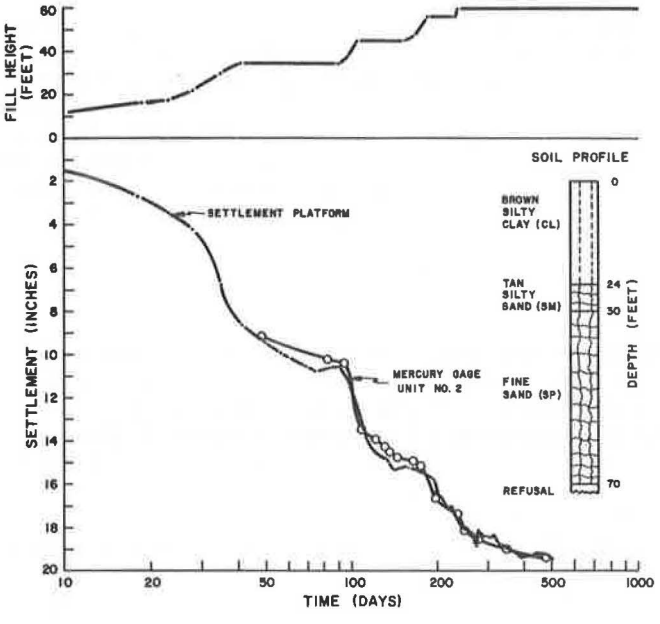

Figure 5. Settlement-logarithm time curves for north approach foundation, Green River site.

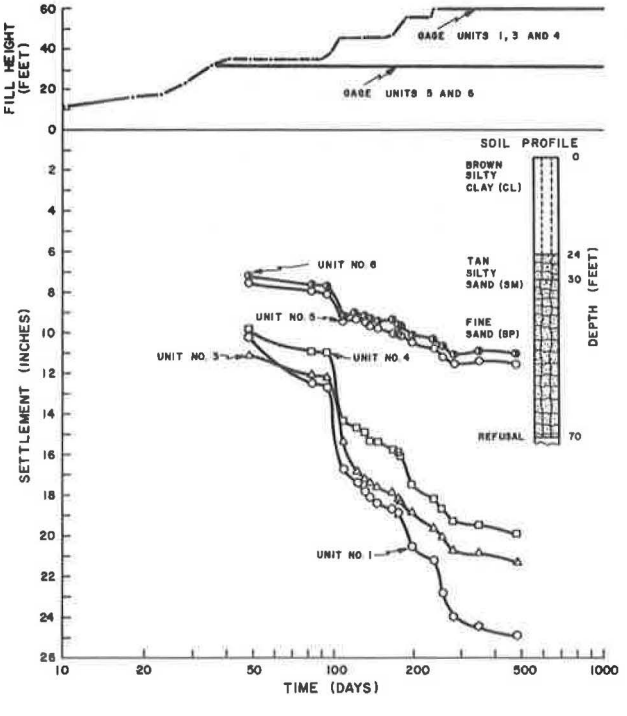

Figure 6. Settlement curves for south approach foundation, Green River site.

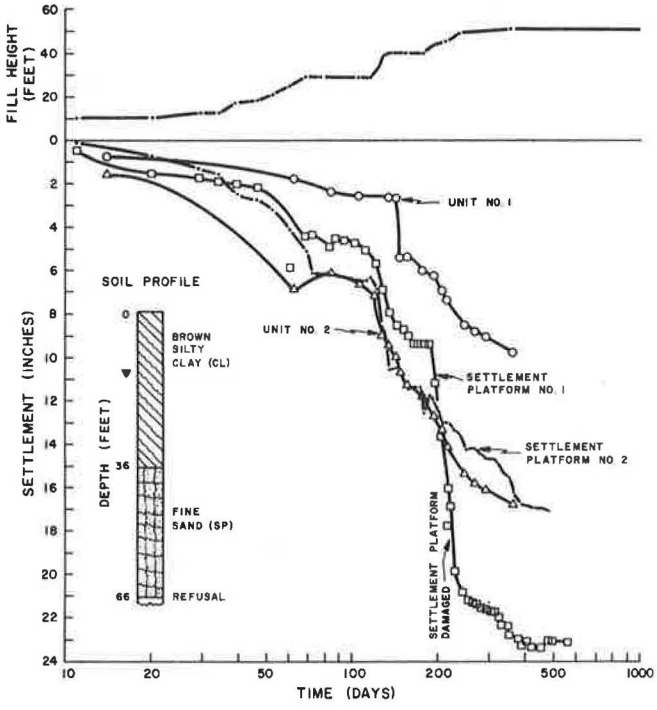

Figure 7. Settlement-logarithm time curves for south approach foundation, Green River site.

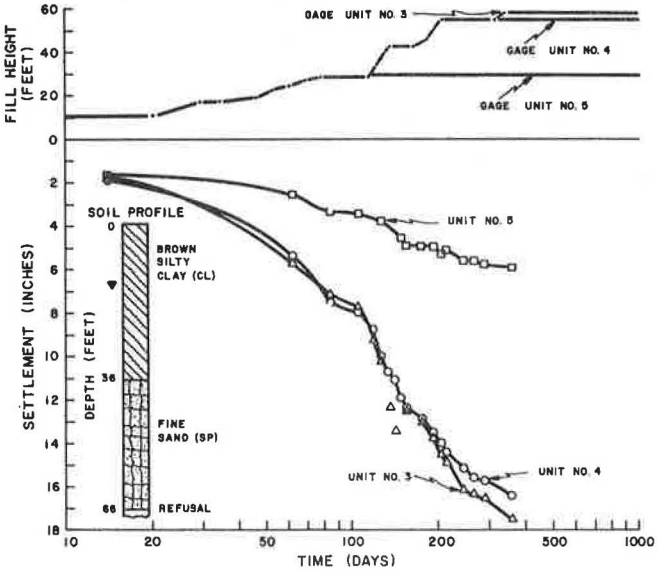

apparently exerted sufficient negative frictional forces on the pipe risers to overload the settlement platform, resulting in measurements of greater settlements than had actually occurred. The settlement platform curve dipped noticeably during each of those periods.

Settlement- and fill height-logarithm time curves for mercury gauge points located on the northern foundation are shown in Figure 5. Gauge units 5 and 6 were located within 3 ft of each other. The height of fill over unit 5 was slightly larger than that over unit 6. Settlement-logarithm time curves shown in Figure 5 are approximately parallel. In 80 percent of the settlement measurements obtained from those two points, variations of the differences of the two readings from the initial difference of 0.34 in. was within 0.10 in.

Comparisons of settlement-logarithm time curves obtained from settlement platforms (SP 1 and SP 2, Fig. 3) and from mercury gauge units (M1 and M2) on the southern foundation are shown in Figure 6. Meaningful comparisons of readings obtained from the mercury gauge and settlement platforms could not be made because pipe risers of the platforms were damaged on several occasions by the contractor's equipment. Figure 7 shows settlement-logarithm time curves for mercury gauge units 3, 4, and 5.

CONCLUSIONS

Experience with the mercury gauge since 1966 at 10 highway construction sites has shown that settlements as large as 3 ft can be measured with no difficulties; however, the gauge has the capacity to measure settlements as large as 10 ft, if properly positioned. The monitoring unit can be located either above or below the settlement units. Errors occurring in the measurements because of volume changes of the tubing and effects of temperature on the unit weight of mercury can be corrected or made small and ignored, depending on the accuracy required.

Thus far, length of gauge has not been a factor in limiting its use. Readings from gauges as long as 370 ft have been obtained successfully for as long as 2 years. An almost continuous settlement profile can be obtained with the mercury gauge. Two settlement measurements per foot of gauge can be obtained. Thus far, 6 to 10 units have been installed per gauge.

Generally, settlement measurements obtained from a mercury gauge unit and a settlement platform were within a range of ±0.14 in. of the mean of the two measurements. Field studies show that, at any given time, readings can be repeated within an accuracy of 0.1 in., the resolution of the manometer used to obtain the readings.

ACKNOWLEDGMENT

The contents of this report reflect the views of the authors who are responsible for the facts and accuracy of the data presented. The contents do not necessarily reflect the official views or policies of the Kentucky Department of Highways or the Federal Highway Administration. This report does not constitute a standard, specification, or regulation.

PLACEMENT RATES FOR HIGHWAY EMBANKMENTS

Raymond J. Krizek and Peter K. Krugmann, Department of Civil Engineering, Northwestern University

ABRIDGMENT

•THE problems of increased urban development, zoning regulations, high land values, and high construction costs, together with the economic necessity to utilize the shortest and most direct routing, make it necessary to construct many highways on soft soils, such as organic silt, sensitive clay, peat, soft marl, muck, etc. Because the rapid construction of an embankment on a soft soil may result in excessively large settlements or a foundation failure or both, measures must be taken to ensure stability of the embankment during and after construction and to eliminate excessive settlements that would adversely affect the pavement performance or riding characteristics of the roadway. These problems usually have more than one solution, and the various techniques that may be employed to achieve the solution include removal of unsuitable soil by excavation or displacement, controlled rate of construction, stabilizing berms, sand drains, lightweight fill, and surcharging. The first method requires removal of the soil, and it is usually quite expensive. Whenever the situation permits, the controlled rate of construction method, perhaps in combination with one or more of the latter methods, is normally most economical. One of its main advantages is that it requires few if any additional construction materials; its major disadvantage is the time required.

The problem considered in this study involves the construction of a highway embankment on a layer of soft soil underlain by a relatively firm or rigid substratum, and the analysis entails two main aspects—stability and differential settlement, both with respect to time. On one hand, it is desired to apply the load as rapidly as possible, so as to accelerate the consolidation process and the resulting strength gain; however, on the other hand, if the load is applied too rapidly, the required strength gain does not have time to occur, and a bearing capacity failure may result. Because the controlled rate of construction technique takes advantage of the soil strength increase resulting from consolidation, soft soil deposits can often be made suitable for the support of highway embankments.

The companion problem to that of stability is concerned with differential settlements. Very often, embankments are constructed to surcharge levels to decrease post-construction settlements and not necessarily to increase the stability under the final design load. In many cases vertical sand drains have served to accelerate the consolidation process and to shorten the time required for large settlements to occur; desirably, of course, the settlement should take place prior to construction of the pavement.

OBJECTIVE

The objective of this study is to provide a series of charts and computer programs that the practicing engineer may employ as guidelines in establishing a suitable rate at which a highway embankment resting on a layer of soft soil may be preloaded without exceeding the bearing capacity of the soft layer and the associated settlements.

Publication of this paper sponsored by Committee on Embankments and Earth Slopes and Committee on Mechanics of Earth Masses and Layered Systems.

GENERAL APPROACH

As considered herein (1, 2, 3), the problem is divided into four parts that deal with the initial distribution of excess pore water pressures due to the applied load, the process of consolidation, the resulting settlements, and the stability of the embankment-foundation system. The pore water pressures are computed by means of Skempton's pore pressure coefficients A and B and a solution for the total stress distribution. Based on the assumption of plane strain conditions and Poisson's ratio equal to one-half, the stresses are determined for the mixed boundary value problem in which a vertically loaded layer of finite thickness and infinite extent rests on a rough, rigid substratum. The dissipation of pore water pressures is evaluated by means of an extended consolidation theory, which includes radial flow toward sand drains, variable coefficients of consolidation, and partial saturation; the associated nonlinear partial differential equation is solved by use of a numerical procedure. Total settlements are computed on the basis of consolidation test results, excluding immediate and secondary effects; increases in effective stresses are assumed to be equal to the dissipated pore water pressures at any given time. The stability analysis is performed in terms of total stresses, and shear strength increases of the underlying soft soil due to consolidation are taken into account by means of the $c/\bar{p}$ ratio.

SUMMARY OF RESULTS

The results of this study are presented (1, 2, 3) in a series of charts and a set of computer programs. The charts include the following:

1. Maximum embankment height versus subsoil thickness—These charts, which have been established for a commonly used set of soil parameters, allow the determination of the maximum embankment height corresponding to a safety factor of unity against failure along a circular arc.
2. Stability charts—These charts are dimensionless and allow the determination of the factor of safety against failure along a circular arc for the cases where the undrained strength of the subsoil is a fraction of the strength of the embankment material.
3. Average pore water pressures under symmetrical trapezoidal loads—These charts have been established for a fully saturated soil with Poisson's ratio equal to one-half and the pore pressure coefficient A equal to one-half or unity. They can be conveniently used to estimate the ultimate consolidation settlements that can be expected under a trapezoidal embankment load.
4. Increases in shearing resistance due to complete dissipation of excess pore water pressures—These charts have been established for a specific set of soil parameters and the assumption that the maximum possible trapezoidal load is applied at time equal to zero. After complete consolidation under this load, the observed nonuniform strength increase is evaluated for two different $c/\bar{p}$ ratios and two different pore pressure coefficients A. This nonuniform distribution is then converted to an equivalent uniform strength increase such that the same factor of safety is obtained for both cases. These charts may be used to determine whether the controlled rate of construction procedure can be used successfully for the case where the initial shear strength of the subsoil is insufficient to sustain the final embankment load.
5. Consolidation-time curves—These curves represent the average degree of consolidation versus a dimensionless time factor for linearly increasing construction loads and for different ratios of the sand drain radius and the subsoil thickness to the radius of influence of the sand drain installation. These charts can be used to estimate the time dependency of the consolidation settlements and the strength increase.

Although the charts can be used most advantageously for preliminary design purposes, the computer programs can best be employed for a detailed final design or for checking an existing embankment-subsoil system. The set of computer routines consists of the main programs SAND and DETR plus 24 subroutines, and all programs are written in FORTRAN IV. Program SAND determines the times at which new load steps can be applied, depending on whether a specified portion of the ultimate consolidation settlement under a reference load or a specified factor of safety or both are obtained at the

time of the new load application. If the different load increments and the times of load application are provided as input, the program can also be used to analyze the consolidation process and the time dependency of settlements without performing any stability analyses.

Program DETR determines the sand drain spacing by checking whether a specified amount of settlement or factor of safety or both at a specified time are ensured for the case where the load intensity increases linearly from time equal to zero to the full intensity at some specified time. Although program SAND allows the use of variable coefficients of consolidation, program DETR requires that these coefficients be constant.

ACKNOWLEDGMENT

This research was performed by the Department of Civil Engineering, Northwestern University, in cooperation with the Illinois Department of Transportation and the Federal Highway Administration.

ANNOTATED REFERENCES

1. Krizek, R. J., and Krugmann, P. K. Placement Rates for Highway Embankments Volume 1: Development of Design Charts and Computer Programs. Dept. of Civil Engineering, Northwestern Univ., June 1972.

The controlled rate of construction procedure is investigated with regard to highway embankments resting on a soft, compressible soil layer that is underlain by a firm substratum. Special attention is given to the advantages of using vertical sand drains, and typical soil conditions, as well as sand drain installation procedures and their effect on the performance of a sand drain design, are considered. A precompression analysis involves problems associated with the distribution of initial excess pore water pressures, the dissipation of these excess pore water pressures, the resulting settlements, and the stability of the embankment-subsoil system. Solutions to each of these problems are presented, and charts are given to facilitate a preliminary precompression design. A well-documented set of computer programs, to illustrate the handling of input parameters, together with flow diagrams, is included to aid in making the final design or in checking a given design. Three examples are presented to elucidate the use of the programs.

2. Krizek, R. J., and Krugmann, P. K. Placement Rates for Highway Embankments, Volume 2: Listings and Flow Charts for Computer Programs. Dept. of Civil Engineering, Northwestern Univ., June 1972.

Given in this volume is a self-contained set of computer programs that can be used to analyze the behavior of an embankment constructed on soft soil. The individual routines, consisting of the main programs SAND and DETR and 24 subroutines, are written in FORTRAN IV. Complete listings are given for all programs, and detailed flow diagrams are provided for the main programs. Based on consideration involving the consolidation process and the stability of the embankment-subsoil system, program SAND determines the times at which new load increments can be applied; the criteria depend on whether a specified portion of the ultimate consolidation settlement under a reference load or a specified factor of safety or both are obtained at the time of a new load application. If the load increments and the times of load application are provided as input, the program can also be used to analyze the consolidation process and the time-dependency of settlements without performing a stability analysis. Program DETR calculates the required spacing of vertical sand drains by checking whether a specified amount of settlement or a specified factor of safety or both are ensured at a specified time. Although program SAND can handle variable coefficients of consolidation, program DETR requires that these coefficients be constant.

3. Krizek, R. J., and Krugmann, P. K. Placement Rates for Highway Embankments, Volume 3: Theoretical Background and Programmed Formulae. Dept. of Civil Engineering, Northwestern Univ., June 1972.

The general precompression analysis for a highway embankment resting on a soft soil can be divided into four parts that deal with the initial increase in pore water pres-

sures due to the application of an embankment load, the associated settlements, the process of consolidation, and the stability of the embankment-foundation system. The four problem areas are described, possible approaches reported in the literature are investigated, and the formulas incorporated into the computer programs are derived. The pore water pressures are computed by use of Skempton's pore pressure coefficients A and B and a solution for the total stress distribution, assuming linear elasticity and plane strain conditions. The dissipation of excess pore water pressures is evaluated by means of an extended consolidation theory, which includes radial flow toward sand drains, variable coefficients of consolidation, and partial saturation. Total settlements are computed on the basis of consolidation test results, excluding immediate and secondary effects. The stability analysis is performed in terms of total stresses, and shear strength increases of the soft soil due to consolidation are taken into account by means of the $c/\bar{p}$ ratio.

STRESSES AND DEFORMATIONS IN JAIL GULCH EMBANKMENT

Jerry C. Chang and Raymond A. Forsyth,
California Division of Highways

Presented is a comprehensive case history of stress and deformation measured by field instrumentation in a 200-ft high Jail Gulch highway embankment. Theoretical analyses in which the finite-element method was used were conducted to predict stresses and deformations within the embankment. Theoretical equations were developed for calculating the nonlinear, stress-dependent tangent modulus of elasticity of soil; parameters obtained from triaxial compression tests on soil samples were used. When a constant value of Poisson's ratio was used, a Poisson's ratio of 0.3 was found to yield results best agreeing with the field data. The stresses and deformations calculated by the finite-element method of analysis agreed reasonably well with the field-measured data.

•THE California Division of Highways has conducted field performance studies to determine the stresses and deformations in several highway embankments over 200 ft in height. This paper presents the results of the field studies and theoretical analysis by finite-element method for the Jail Gulch embankment. A more detailed report of this research project has been presented by Chang et al. (2).

The Jail Gulch embankment was constructed on I-5 about 8 miles north of Yreka, California, during June through December 1968. The maximum height of the embankment is about 200 ft at the centerline of the roadway. The side slopes of the embankment are 1.5 to 1 normal and about 1.6 to 1 on the instrumented section due to a slight skew.

The embankment material consists of hard, metamorphic rock (greenstone) excavated from adjacent cuts. It is very coarse-graded with only a small percentage of fines. Geologic exploration in the nearby area indicated that there was a very thin overburden of about 3 to 4 ft over foundation rock consisting of weathered and broken greenstone to a depth of about 20 ft and underlain by hard hornblende andesite.

The test section of the Jail Gulch embankment is instrumented to measure horizontal movement, vertical settlement, and soil stresses at four levels.

FIELD MEASUREMENTS

Horizontal Movement

The horizontal movements were measured by horizontal movement platforms and turn pots placed within the fill and surveys on surface monuments. The most significant horizontal movement for all movement platforms and surface monuments occurred in the period from the beginning to about 100 days after completion of the embankment. Figure 1 shows the contours of the horizontal displacements at 15 months after completion of construction. The largest movements occurred near the midheight of the embankment. Because of the unsymmetrical configuration of the embankment, the contour of zero movement occurred to the right of the centerline.

Publication of this paper sponsored by Committee on Embankments and Earth Slopes.

Vertical Movement

Vertical movements were measured by settlement platforms and surveys on surface monuments. Contours of vertical settlements 15 months after completion of construction are shown in Figure 2. The magnitude of settlement at any point at each level depends on the height of fill above that level and the depth between the instrumentation level and the foundation rock surface. A maximum settlement of 1.53 ft was measured at the B-instrumentation level on centerline on completion of the embankment. The settlements at this point were 1.66 ft and 1.74 ft respectively at 100 days and 15 months after completion of construction. It was expected that the maximum settlement would occur near C-level where the midheight of the embankment is located. The depth of overburden including weathered rocks above the foundation rock was assumed to be approximately 20 ft based on explorations at adjacent areas, and it was anticipated that the settlement, because of compression of the foundation overburden, would be small. The fact that the maximum settlement occurred at the B-level indicates a possibility that the actual depth of overburden and weathered rock was greater than anticipated, resulting in larger settlement due to compression in the foundation overburden. No borings were made to investigate the actual depth of overburden at the test section. Because there are no settlement data measured at the foundation boundary, the contours were connected by dashed lines based on estimates. Settlement platforms should be installed in the foundation overburden in future research projects.

Soil Stresses

Soil pressure cell groups were embedded in the embankment to measure vertical, horizontal, and inclined stresses. Although the measured soil pressures generally conform to the increase in embankment overburden pressure, the magnitude of measured pressure was found to vary somewhat with the type of bedding material. Generally, the cells embedded in sand indicated more consistent measurements compared to those embedded in clay or random fill material.

The soil stresses measured at completion of the fill are given in Table 1. These data indicate that the vertical stresses measured at PCG-1, -4, and -7 are generally in reasonably good agreement with the embankment overburden pressure with a difference of only 5 to 10 percent. The embankment overburden pressures were computed assuming a constant unit weight of 140 lb/ft^3 for the fill. The measured lateral horizontal stresses vary from 10 to 60 percent of embankment overburden. The longitudinal horizontal stresses and the 45-deg inclined stresses are within 10 to 80 percent of embankment overburden except at PCG-2 where 125 percent of embankment overburden was recorded. The major and minor principal stresses and the maximum shear stresses were also calculated from the measured stresses (Table 1). These calculated stresses appear to be of the proper order of magnitude.

FINITE-ELEMENT ANALYSIS

A computer program using finite-element method of analysis was developed for this project. This program permits the use of nonhomogeneous and nonlinear material properties in the evaluation of stresses and deformations in an embankment. It also permits an incremental construction analysis to simulate more closely the placement of successive layers of embankment materials during construction. A finite-element analysis of such nature has been used previously (3, 5, 9).

A finite-element analysis requires evaluation of the elastic constants of the embankment material. One method of calculating the nonlinear tangent modulus of soils was proposed by Duncan (4) using initial tangent modulus, shear strength parameters, and principal stresses at failure.

Chang et al. (2) proposed a basic equation for calculating the tangent modulus, E_t, of soils as

$$E_t = E_i \left[1 - \frac{\gamma H \sin \phi \, (1 - \sin \phi)}{2c \cos \phi + 2q \sin \phi}\right]^2 \qquad (1)$$

Figure 1. Contours of horizontal displacement.

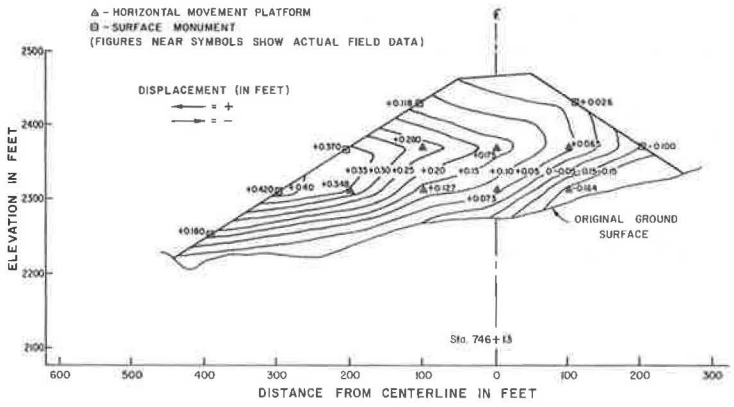

Figure 2. Contours of settlement.

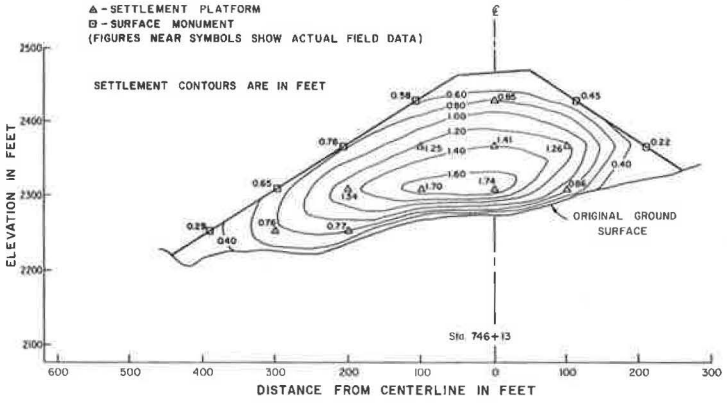

Table 1. Summary of soil stress measured at completion of fill.

Designation	Orientation	Stress Location PCG-1	PCG-2	PCG-3	PCG-4	PCG-5	PCG-6	PCG-7	PCG-8	PCG-9
σ_a	Vertical	58[a] (110)	110[a] (105)	20[a] (40)	100[a] (90)			50[a] (90)	42[a] (45)	35[a] (65)
σ_b	Lateral horizontal	18[a] (30)	35[a] (32)	30[a] (60)	35[a] (32)			0[a] (0)	60[a] (60)	6[a] (10)
σ_c	Longitudinal horizontal	42 (80)	53 (50)	30 (55)	33 (30)			10 (20)	40 (40)	10 (20)
σ_d	Laterally inclined 45 deg	17[a] (30)	45[a] (40)	16[a] (30)	24[a] (20)	36 (25)	90 (80)	16[a] (30)	43[a] (45)	40[a] (75)
σ_e	Laterally inclined 45 deg		132 (125)		60 (55)				40 (40)	
σ_f	Longitudinally inclined 45 deg				60 (55)					
σ_g	Longitudinally inclined 45 deg				30 (25)					
σ_1	Major principal	67 (127)	119 (114)	35 (70)	122 (110)			52 (93)	63 (68)	45 (84)
σ_2	Minor principal	9 (17)	26 (25)	15 (30)	13 (12)			2 (4)	39 (42)	-4 (7)
τ_{max}	Maximum shear	25 (46)	47 (45)	10 (20)	55 (50)			25 (45)	12 (13)	25 (46)

Note: Numbers without parentheses give soil stresses in psi; numbers within parentheses give soil stress in percentage of embankment pressure directly above each pressure cell group.

[a]Used to compute the major and minor principal stresses and the maximum shear stresses.

where

E_t = initial tangent modulus in pounds per square foot,
c, ϕ = shear strength parameters determined from ultimate strength criterion (c is expressed with unit in pounds per square foot),
γ = density of soil in pounds per cubic foot,
H = height of embankment overburden in feet,
$N_\phi = \tan^2(45 \text{ deg} + \phi)$, and
$q = \frac{\gamma H}{N_\phi} - \frac{2c}{(N_\phi)}$.

The initial tangent modulus can be expressed in a linear form as suggested by Scheidig (11)

$$E_t = A + B\sigma_3 \tag{2}$$

and by Janbu (8) in an exponential form,

$$E_t = K(\sigma_3)^n \tag{3}$$

Based on the finding by Jaky (7) and Brooker and Ireland (1), the principal stress σ_3 can be expressed as

$$\left.\begin{aligned} \sigma_3 &= (1 - \sin\phi)\sigma_1 \\ \sigma_3 &= (1 - \sin\phi)\gamma H \end{aligned}\right\} \tag{4}$$

where σ_1 is assumed to be equal to the vertical embankment overburden pressure. The constants A, B, K, and n are determined from arithmetic and log-log plots using the values of E_t and the confining pressures, σ_3, obtained from triaxial compression tests. The Poisson's ratio was also calculated by using the stress-strain and volume change data obtained from triaxial compression tests of the Jail Gulch material and by using the equation proposed by Duncan (4).

$$\mu = \frac{\Delta\xi_v - \Delta\xi_a}{2\Delta\xi_a} \tag{5}$$

where

μ = Poisson's ratio,
$\Delta\xi_a$ = incremental axial strain, and
$\Delta\xi_v$ = incremental volumetric strain.

The relation between the calculated values of Poisson's ratio and the corresponding deviator stress is shown in Figure 3. This figure indicates that, for a given confining pressure, the Poisson's ratio increases approximately linearly with deviator stress. All values of μ fell within a range of 0.05 to 0.5 regardless of the magnitude of confining pressure. Poisson's ratio values of 0.25, 0.3, and 0.4, which are near the midpoints of the test data shown in Figure 3, were selected for use in the finite-element analysis.

In the finite-element method of analysis, the cross section of a solid mass is divided into a finite number of elements connected at nodal points. The finite-element mesh model for the Jail Gulch embankment is shown in Figure 4. Based on the exploration data of the surrounding area, an overburden of 20 ft in depth was assumed in the foundation. Boundary limits of zero deformation were assumed at 100 ft in the foundation rock and 100 ft and 150 ft away from the right and left toes of the embankment respectively. The embankment was divided into nine horizontal layers to simulate incremental construction. Incremental construction analysis involves calculation of stresses and deformations in a successive superposition procedure.

The foundation rock and overburden were assumed to be weightless. The modulus of elasticity of the foundation rock was estimated to be 4.4×10^8 lb/ft^2 based on Fairhurst (6). The modulus is the dynamically determined in situ modulus for andesite rock.

The modulus of the foundation overburden was assumed to be the same as that obtained from the JG-1 sample material. The nonlinear tangent moduli were calculated in accordance with the embankment load corresponding to the assumed sequence of incremental construction. As mentioned previously, Poisson's ratios of 0.25, 0.30, and 0.40 were introduced separately in the analysis. However, it was found that the magnitude of the maximum displacement, calculated from the trial analyses using tangent modulus values computed from the linear expression for initial tangent modulus and a Poisson's ratio of 0.30, was in best agreement with the maximum measured value of the field displacement. This Poisson's ratio value of 0.3 is consistent with the finding by Richart, Hall, and Woods (10) for soils of this type. The results of the finite-element analysis are presented as follows.

Vertical Displacements

The contours of the calculated settlements from finite-element analysis are shown in Figure 5. The calculated maximum settlement was 1.94 ft, which compares reasonably well with the largest measured settlement of 1.74 ft at 15 months after completion of the embankment. However, the distribution pattern of the calculated settlement does not compare as favorably with that measured (Fig. 2). The maximum field settlement occurred near the bottom third of the embankment, whereas the calculated maximum settlement was located near the midpoint.

The discrepancies are thought to be attributed largely to initial settlement. The actual initial settlement that occurred below any settlement platform level was undetected in the construction process because the fill was placed to the planned elevation. However, in the computer analysis, the calculated settlement includes the initial settlements of each layer of fill placed due to the increase in gravity load of subsequently placed layers. Thus, the calculated results indicate a greater value of settlement and a higher elevation of the maximum settlement to occur in the embankment.

Horizontal Displacements

The contours of calculated theoretical horizontal displacements are shown in Figure 6. A comparison of this figure with the measured horizontal movements in Figure 1 shows that the calculated values are generally larger than those measured near the slopes of the embankment, particularly on the left side. Good agreements are seen in surface horizontal movements and the position of zero horizontal movement contour.

Stresses

The magnitude of calculated vertical stresses agrees reasonably closely with the embankment overburden pressure. Contours of the calculated vertical stresses are shown in Figure 7. The measured vertical stresses are also shown in this figure with the magnitude indicated in parentheses.

Contours of the calculated lateral stresses are shown in Figure 8 along with field-measured stresses. The agreement between measured and calculated lateral stresses is generally good except at PCG-8.

Generally, the results of the finite-element analysis of stresses and deformations correspond quite closely with observed behavior in both the magnitude and pattern of movements. Some factors that could influence the accuracies of the analysis results are believed to be as follows:

1. A two-dimensional finite-element analysis was made. The Jail Gulch embankment is constructed across a V-shaped canyon where three-dimensional analysis would have been more appropriate. Some longitudinal strains were detected by turn pot 13 along the longitudinal axis of the embankment, which indicates the possible error due to the two-dimensional assumption.

Figure 3. Variation of Poisson's ratio with deviator stress and confining pressure.

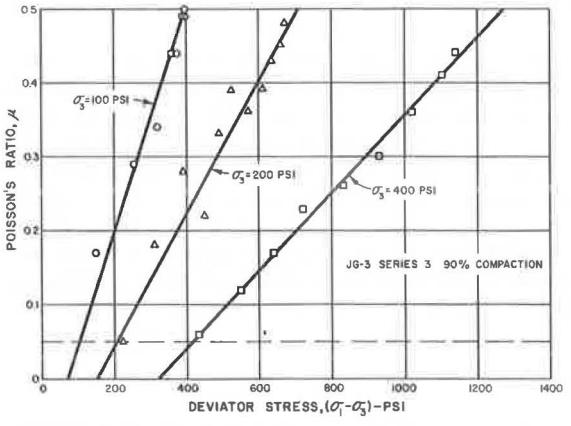

Figure 4. Finite-element mesh for Jail Gulch embankment (station 746+13).

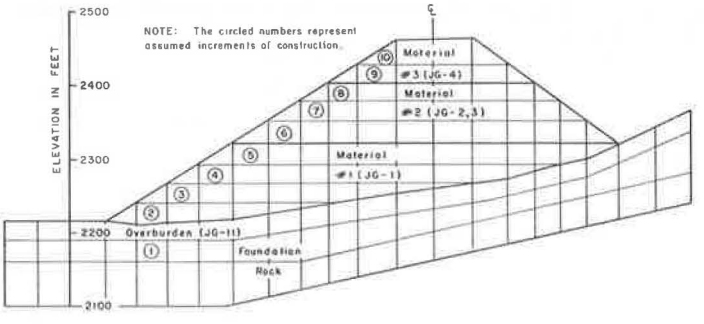

Figure 5. Contours of theoretical settlement.

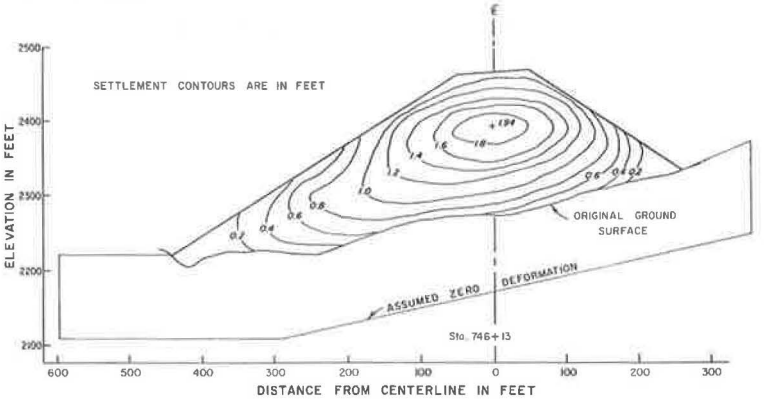

Figure 6. Contours of theoretical horizontal movement.

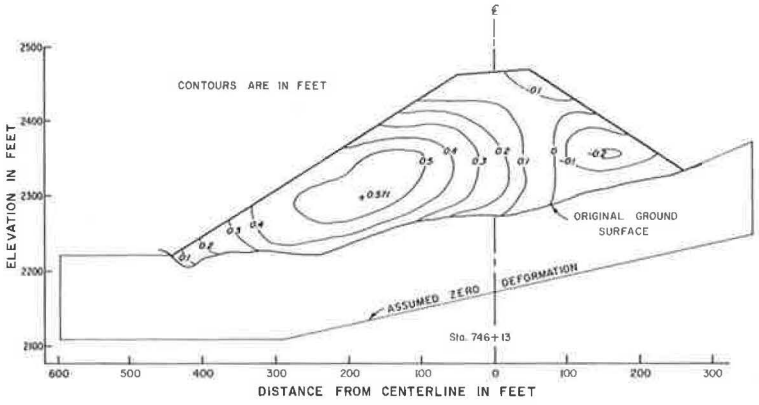

Figure 7. Contours of theoretical vertical stress.

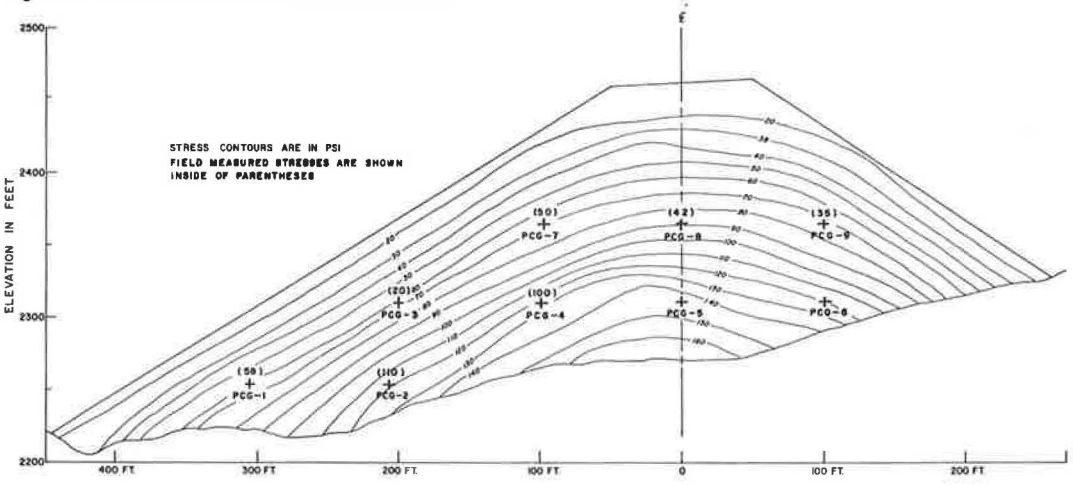

Figure 8. Contours of theoretical lateral stress.

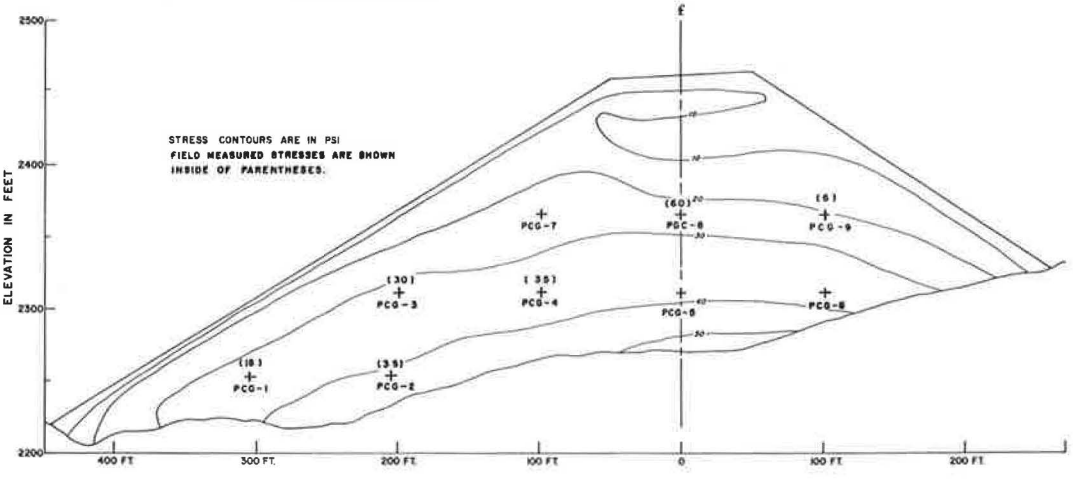

2. The embankment material was nonuniform. The embankment was assumed to consist of only three types of soils with different elastic properties as determined from the laboratory tests on four soil samples. These did not include the large rocks prevalent in the actual embankment.

3. The equations for tangent modulus were simplified by assuming that (σ_1) ult = (σ_1) even though the theoretical maximum stresses in the embankment do not reach the plastic equilibrium condition at any point. These equations were further simplified by assuming that the embankment pressure represents the major principal stress in order to eliminate the unlimited iteration in the computing process. In addition, nonlinearity of the Poisson's ratio was not introduced into the finite-element analysis because of the limitation of available laboratory test data. A constant value of 0.3 was selected to represent the Poisson's ratio in the entire embankment material in the final analyses.

CONCLUSIONS

The study substantiates the following conclusions:

1. Most of the soil stresses measured by pressure cells in the Jail Gulch embankment responded proportionally to the embankment load. The soil stresses generally became stabilized when the fill reached its final grade directly above the point where the soil stresses were measured.

2. The measured deformations in the Jail Gulch embankment increased generally in proportion to the height of the embankment. However, these deformations continued at a significant rate until approximately 100 days after completion of fill. The deformations increased continuously through the observation period of 15 months after completion of fill, but the rate of increase became progressively smaller.

3. The theoretical calculations of stresses and deformations using two-dimensional finite-element analysis in general compare favorably with measured values. In the method of analysis used, the evaluation of the elastic constants was found to be the most important factor in the prediction of the embankment performance.

4. The successful application of finite-element method in evaluating the performance of the Jail Gulch embankment indicates that this method may be more extensively used in the future as a design tool.

ACKNOWLEDGMENTS

The contribution by L. R. Herrman, University of California, Davis, in developing the computer program for the finite-element analysis of embankment under a service contract for this research project is appreciated. This work was done under the HPR Work Program in cooperation with the Federal Highway Administration. The contents of this paper reflect the views of the authors who are responsible for the facts and the accuracy of the data presented herein. The contents do not necessarily reflect the official views or policies of the state of California or the Federal Highway Administration. This paper does not constitute a standard, specification, or regulation.

REFERENCES

1. Brooker, E. W., and Ireland, H. O. Earth Pressures at Rest Related to Stress History. Canadian Geotechnical Jour., Vol. 2, Feb. 1965.
2. Chang, J. C., Forsyth, R. A., Shirley, E. C., and Smith, T. W. Stresses and Deformations in Jail Gulch Embankment. California Division of Highways, Interim Rept. MR632509, Feb. 1972.
3. Clough, R. W., and Woodward, R. J. Analysis of Embankment Stresses and Deformation. Jour. Soil Mech. and Found. Div., Proc. ASCE, Vol. 93, No. SM4, July 1967.
4. Duncan, J. M. Stress Deformation and Strength Characteristics, Including Time Effects. Proc. 7th Internat. Conf. on Soil Mech. and Found. Eng., Mexico City, 1969, p. 164.
5. Duncan, J. M., and Chang, C. Y. Nonlinear Analysis of Stress and Strain in Soils. Jour. Soil Mech. and Found. Div., Proc. ASCE, Vol. 96, No. SM5, Sept. 1970.

6. Fairhurst, C. Proc. 5th Symposium on Rock Mechanics. Pergamon Press, 1963, p. 528.
7. Jaky, J. Pressure in Soils. Proc. 1st Conf. on Soil Mech. and Found. Eng., Rotterdam, 1948.
8. Janbu, N. Soil Compressibility as Determined by Oedometer and Triaxial Tests. European Conf. on Soil Mech. and Found. Eng., Wiesbaden, Vol. 1, 1963.
9. Kulhawy, F. H., and Duncan, J. M. Nonlinear Finite Element Analysis of Stresses and Movements in Oroville Dam. Dept. of Civil Engineering, Univ. of California, Berkeley, Rept. TE-70-2, 1970.
10. Richart, F. E., Jr., Hall, J. R., Jr., and Woods, R. D. Vibrations of Soils and Foundations. Prentice-Hall, Inc., Englewood Cliffs, New Jersey, 1970, p. 352.
11. Scheidig, A. Tests on the Deformation of Sand and Their Application to the Settlement Analysis of Buildings. MS thesis, Vienna, 1931.

STRESSES AND STRAINS IN VISCOELASTIC MULTILAYER SYSTEMS SUBJECTED TO MOVING LOADS

Y. H. Huang, University of Kentucky

A method programmed for a high-speed computer is developed for determining the stresses and strains in viscoelastic multilayer systems subjected to moving loads. The method, which can be applied to systems consisting of any number of layers and any type of linear viscoelastic materials, is based on the principle of elastic-viscoelastic correspondence and an approximate procedure of collocation. Numerical solutions, which do not consider the inertia effect, are presented for the stresses and strains in a four-layer system. Of particular interest are the compressive stresses and strains on the surface of the subgrade, layer 4, and the tensile strains at the bottom of the asphalt-bound layer, layer 1, because these stresses and strains have been suggested as criteria for pavement design and evaluation. A study of these critical stresses and strains shows that they all decrease with the increase in speed of the moving load. If the compressive stress on the subgrade is considered as a criterion, either the vertical or the principal stress can be used with little difference. However, if the compressive strain on the subgrade or the tensile strain in the asphalt-bound layer is considered, a criterion based on the vertical or the radial strain will be certainly quite different from that based on the principal strain because of the significant effect of the shear strain.

•BECAUSE of the time-dependent behavior of paving materials, there has been a growing belief that pavement design and evaluation should be based on viscoelastic theory rather than the conventional elastic theory. Although elastic theory has been used successfully for determining the stresses and strains in flexible pavements under moving loads, its successful application requires the judicious selection of a Young's modulus and a Poisson's ratio for each of the component layers. An alternative, which is more direct and not so arbitrary, is first to determine the viscoelastic properties of the materials forming the component parts of the pavement and then apply the viscoelastic theory for computing the stresses and strains in the pavement under actual moving loads. This approach was employed by Perloff and Moavenzadeh (1) for determining the surface deflection of a viscoelastic half-space, by Chou and Larew (2) for the stresses and displacements in a viscoelastic two-layer system, and by Elliot and Moavenzadeh (3) for those in a three-layer system. For viscoelastic systems of more than three layers, very little work has been done in the case of moving loads, although a method based on the Duhamel superposition integral was presented by Barksdale and Leonards (4) for analyzing four-layer viscoelastic systems under repeated loads, which was later employed by Elliot and Moavenzadeh (3) for analyzing both the repeated and the moving loads. Because actual flexible pavements are generally composed of multiple layers, an analysis of viscoelastic multilayer systems subjected to moving loads is of practical significance.

The purpose herein is to present a new and more effective method, programmed for a high-speed computer, for determining the stresses and strains in a viscoelastic

Publication of this paper sponsored by Committee on Mechanics of Earth Masses and Layered Systems.

multilayer system due to a circular load moving at a constant speed on the surface. Although the example given is limited to a four-layer system with each layer characterized by a constant Poisson's ratio and a simple mechanical model, the method can be applied to systems consisting of any number of layers and any type of linear viscoelastic materials. In view of the general belief that the fatigue cracking of asphalt pavements is caused by the repeated application of excessive tensile strains at the bottom of the asphalt-bound layer and that the rutting of pavement surfaces is caused by excessive compressive stresses or strains at the surface of the subgrade (5, 6), numerical results on the strains at the bottom of the first layer and the stresses and strains at the top of the fourth layer are presented to illustrate the effect of time and speed on these critical stresses and strains. In line with all previous studies, inertia forces are not considered in the analysis.

STATEMENT OF PROBLEM

Figure 1 shows an n-layer system, the Young's modulus and the Poisson's ratio of the j th layer being $(E)_j$ and $(\nu)_j$ respectively. For a linear elastic system, both $(E)_j$ and $(\nu)_j$ are constants independent of time; for a linear viscoelastic system, they are linear time operators. A uniform load of intensity q is applied on the surface over a circular area of radius a and moves with a constant velocity, v, from a distant point toward a point 0 on the surface along a straight path. It is convenient to consider the time as zero, i.e., t = 0, when the center of the load just arrives at point 0, as negative before the load reaches point 0, and as positive after the load passes point 0. The distance, r, between the load and point 0 at any given time, t, is $r = v|t|$. The problem now on hand is to determine the stresses and strains at any point directly beneath point 0 as a function of time. The restriction that the load moves toward point 0 along a straight path is a practical way to simplify the problem because experience indicates that most pavement distress is along the wheelpath; so point 0 may be considered as a given point in the wheelpath.

It is further assumed that the layers are in continuous contact as indicated by the continuity in vertical stress, shear stress, vertical displacement, and radial displacement and that the surface is free of shear stress.

ELASTIC SOLUTION

Before viscoelastic solutions can be developed, elastic solutions must be obtained. The stresses in an elastic multilayer system under a circular loaded area can be expressed as (7)

$$\sigma_z = q\alpha \int_0^\infty J_1(m\alpha)J_0(m\rho)\phi(m)dm \tag{1a}$$

$$\sigma_r = q\alpha \int_0^\infty J_1(m\alpha)\left\{\left[J_0(m\rho) - \frac{J_1(m\rho)}{m\rho}\right]\phi_1(m) + J_0(m\rho)\phi_2(m)\right\} dm \tag{1b}$$

$$\sigma_\theta = q\alpha \int_0^\infty J_1(m\alpha)\left[\frac{J_1(m\rho)}{m\rho}\phi_1(m) + J_0(m\rho)\phi_2(m)\right] dm \tag{1c}$$

$$\tau_{rz} = q\alpha \int_0^\infty J_1(m\alpha)J_1(m\rho)\phi_3(m)dm \tag{1d}$$

in which σ_z, σ_r, σ_θ, and τ_{rz} = vertical, radial, tangential, and shear stresses respectively; q = intensity of the uniformly applied load; α = a/H; a = radius of loaded area;

H = depth from surface to the upper boundary of the lowest layer; J_0 and J_1 = Bessel functions of the first kind and order, 0 and 1 respectively; $\rho = r/H$; r = radial distance from the center of loaded area to the point at which stresses are to be determined; m = a parameter of integration; and ϕ, ϕ_1, ϕ_2, and ϕ_3 = functions of elastic constants, layer thicknesses, the vertical coordinate of the point in question, as well as the parameter of integration, m. Once the stresses are known, the strains can be determined by

$$(\epsilon_z)_j = \frac{1}{(E)_j}\left[\sigma_z - (\nu)_j(\sigma_r + \sigma_\theta)\right] \tag{2a}$$

$$(\epsilon_r)_j = \frac{1}{(E)_j}\left[\sigma_r - (\nu)_j(\sigma_\theta + \sigma_z)\right] \tag{2b}$$

$$(\epsilon_\theta)_j = \frac{1}{(E)_j}\left[\sigma_\theta - (\nu)_j(\sigma_z + \sigma_r)\right] \tag{2c}$$

$$(\gamma_{rz})_j = \frac{1}{(G)_j}\tau_{rz} \tag{2d}$$

in which ϵ_z, ϵ_r, ϵ_θ, and γ_{rz} = vertical, radial, tangential, and shear strains respectively; E = Young's modulus; ν = Poisson's ratio; and the subscript j outside the parentheses indicates the j th layer.

VISCOELASTIC SOLUTION

In presenting numerical results, it is desirable to use a dimensionless velocity, V, and a dimensionless time, T, defined as

$$V = \frac{v\tau^*}{H} \tag{3}$$

$$T = \frac{t}{\tau^*} \tag{4}$$

in which τ^* is one of the retardation times used for describing material properties. Note that $\rho = V|T|$.

For brevity, only the vertical stress, σ_z, will be used for illustration. It must be borne in mind that the same procedure can be employed for determining other stresses and strains as well.

The viscoelastic solution can be obtained by applying the elastic-viscoelastic correspondence principle originally developed by Lee (8). Instead of considering directly the stress, strain, and load, the Laplace transform of stress, the Laplace transform of strain, and the Laplace transform of load are considered. Application of the correspondence principle involves the following steps:

1. Taking the Laplace transform of the time-dependent boundary conditions;
2. Changing the elastic field equations by replacing E, which is a ratio between stress and strain, with $\overline{E}(p)$, which is a ratio between the Laplace transform of stress and the Laplace transform of strain, and also replacing ν with $\overline{\nu}(p)$;
3. Solving the resulting problem in terms of the transformed variable p; and
4. Inverting the solution involving the transformed variables into time variable.

Based on the preceding principle, Eq. 1a, which is based on elasticity, can still be applied for viscoelastic media, if the stress, σ_z, is replaced by the Laplace transform of stress, $\overline{\sigma}_z$, the time-dependent boundary or the moving load $qJ_o(mV|T|)$ by $q\overline{J}_o(mV|T|)$, as indicated in step 1, and $\phi(m)$, which involves E and ν, by $\overline{\phi}(m,p)$, as indicated in step 2. Note that $\overline{\phi}(m,p)$ is obtained by replacing E and ν in the expression for $\phi(m)$ by $\overline{E}(p)$ and $\overline{\nu}(p)$. Consequently, the resulting problem in terms of p, as indicated in step 3, can be written as

$$\bar{\sigma}_z = q\alpha \int_0^\infty J_1(m\alpha)\bar{J}_0(mV|T|)\bar{\phi}(p, m)dm \tag{5}$$

The bar on top of σ_z, J_0, and ϕ denotes the Laplace transform and implies that they are functions of the transformed variable p. Note that $\bar{J}_0$ is a function of load, and $\bar{\phi}$ is a function of material properties. The determination of $\bar{\phi}$ from material properties was described elsewhere (9). To complete step 4, Eq. 5 can be inverted by the convolution theory as

$$\sigma_z = q\alpha \int_0^\infty \int_{-\infty}^{T} J_1(m\alpha)\left[J_0(mV|\tau|)\ \phi(T - \tau, m)d\tau\right]dm \tag{6}$$

The same procedure can be used for determining other stresses. The radial stress has three terms involving Bessel functions $J_0(mV\ |\tau|)$ and $J_1(mV\ |\tau|)$; each must be evaluated independently and then combined. The same is true for the tangential stress, which involves two terms to be evaluated.

By the correspondence principle, Eq. 2a can be written as

$$(\bar{\epsilon}_z)_j = \frac{\bar{\sigma}_z}{(\bar{E})_j} - \frac{(\bar{\nu})_j}{(\bar{E})_j}\bar{\sigma}_r - \frac{(\bar{\nu})_j}{(\bar{E})_j}\bar{\sigma}_\theta \tag{7}$$

$\bar{\sigma}_z/(\bar{E})_j$ can be inverted in the same way as $\bar{\sigma}_z$, except that $\bar{\phi}$ is replaced by $\bar{\phi}/(\bar{E})_j$. The same procedure can be applied to $-(\bar{\nu})_j\bar{\sigma}_r/(\bar{E})_j$ and $-(\bar{\nu})_j\bar{\sigma}_\theta/(\bar{E})_j$; their summation gives the vertical strain $(\epsilon_z)_j$.

LAPLACE INVERSION

The major difficulty of the preceding procedure lies in the Laplace inversion of $\bar{\phi}(p, m)$ to $\phi(T, m)$. Because exact inversion is difficult, if not impossible, for a multilayer system, an approximate method of collocation is employed.

The function of $\bar{\phi}(p, m)$ is a ratio of two polynomials in p. Depending on the stress or strain to be determined and the models used to characterize the materials, the degree of the polynomial in the denominator may be equal to or greater than that in the numerator. If both have the same degree, $\bar{\phi}(p, m)$ must be separated into a constant, s_o, plus a ratio, $\bar{\Psi}(p, m)$, the denominator of which has degrees higher than the numerator.

$$\bar{\phi}(p, m) = s_o + \bar{\Psi}(p, m) \tag{8}$$

The value of s_o can be determined from $\bar{\phi}(p, m)$ by assigning a very large value, e.g., 10^{10}, to p.

$$s_o = [\bar{\phi}(p, m)]_{p=10^{10}} \tag{9}$$

If the denominator of $\bar{\phi}(p, m)$ has a higher degree, s_o automatically approaches zero when a large p is assigned. Substituting Eq. 8 into Eq. 5 gives

$$\bar{\sigma}_z = q\alpha \int_0^\infty J_1(m\alpha)\ \bar{J}_0(mV|T|)\ [s_o + \bar{\Psi}(p, m)]dm \tag{10}$$

The inversion of Eq. 10 is

$$\sigma_z = q\alpha \int_0^\infty J_1(m\alpha)\left[s_o J_0(mV|T|) + \int_{-\infty}^{T} J_0(mV|\tau|)\ \Psi(T - \tau, m)d\tau\right]dm \tag{11}$$

In the collocation method, it is assumed that $\Psi(T, m)$ can be expressed approximately by a Dirichlet series of decaying exponentials

$$\Psi(T, m) = \sum_{i=1}^{n} s_i \exp(-p_i T) \tag{12}$$

in which s_i and p_i = constants and n = number of terms. This approximation is possible because $\Psi(T, m)$ is a monotonic increasing or decreasing function of T. The collocation method cannot be applied directly to the stresses and strains, as in the case of stationary loads, because under moving loads they are not monotonic functions of T. Take the Laplace transforms of Eq. 12 and then multiply by p:

$$p\Psi(p, m) = \sum_{i=1}^{n} \frac{s_i}{1 + \frac{p_i}{p}} \tag{13}$$

In this study, eight exponential terms are used to approximate $\Psi(T, m)$. The assumed values of p_i are 0.02, 0.05, 0.1, 0.2, 0.5, 1, 10, and 100. Theoretically, the values of p selected depend on the time range within which the stresses and strains are to be analyzed. Schapery (10) suggested the relation between p and T as $p = \frac{1}{2}T$, so a range of p from 0.02 to 100 is equivalent to a range of T from 25 to 0.005. By successively assigning p in Eq. 13 to each of the preceding values, eight simultaneous equations are obtained that will give a solution to the unknowns, s_1 through s_8.

$$\begin{Bmatrix} \frac{1}{1+\frac{0.02}{0.02}} & \frac{1}{1+\frac{0.05}{0.02}} \cdots \frac{1}{1+\frac{100}{0.02}} \\ \frac{1}{1+\frac{0.02}{0.05}} & \frac{1}{1+\frac{0.05}{0.05}} \cdots \frac{1}{1+\frac{100}{0.05}} \\ \vdots & \vdots \\ \frac{1}{1+\frac{0.02}{100}} & \frac{1}{1+\frac{0.05}{100}} \cdots \frac{1}{1+\frac{100}{100}} \end{Bmatrix} \begin{Bmatrix} s_1 \\ s_2 \\ \vdots \\ s_8 \end{Bmatrix} = \begin{Bmatrix} p[\bar{\varphi}(p, m) - s_0]_{p=0.02} \\ p[\bar{\varphi}(p, m) - s_0]_{p=0.05} \\ \vdots \\ p[\bar{\varphi}(p, m) - s_0]_{p=100} \end{Bmatrix} \tag{14}$$

Once s_i is known, $\Psi(T, m)$ can be determined from Eq. 12 and σ_z from Eq. 11.

NUMERICAL INTEGRATION

Most of the computer time used in the viscoelastic analysis is for the evaluation of two infinite integrals, one with respect to time and the other to m. Without involving excessive computer times, accuracy can be ensured by selecting the proper increments in performing the numerical integration.

The inner integral in Eq. 11 is evaluated by a five-point Gaussian quadrature formula. The zeros of Bessel functions, J_0 and J_1, and the values of the functions at the five points between 2 zeros are stored in the computer and used repeatedly to save computer time.

When $T \leq 0$, let $x = -mV\tau$; the inner integral in Eq. 11 becomes

$$I = \frac{1}{mV} \int_{mV|T|}^{\infty} J_0(|x|)\Psi(T + \frac{x}{mV}, m)\, dx \tag{15}$$

Equation 15 is integrated numerically from $mV|T|$ to a large value until the integral converges. It is found that integration up to 40 cycles of the Bessel functions is sufficient, so a limit of 40 cycles is imposed to save computer times. A five-point Gaussian quadrature formula is used to evaluate the integral between 2 zeros of the Bessel function and between the starting point and the next nearest zero.

When $T > 0$, the inner integral in Eq. 11 can be divided into two parts:

$$I = \int_{-\infty}^{0} J_0(mV|\tau|)\Psi(T - \tau, m)d\tau + \int_{0}^{T} J_0(mV|\tau|)\Psi(T - \tau, m)\, d\tau \tag{16}$$

Because the shear stress and strain change signs when passing point 0, a negative sign should be used for the integral from 0 to T.

Let $x = -mV\tau$ for the first integral and $x = mV\tau$ for the second; Eq. 16 becomes

$$I = \frac{1}{mV}\int_{0}^{\infty} J_0(|x|)\Psi(T + \frac{x}{mV}, m)dx + \frac{1}{mV}\int_{0}^{mVT} J_0(|x|)\Psi(T - \frac{x}{mV}, m)\, dx \tag{17}$$

The outer integral in Eq. 11 is evaluated by Simpson's one-third rule. The values of m used are 0, 0.01, 0.02, 0.21, 0.4, 0.7, 1.0, and then every 0.5 until the integral converges. Because the increments of integration used in Simpson's rule are 0.005 for $m < 0.02$, 0.085 for $0.02 < m < 0.4$, and 0.1 for $m > 0.4$, a three-point parabolic interpolation formula is used to determine the values of the integrand at the intermediate points.

The analysis of viscoelastic multilayer systems can be summarized as follows:

1. Assign successive values of m starting from zero to a rather large positive value until σ_z converges;
2. For each m, determine s_0 from Eq. 9, s_1 through s_8 from Eq. 14, and the values of the integrand at various times, T, from Eq. 11; and
3. Integrate Eq. 11 by Simpson's rule and parabolic interpolation.

COMPARISON WITH EXISTING METHODS

The method developed in this study is very effective for analyzing multilayer systems and differs significantly from the existing methods by Chou and Larew for two-layer systems and Elliot and Moavenzadeh for three-layer systems (2, 3).

Chou and Larew (2) considered a concentrated moving load instead of a circular load. Because they assumed that the load started from a fixed point at a given distance, R_o, from point 0, they had difficulty in integrating Eq. 6. To obtain correct solutions, they had to exchange the order of integration, i.e., integrating first with respect to m and then with respect to τ. This is a very cumbersome process. First, they divided the time into small increments. At the end of each time increment, a series of m values, e.g., 25, was assumed, and integration was performed with respect to m. If there are 200 time increments, as is usually the case when the load starts from $-\infty$, the collocation method will be applied 200 x 25 or 5,000 times. Therefore, because the computer time for the double integration was just too excessive, they could not obtain numerical results for systems with more than two layers.

The result of this study shows that, by changing the starting point of the load from $-\infty$, instead of from a fixed distance R_o, Eq. 6 could be integrated first with respect to τ and then with respect to m. This means that, for each m, only one collocation is necessary, or a total of only 25 collocations instead of 5,000. The reason that Eq. 6

does not yield correct solutions when the load starts from a fixed distance R_o instead of from $-\infty$ is that the load $J_0(mV|\tau|)$ at the starting time is not negligible when m is small, and the system cannot be considered initially undisturbed as assumed in the Laplace transform of the field equations. However, if the order of integration is exchanged, the problem becomes the determination of stress at various times. Unless R_o is very small, the stress at point 0 when the load starts will be very small, and the system can be considered initially undisturbed.

Elliot and Moavenzadeh (3) employed the Duhamel integral for determining the stresses and displacements under a circular moving load. Their method is different from the author's in that they applied the Duhamel integral, instead of the correspondence principle, in obtaining the viscoelastic solutions. Using the Duhamel integral, the vertical stress in a viscoelastic-layered system, corresponding to Eq. 6, can be written as

$$\sigma_z = q\alpha \int_0^{\infty} \int_{-\infty}^{T} J_1(m\alpha) \left[\frac{\partial}{\partial \tau} J_o(mV|\tau|)\right] \phi_s(T - \tau, m) d\tau dm \qquad (18)$$

in which ϕ_s is the response of the system to a static load and can be obtained by inverting $\bar{\phi}(p, m)/p$. After differentiation, the equation becomes

$$\sigma_z = -q\alpha \int_0^{\infty} \int_{-\infty}^{T} \frac{J_1(m\alpha)}{mV} J_1(mV|\tau|) \phi_s(T - \tau, m) d\tau dm \qquad (19)$$

The reason that the Duhamel integral was not employed in this study is that the differentiation of one term of Bessel function such as J_1 for determining radial, tangential, and shear stresses may generate two terms of Bessel functions, and the evaluation of these additional Bessel functions requires additional computer times. This is particularly significant when determining the strains due to the large number of terms involved.

COMPUTER PROGRAM

The method described in this paper was programmed in FORTRAN IV for an IBM 360 computer available at the University of Kentucky. It is not the intention herein to describe in any detail the computer program. Nevertheless, the capability of the program will be pointed out, so that readers interested in using the program can obtain a complete listing of the program from the author.

Theoretically, the method developed in this study is quite general and can be used to determine the stresses and strains at any point in a multilayer system consisting of any number of layers and any types of linear viscoelastic materials. However, a general program of this type requires considerable computer times and may not be desirable from a practical viewpoint. Consequently, the program was written in a more restrictive way to obtain useful information at a reasonable cost. It is hoped that these restrictions will promote the application of the program instead of limit its usefulness.

The program can only provide solutions for the vertical displacement on the surface and the vertical, radial, tangential, and shear stresses or strains at both the bottom of layer 1 and the top of the lowest layer because these stresses and strains have been considered as important criteria for pavement design and evaluation. The user must specify whether the stresses or strains are to be computed.

In computing the stresses, the transformed shear and bulk moduli of each layer are represented by the quotients of two polynomials, the degrees and coefficients of which must be specified by the user. In computing the strains, the transformed shear moduli and the Poisson's ratios of each layer must be specified. The latter are assumed to be elastic and independent of time. Because the Poisson's ratios have relatively small effect on the strains, this simplification will save a great deal of computer time without affecting the results significantly.

Computer storage is reduced by dimensioning to take care of up to six layers using a maximum of 12 values of the transformed variables for the collocation. The displacement, stresses, or strains at 20 different times are computed simultaneously. These restrictions can easily be removed by merely increasing the dimensions of the parameters involved.

NUMERICAL RESULTS

The applicability of the method is demonstrated by using a four-layer system (Fig. 2) to simulate a highway pavement. It is assumed that the surface course of the pavement is asphaltic concrete, the behavior of which under pure shear is characterized by a Burgers model; the base and subbase courses are granular materials, which are considered as elastic; and the subgrade is a soft clay, which is represented by a Maxwell model. The Poisson's ratios of the layers from top down are assumed to be 0.4, 0.3, 0.3, and 0.5 respectively. The total computer time for obtaining all the data presented in this paper by an IBM 360/65 was about 15 min.

Let $(G_1)_1$ be the shear spring constant and $(\tau_1)_1$ be the shear retardation time of the Kelvin element in layer 1. Because $(G_1)_1$ and $(\tau_1)_1$ are assumed unity in Figure 2, the spring constants and relaxation times shown in the various models are not their actual values but are their ratios to $(G_1)_1$ and $(\tau_1)_1$ respectively. If $T = t/(\tau_1)_1$ and the transformed variable of T is p, the transformed shear moduli of the materials are $(\bar{G})_1 = [20p(p + 1)(G_1)_1]/[(p + 1)(2p + 1) + 20p]$, $(\bar{G})_2 = 2(G_1)_1$, $(\bar{G})_3 = (G_1)_1$, and $(\bar{G})_4 = 5p(G_1)_1/(10p + 1)$. Because the Poisson's ratios are assumed time-independent, the transformed Poisson's ratio and the original Poisson's ratio are the same, so

$$(\bar{E})_j = 2[1 + (\upsilon)_j](\bar{G})_j \tag{20}$$

Once the transformed moduli of elasticity and Poisson's ratios are known, $\bar{\phi}(p, m)$ can be evaluated and the stresses and strains determined by the method presented.

Figures 3, 4, and 5 show the stresses and strains in the four-layer system at nine different dimensionless times, T, i.e., -1, -0.75, -0.5, -0.25, 0, 0.25, 0.5, 0.75, and 1. The narrow range of times from -1 to 1 is used because the most critical stresses and strains generally occur within this range, especially when the velocity is high. Two different dimensionless velocities are used: V = 0.25, as indicated by the small circles, and V = 1 by the small triangles. Integration is carried out to m = 10.

In the figures, compressive stresses and strains are considered positive and tensile stresses and strains negative. In addition to the tangential stress or strain, which is one of the principal stresses or strains, two other principal stresses or strains are also shown, the major and minor principal stress or strain. These are the major and minor principal stresses or strains in the rz plane only and may not always be the largest or the smallest of the three principal stresses or strains.

Figure 3 shows the vertical, radial, tangential, shear, and principal stresses at the top of layer 4. The vertical, tangential, and major principal stresses decrease with the increase in speed and become maximum sometime after the load passes point 0. The fact that all three principal stresses are positive implies the nonexistence of tensile stresses. The nearly equal magnitude of vertical and major principal stresses in this critical range indicates that, if rutting is caused by excessive stress in the subgrade, either vertical or major principal stress can be used as a criterion with no significant difference.

Figure 4 shows the vertical, radial, tangential, shear, and principal strains at the top of layer 4. Although both the vertical and the major principal strains decrease with increasing speed, the maximum vertical strain occurs after the load passes point 0, whereas the maximum major principal strain, because of the large component of the shear strain, occurs before the load reaches point 0. In this particular case, where shear strains are large and contribute to a significant portion of the principal strains, a criterion based on the vertical compressive strain will certainly be different from that based on the major principal strain. Note that part of the radial strains and all of the tangential and minor principal strains are negative, even though all stresses are positive at the top of layer 4.

Figure 1. A multilayer system subjected to a moving load.

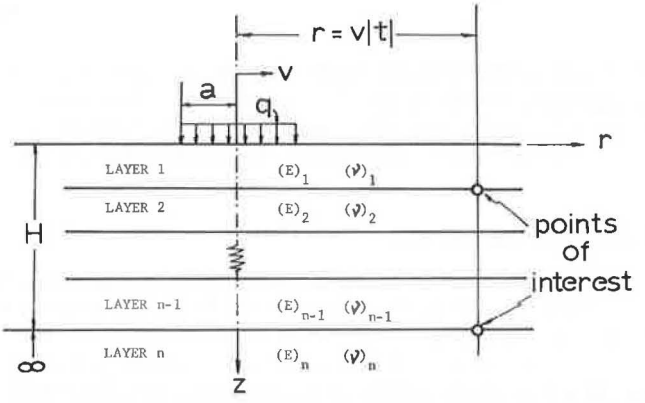

Figure 2. Models characterizing a four-layer system.

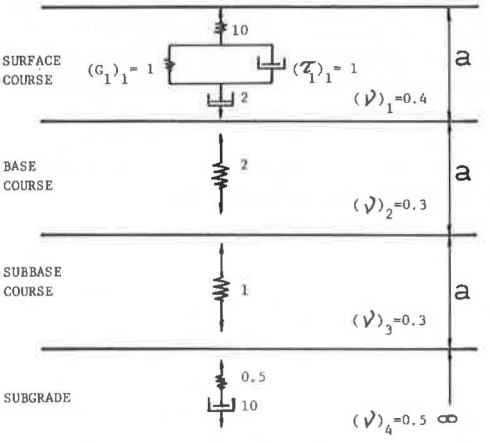

Figure 3. Stresses at top of layer 4.

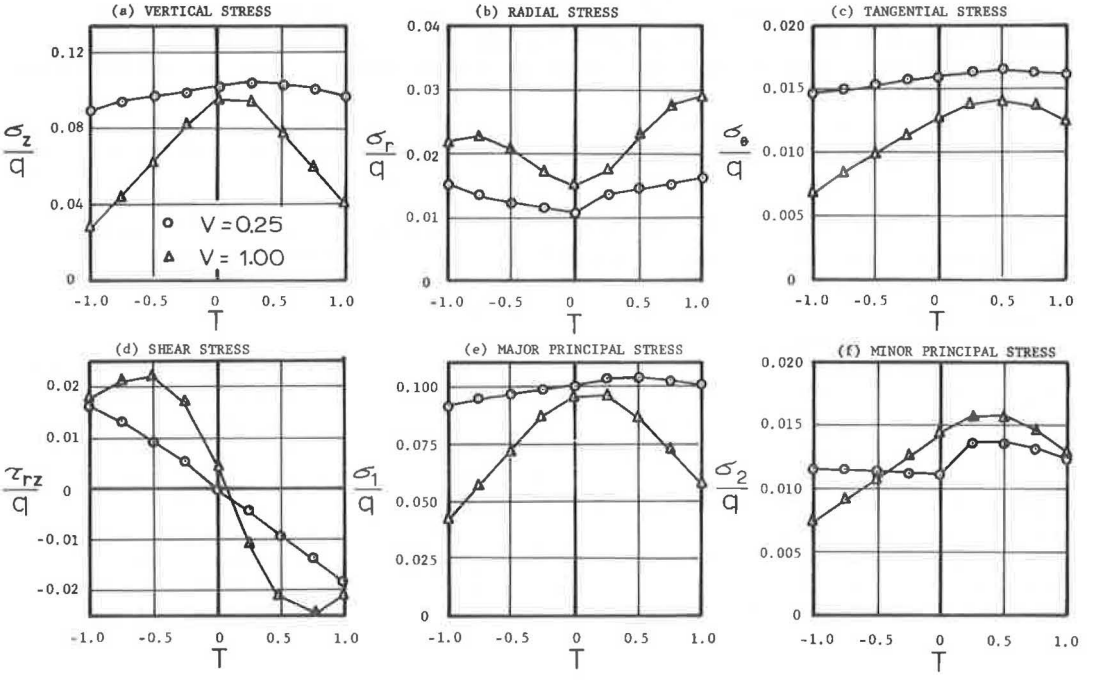

Figure 4. Strains at top of layer 4.

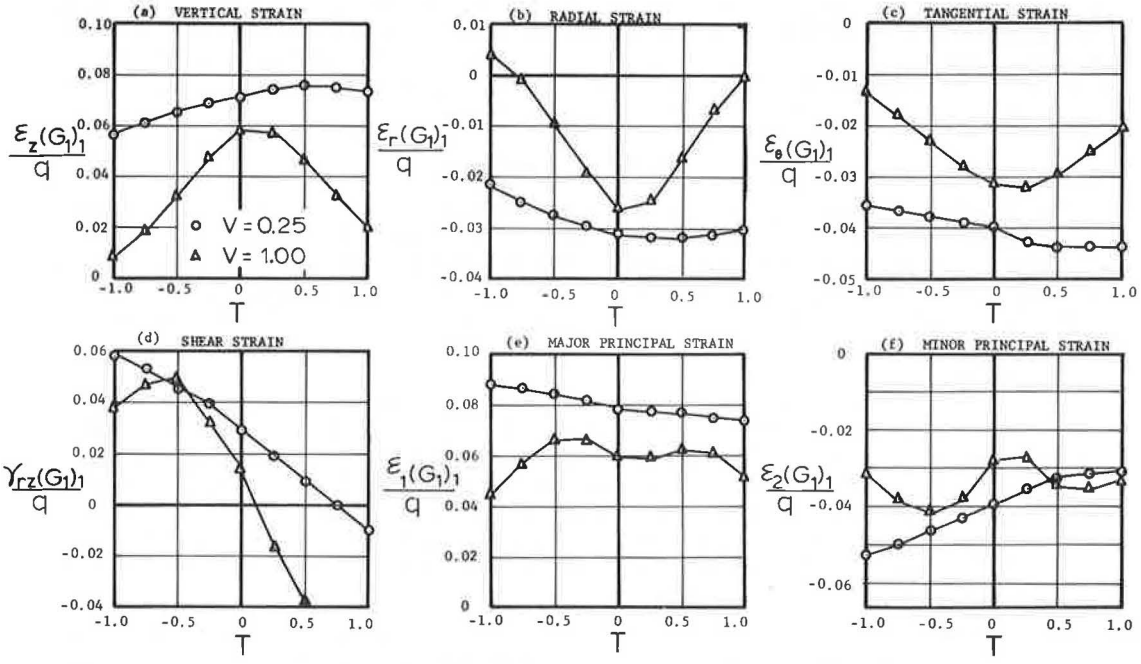

Figure 5. Strains at bottom of layer 1.

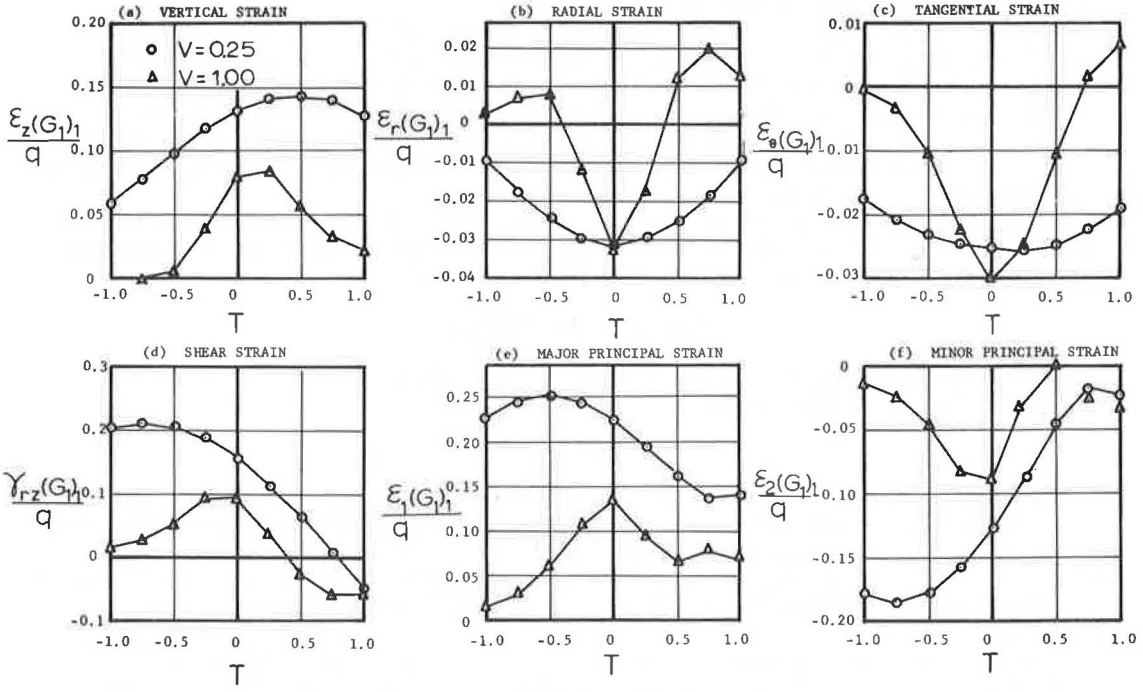

Figure 5 shows the vertical, radial, tangential, shear, and principal strains at the bottom of layer 1. The general trend for the change of strain with time is quite similar to that at the top of layer 4. Because fatigue is caused by excessive tensile strains at the bottom of the asphalt-bound layer, the minor principal strains are of particular interest. The principal tensile strains also decrease appreciably with the increase in speed and arrive at a maximum value before point 0 is reached.

CONCLUSIONS

A method programmed for a high-speed computer is presented for determining the stresses and strains in viscoelastic multilayer systems subjected to moving loads. The elastic solution is briefly described, and the application of the elastic-viscoelastic correspondence principle to change the viscoelastic problem to an associated elastic problem is illustrated. The inversion of the associated elastic problem to the viscoelastic problem is facilitated by using the convolution theory and an approximate method of collocation.

Numerical results are presented for the stresses and strains in a four-layer system consisting of an asphalt-bound surface course, granular base course, granular subbase course, and soil subgrade. Of particular interest are the vertical and principal compressive stresses and strains on the surface of the subgrade, layer 4, and the principal tensile strains at the bottom of the asphalt-bound layer, layer 1, because these stresses and strains have been suggested as criteria for pavement design and evaluation. A study of these critical stresses and strains in the four-layer system subjected to moving loads reveals the following facts:

1. Both the vertical compressive stresses and the major principal stresses at the top of layer 4 decrease with the increase in speed; their maximum values occur at or immediately after the load passes point 0. The predominant contribution of the vertical stress to the principal stress indicates that, if rutting is caused by excessive stresses in the subgrade, there is very little difference whether the design or evaluation is based on the vertical or the principal stress.
2. The vertical compressive strains and the major principal strains at the top of layer 4 also decrease with the increase in speed. However, the maximum vertical strain occurs after the load passes point 0, whereas the maximum principal strain, because of the large component of shear strain, occurs before the load reaches point 0. When shear strains are large and contribute to a significant portion of the principal strains, a criterion based on the vertical compressive strain will certainly be different from that based on the major principal strain.
3. The principal tensile strains at the bottom of layer 1 also decrease with the increase in speed, and, because of the existence of the large shear strain, the maximum principal tensile strain occurs before point 0 is reached.

ACKNOWLEDGMENT

The support given by the University of Kentucky Computing Center for the use of the IBM 360 computer is appreciated.

REFERENCES

1. Perloff, W. H., and Moavenzadeh, F. Deflection of Viscoelastic Medium Due to Moving Load. Proc. 2nd Internat. Conf. on the Structural Design of Asphalt Pavements, Univ. of Michigan, 1967, pp. 269-276.
2. Chou, Y. T., and Larew, H. G. Stresses and Displacements in Viscoelastic Pavement Systems Under a Moving Load. Highway Research Record 282, 1969, pp. 25-40.
3. Elliot, J. F., and Moavenzadeh, F. Analysis of Stresses and Displacements in Three-Layer Viscoelastic Systems. Highway Research Record 345, 1971, pp. 45-57.
4. Barksdale, R. D., and Leonards, G. A. Predicting Performance of Bituminous Surfaced Pavements. Proc. 2nd Internat. Conf. on the Structural Design of Asphalt Pavements, Univ. of Michigan, 1967, pp. 321-340.

5. Peattie, K. R. A Fundamental Approach to the Design of Flexible Pavements. Proc. Internat. Conf. on the Structural Design of Asphalt Pavements, Univ. of Michigan, 1962, pp. 403-411.
6. Dorman, G. M., and Metcalf, C. T. Design Curves for Flexible Pavements Based on Layered System Theory. Highway Research Record 71, 1965, pp. 69-84.
7. Huang, Y. H. Stresses and Displacements in Nonlinear Soil Media. Jour. Soil Mech. and Found. Div., Proc. ASCE, Vol. 84, No. SM1, Jan. 1968, pp. 1-19.
8. Lee, E. H. Stress Analysis of Viscoelastic Material. Quarterly of Applied Mathematics, Vol. 13, 1955, pp. 183-190.
9. Huang, Y. H. Stresses and Displacements in Viscoelastic Layered Systems Under Circular Loaded Areas. Proc. 2nd Internat. Conf. on the Structural Design of Asphalt Pavements, Univ. of Michigan, 1967, pp. 225-244.
10. Schapery, R. A. Approximate Methods of Transform Inversion for Viscoelastic Stress Analysis. Proc. 4th National Congress of Applied Mechanics, 1962, pp. 1075-1085.

SPONSORSHIP OF THIS RECORD

GROUP 2—DESIGN AND CONSTRUCTION OF TRANSPORTATION FACILITIES
John L. Beaton, California Division of Highways, chairman

SOIL MECHANICS SECTION
Carl L. Monismith, University of California, Berkeley, chairman

Committees as of December 31, 1972

Committee on Embankments and Earth Slopes
Lyndon H. Moore, New York State Department Transportation, chairman
Raymond A. Forsyth, David S. Gedney, Roger D. Goughnour, Wilbur M. Haas, C. W. Heckathorn, William P. Hofmann, Henry W. Janes, Philip Keene, Charles C. Ladd, Richard E. Landau, Ivan C. MacFarlane, Harry E. Marshall, Glen L. Martin, R. M. Mattox, Melvin W. Morgan, Robert L. Schuster, Edgar Pierron Ulbricht, David J. Varnes, Walter C. Waidelich, William G. Weber, Jr.

Committee on Mechanics of Earth Masses and Layered Systems
Russell A. Westmann, University of California, Los Angeles, chairman
Richard G. Ahlvin, Richard D. Barksdale, A. Alexander Fungaroli, Delon Hampton, M. E. Harr, Robert L. Kondner, Raymond J. Krizek, Fred Moavenzadeh, Keshavan Nair, Robert L. Schiffman, Frank H. Scrivner, Robert D. Stoll, Aleksandar S. Vesic, Harvey E. Wahls, William G. Weber, Jr., T. H. Wu

John W. Guinnee, Highway Research Board staff

The sponsoring committee is identified by a footnote on the first page of each report.